

**Ministry of Higher Education and Scientific Research  
University of Baghdad  
Institute of Laser for Postgraduate Studies**



# **Design and Implementation of In Line Fiber Pulse Compression using Photonic Crystal Fiber**

**A Thesis Submitted to the Institute of Laser for  
Postgraduate Studies, University of Baghdad in Partial  
Fulfillment of the Requirements for the Degree of  
Master of Science in Laser / Electronic and  
Communication Engineering**

**By**

**Ali Ahmed Dawood  
B.Sc. Communication Engineering  
2008**

**Supervisor**

**Asst. Prof. Dr. Tahreer Safa'a Mansour**

**2020 AD**

**1441 AH**

بِسْمِ اللَّهِ الرَّحْمَنِ الرَّحِيمِ

قَالُوا سُبْحَانَكَ لَا عِلْمَ لَنَا إِلَّا مَا عَلَّمْتَنَا إِنَّكَ أَنْتَ  
الْعَلِيمُ الْحَكِيمُ

صدق الله العلي العظيم

الآية (32) سورة البقرة

## **Certification**

I certify that this thesis was prepared under my supervision at the Institute of Laser for Postgraduate Studies, University of Baghdad, as a partial fulfillment of requirements for the degree of "Master of Science in Laser/ Electronic and Communication Engineering".

Signature:

Name: **Dr. Tahreer Safa'a Mansour**

Title: **Asst. Professor**

Address: Institute of Laser for Postgraduate studies,  
University of Baghdad.

Date: / / 2020  
(Supervisor)

In view of the available recommendation, I forward this thesis for debate by Examining Committee.

Signature:

Name: **Asst. Prof. Dr. Hanan Jaafar Taher**

Title: Head of the Scientific Committee.

Address: Institute of Laser for Postgraduate studies,  
University of Baghdad.

Date: / / 2020

## Examination Committee Certification

We certify that we have read this thesis "In Line Fiber Pulse Compression" and as Examination Committee, we examined the student in its content and in our opinion, it is adequate with standards as a thesis for a degree of Master in science in Laser /Electronic and Communication Engineering.

**Signature:**

**Name:** Dr. Hussein A. Jawad.

**Title:** Assistant Professor.

**Address:** Institute of Laser for Postgraduate Studies / University of Baghdad.

**Date:** / / 2020

(Chairman)

**Signature:**

**Name:** Dr. Sinan M. Abdul Satar.

**Title:** Assistant Professor

**Address:** Laser and Optoelectronics /  
University of Technology

**Date:** / / 2020

(Member)

**Signature:**

**Name:** Jawad A. Hasan

**Title:** Lecturer.

**Address:** Institute of Laser for Postgraduate  
Studies / University of Baghdad

**Date:** / / 2020

(Member)

**Signature:**

**Name:** Dr. Tahreer Safa'a Mansour

**Title:** Assistant Professor.

**Address:** Institute of Laser for Post graduate  
Studies / University of Baghdad

**Date:** / / 2020

(Supervisor)

Approval by the Deanship of Institute of Laser for Post graduate Studies,  
University of Baghdad.

**Signature:**

**Name:** Assistant Prof. Dr. Hussein A. Jawad

**Title:** Dean.

**Address:** Institute of Laser for Postgraduate  
Studies / University of Baghdad.

**Date:** / / 2020

# *Dedication*

This thesis is dedicated to...

My family and my country...

The people who support and encourage me.

## Acknowledgement

I'm so honored to have this opportunity to thank all the people who have helped me over the past two years.

First of all, I am grateful to the creator "ALLAH" for giving me the strength, enablement, knowledge and understanding required to complete this work. I would like sincerely thank my supervisor, **Asst. Prof. Dr. Tahreer Safa'a**, for her great contribution, scientific generosity, continuous support and encouragement during the research period. My grateful thanks go to **Prof. Dr. Abdul Hadi M. Al-Janabi**, Dean of the Institute of Laser for Postgraduate Studies, for his unlimited encouragement, and support during my research work. Special thanks are to **Dr. Mahmoud Shaker Mahmoud**, Asst. Dean of the Institute of Laser for Postgraduate Studies and **Asst. Prof. Dr. Mohammed K. Dhahir**, head of the Engineering and Industrial Applications Department, for his continuous advice and support. Many thanks go to all the faculty members and staff of Institute of Laser for Postgraduate Studies, University of Baghdad, especially to **Asst. Prof. Dr. Shelan Khasro Tawfeeq**, for her encouragement, help, and support during my research work. Special gratitude to **Eng. Laith T. Mohammed** who gave me great assistances to complete my work and getting excellent results.

Finally, I am indebted to my family and colleagues whom were very patient, kind and encouraging during the period of my study.

*Asi*

## Abstract

Optical pulse compression is an important process that can be used to reduce pulse duration, for that future it can be used in many advanced optical communication systems for high data rate applications such as orthogonal frequency division multiplexing (OFDM) and dense wavelength division multiplexing (DWDM).

In this work, the in line fiber pulse compression is designed and constructed using very narrow pulse laser which designed to couple the two interferometers by using electronically chopped circuit that has 10 ns pulse duration, 286 pm full width at half maximum (FWHM), peak power ( $P_p$ ) of 1229.271  $\mu$ W and centered at 1546.7 nm and propagate via these types of fiber interferometers. The first interferometer is etalon Fabry–Perot interferometer that formed by splicing two hollow core photonic crystal fibers HC-PCFs (7 & 19 cell) between two single mode fibers smf-28 fibers while the second interferometer is Mach-Zhender interferometer that was constructed using two types of solid core photonic crystal fibers SC-PCFs (PM-1550-01 & ESM-12B) with 30 cm length spliced in between two single mode fibers (smf-28). It is worthy to be mentioned that the two types of interferometers are centered in 1546.7 nm. Minimum FWHM was obtained in the case of 7 cm 19 cell hollow core photonic crystal fiber (HC-PCF) which was equal to 117.26 pm with 2.43 compression factor. This output was enhanced, compressed, by changing the effective refractive index ( $n_{eff}$ ) after replacing the air holes of 19 cell HC-PCF with two organic compound that are ethanol and acrylic acid solution. Good compression factor that is equal to 4.9 with FWHM of 58 pm was extracted in the case of acrylic acid solution after dilute 25% acrylic acid that has a refractive index of 1.5 with 75% ethanol and 1.3369 refractive index (both refractive indices of organic compound are to be measured at 1550 nm and 25C<sup>o</sup>) and using refractometer.

## List of Contents

<b>Abstract</b>		i		
<b>List of Contents</b>		iii		
<b>List of Abbreviations</b>		vii		
<b>List of Symbols</b>		viii		
<b>List of Tables</b>		x		
<b>List of Figures</b>		xi		
<b>Chapter One : Introduction and Basic Concepts</b>				
1.1	Introduction	1		
1.2	Aim of the work	3		
1.3	Photonic crystal fibers	3		
	1.3.1	Guiding Mechanism in Photonic Crystal Fiber	4	
	1.3.2	Challenges in Splicing of PCF	6	
		1.3.2.1	Hole Collapse	6
		1.3.2.2	Splice Loss	8
1.4	Interferometers	10		
	1.4.1	In Line Fiber PCF as Michelson Interferometer	10	
	1.4.2	In Line PCF as Sagnac Interferometers	11	
	1.4.3	Mach-Zehnder Interferometers (MZI) using PCF	12	
		1.4.3.1	Mach-Zehnder Interferometer based on Mode Mismatch	13
	1.4.4	HC-PCF as Fabry-Perot Interferometers	14	
		1.4.4.1	In Line Photonic Crystal Fiber Fabry-Perot interferometers	16
		1.4.4.2	In Line HC-PCF FPI	16
1.5	Degradation of the Propagated Signals in Optical Fibers	17		
	1.5.1	Transmission Loss of Optical Fiber	17	
	1.5.2	Confinement loss	19	
	1.5.3	Bending loss	20	
	1.5.4	Dispersion	20	
		1.5.4.1	Chromatic Dispersion	20
		1.5.4.2	Intermodal Dispersion	23
		1.5.4.3	Polarization Mode Dispersion	24

	1.5.5	Nonlinearities phenomena		24
		1.5.5.1	Intensity-Dependent Refractive Index	25
		1.5.5.2	Self-Phase Modulation	26
		1.5.5.3	Cross-phase modulation	28
		1.5.5.4	Stimulated Raman Scattering	28
		1.5.5.5	Effective length	29
1.6	All-Fiber Pulse Compression			30
	1.6.1	Linear Pulse Compression		30
		1.6.1.1	Linear pulse compression based Fibers Dispersion	31
		1.6.1.2	Linear Pulse Compression using Fiber Bragg Grating	31
	1.6.2	Fiber Nonlinear Pulse Compression		32
		1.6.2.1	Nonlinear Pulse Compression using Dispersive Compressor	32
		1.6.2.2	Nonlinear Pulse Compression using Hollow Core Photonic Crystal Fiber	32
		1.6.2.3	Nonlinear Pulse Compression using Higher-Order Soliton	33
		1.6.2.4	Nonlinear Pulse Compression using Adiabatic Soliton	33
		1.6.2.5	Nonlinear Pulse Compression using Self – Similar Technique	34
1.7	Compression factor ( $F_c$ )			35
1.8	Literature survey			35
1.9	Thesis layout			41
<b>Chapter Two : Experimental Setups</b>				
2.1	Introduction			43
2.2	key Components and Equipment			44
	2.2.1	Laser Source		45
		2.2.1.1	CW Laser Source	45
		2.2.1.1	A Laser diode controller (driver circuit)	45
		2.2.1.1	B Electronic Chopping Circuit	46
	2.2.2	Erbium-Doped Fiber Amplifier		48

	2.2.3	Interferometer		48
		2.2.3.1	Fiber	49
		2.2.3.2	Procedures of Constructing Interferometers	58
		2.2.3.3	Coupling Laser to Interferometers	62
	2.2.4	Polarization Controller (PC)		63
	2.2.5	System Visualizers		63
		2.2.5.1	Optically Visualize	63
		2.2.5.2	Temporally visualize	64
		2.2.5.3	Power Meter	65
		2.2.5.4	Thermometer	65
2.3	In Line Pulse Compression Techniques			65
	2.3.1	Pulse Compression Based on Solid Core Photonic Crystal Fiber		65
	2.3.2	Pulse Compression Based on HC-PCF		66
	2.3.3	Pulse Compression Based on Infiltration of HC-PCF 19 cell		67
		2.3.3.1	Ethanol	68
		2.3.3.2	Acrylic Acid	69
<b>Chapter Three : Results and Discussions</b>				
3.1	Introduction			71
3.2	Characterization of the Pulsed Laser Source			71
3.3	Pulse Compression Using Fabry-Perot Etalon Interferometers			74
	3.3.1	Pulse Compression Based on HC-PCF without infiltration		74
		3.3.1.1	Pulse Compression Based on HC-PCF (19 cells)	74
		3.3.1.2	Pulse Compression Based on HC-PCF (7 cells)	80
	3.3.2	Pulse Compression Based on Infiltrated HC-PCF (19 cells)		86
		3.3.2.1	Pulse Compression using Infiltrated HC 19-1550 PCF with Ethanol	86
		3.3.2.3	Pulse Compression Based on Infiltrated HC-PCF (19 cells) with Acrylic Acid	87
3.4	Pulse Compression Based on SC-PC			89

	3.4.1	Pulse Compression Based on PM	89
	3.4.2	Pulse Compression Based on ESM	90
3.5	Performance comparison of 19 cells HC-PCF		91
3.6	Conclusion		94
3.7	Future Work		95
	<b>References</b>		96
	<b>Appendix A</b>		A-1
	<b>Appendix B</b>		B-1
	<b>Appendix C</b>		C-1

### List of abbreviations

Abbreviation	Meaning
CL	Confinement loss.
CW	Continuous Wave.
DWDM	Dense Wavelength Division Multiplexing.
d	Air Hole Size Diameter
D	Hole Diameter
EFFPI	Extrinsic Fiber Fabry-Perot Interferometer.
FP	Fabry-Perot.
FC	Ferrule Connector.
$F_c$	Compression Factor.
FWHM	Full Width at Half Maximum
GVD	Group Velocity Dispersion.
HC-PBGFs	Hollow-Core Photonic Bandgap Fibers.
IGPCFs	Index Guiding Photonic Crystal Fiber.
IFFPI	Intrinsic Fiber Fabry-Perot Interferometer.
ID	Inner Diameter.
IC	Integrated Circuit.
ILFE	In-Line Fiber Etalon.
LD	Laser Diode.
MZI	Mach-Zender Interferometer
MFD	Mode Filed Diameter
OSA	Optical Spectrum Analyzer.
OD	Outer Diameter.
OFC	Optical Fiber Coupler.
OFI	Optical Fiber Interferometer.
OFDM	Optical Orthogonal Frequency Multiplexer.
OKE	Optical Kerr Effect.
PMD	Polarization Mode Dispersion.
PBG	Photonic Bandgap Fiber.
PC	Polarization Controller.
PCF	Photonic Crystal Fiber.
PBGFs	Photonic Bandgap Fibers.
RI	Refractive Index.
SMF	Single Mode Fiber.
SPM	Self-Phase Modulation.
SRS	Stimulated Raman Scattering.
TTL	Transistor-to-Transistor Logic.
TIR	Total Internal Reflection.
UV	Ultraviolet.
USPs	Ultrashort Pulses.
XPM or CPM	Cross Phase Modulation.
$\Lambda$	Hole-to-Hole Spacing.

### List of symbols

<b>Symbol</b>	<b>meaning</b>	<b>unit</b>
$\beta^2$	GVD parameter.	ps <sup>2</sup> /km
$\lambda$	Laser wavelength.	nm
R	Radius of curvature of bends.	nm
K	Wave vector	nm <sup>-1</sup>
NA	Numerical aperture.	-
W	Mode field radius	cm
$\beta(\omega)$	Mode-propagation constant of frequency $\omega$ .	Rad/nm <sup>-1</sup>
f	Air filling fraction	-
$n_{air}$	Refractive index of air	-
$n_{silica}$	Refractive index of silica	-
$L_{eff}$	Effective sample length	m
L	Fiber length.	m
$\lambda_0$	Free space wavelength	nm
$\Omega$	Angular velocity	Rad/sec
$\theta$	Angle for reflected mode.	degree
r	Core radius.	$\mu\text{m}$
$\alpha$	Attenuation coefficient.	cm <sup>-1</sup>
$n_{co}$	Refractive index of core	-
$n_{cl}$	Refractive index of cladding	-
$n^2$	Nonlinear refractive index	m <sup>2</sup> /W
$n_0$	Ordinary refractive index.	m <sup>2</sup> /W
ac	Cauchy coefficient	-
$\chi^{(3)}$	Third order nonlinear susceptibility	-
$\epsilon_0$	Permittivity of free space	F/m
$\Delta$	Difference between core and cladding refractive indices.	-
bc	Cauchy coefficient	nm <sup>+2</sup>
cc	Cauchy coefficient	nm <sup>+4</sup>
$n_{eff}$	Effective refractive index.	-
D	Dispersion parameter.	ps/(km. nm)
$D_M$	Material dispersion	ps/(km. nm)
$D_W$	Waveguide dispersion.	ps/(km. nm)
FWHM	Full width at half maximum.	pm
$\tau$	Pulse duration.	$\mu\text{s}$ , ns
PRR	Pulse repetition rate.	Hz
$\gamma$	Nonlinear coefficient.	W <sup>-1</sup> m <sup>-1</sup>

$P_i$	Input power.	W
$P_o$	Output power.	W
$\omega_s$	Resonance frequency	rad/s
$E$	Electric field	V/m
$P$	Polarizability	Coul./m <sup>2</sup>
$I_{eff}$	Optical power per fiber effective area	W/m <sup>2</sup>
$A_{eff}$	Fiber effective area	m <sup>2</sup>
$\alpha_m$	Attenuation constant	dB/m
$\alpha_{mic}$	Micro bend loss	dB/m
$\Delta\phi$	Phase different between modes.	rad
$\Phi_{NL}$	Nonlinear phase shift	rad
$\lambda_c$	Central wavelength	nm
$\omega$	Angular frequency	Rad
$V_g$	group velocity	m/s
$n_g$	group index	-

## List of Table

<b>Table No.</b>	<b>Ttle of the table</b>	<b>Page No.</b>
Table 1.1	Compare experimental results of literature survey and this thesis	42
Table 2.1	Parameters of chopped laser source.	46
Table 2.2	Geometrical properties for HC-PCF (19 cells HC19-1550) obtained from microscope.	52
Table 2.3	Optical parameters of HC-PCF (19 cells HC19-1550).	52
Table 2.4	Geometrical properties for 7 cell HC-PCF (HC-1550-02) obtained from microscope	54
Table 2.5	Optical parameters of HC-PCF (7 cell HC-1550-02).	54
Table 2.6	General properties of PM-1550-01 fiber.	55
Table 2.7	Shows general properties of the ESM fiber.	57
Table 2.8	General properties of fiber	58
Table 2.9	Setting parameters of the arc fusion splicer for HC-PCF, SC- PCF, DCF38.	60
Table 2.10	Ethanol properties [65]	68
Table 2.11	Acrylic Acid properties	69
Table 3.1	Relationship between 19 cells HC-PCF length, FWHM and compression factor.	79
Table 3.2	Relationship between 7 cells HC-PCF length, FWHM and compression factor.	85
Table 3.3	Refractive index for chemical liquids.	88
Table 3.4	Effects of infiltration on compression factor and full width at half maximum.	93
Table 3.5	percentage values of $F_c$ and FWHM	93

## List of Figures

Figure No.	Title of the Figure	Page No.
Fig.1.1	A schematic configuration of in line PCF as Michelson interferometer Fig. [5].	4
Fig.1.2	A schematic configuration of in line PCF as Sagnac interferometer [6].	5
Fig.1.3	A schematic configuration of in line PCF as MZI interferometer [11].	6
Fig.1.4	Schematic of the interferometer based on core mismatch Technique [8].	7
Fig.1.5	Fig.1.0.5 a) Fabry-Perot based on the light transmission, b) Fabry-Perot based on the light reflection [7].	8
Fig.1.6	Schematic configurations of three IFFPI [7].	8
Fig.1.7	Schematic configurations of four EFFPI [7].	9
Fig.1.8	A schematic configuration of fiber in line HC-PCF as etalon interferometer [14].	10
Fig.1.9	Cross section and refractive index profiles of a) conventional step-index, b) a solid-core PCF. The gray and black regions correspond to silica material and air, respectively [16].	11
Fig.1.10	Photonic Crystal Fiber designs, a) Bragg fiber, b) hollow-core fiber and, c) solid-core fiber. [17]	12
Fig.1.11	Attenuation spectrum of optical fiber [32].	18
Fig.1.12	Attenuation and group velocity dispersion spectra of photonic crystal fiber 19 cells [35].	19
Fig.1.13	Attenuation and group velocity dispersion spectra of photonic crystal fiber 7 cells [36].	19
Fig.1.14	Variation in polarization states of an optical pulse at it passes through a fiber [48].	24
Fig.1.15	The effect of SPM on un chirped pulse [52].	27
Fig.1.16	The effect of SPM on the spectrum [52].	28
Fig.1.17	Energy level diagrams describing, a) Raman Stokes scattering and b) Raman anti-Stokes scattering [42].	29
Fig.1.18	Effective transmission length calculation, a) A typical distribution of the power along the length L of a link. The peak power is $p_0$ , b) A hypothetical uniform distribution	30

	of the power along a link up to the effective length $L_{\text{eff}}$ . This length $L_{\text{eff}}$ is chosen such that the area under the curves (a) and (b) is equal [55].	
Fig.1.19	Re-shaped the pulse by using chirped Fiber Bragg Grating [59].	31
Fig.1.20	Compression using dispersive compressor [61].	32
Fig.1.21	A schematic configuration for high order soliton compression [62].	33
Fig.1.22	A schematic configuration for pulse compression by using self-similar technique [64].	34
Fig. 2.1	Flow chart of the work's steps.	43
Fig. 2.2	Pulse compression, a) Schematic diagram, b) experimental setup.	44
Fig. 2.3	Electronic Chopping Circuit, a) Schematic diagram b) simulation by Optisystem, c) experimental image.	47
Fig. 2.4	Side view for the SMF fiber under microscope.	49
Fig. 2.5	Cross section of top view and side view for the 19 cells under microscope (a,b,c,d,e) top view, and (f) side view	51
Fig. 2.6	Cross section of top view and side view for the 7 cells under microscope (a,b,c,d,e) top view, and (f) side view	53
Fig. 2.7	Shows a cross sectional view of PM-1550-01 fiber.	55
Fig. 2.8	a) side view of ESM, b) cross sectional view of ESM.	56
Fig. 2.9	Cross sectional view of DCF38.	57
Fig.2.10	procedure of the splicing HC-PCF with SMF, a) splicing region for 30 cm, b) splicing region for 20 cm during arcing	61
Fig.2.11	Images show splicing joints during the splicing of seven cells with SMF, a) splicing region for seven cells at 30 cm length of PCF, b) splicing of same fiber but different length of 20 cm	61
Fig.2.12	Images show the splicing joints during the splicing of SC-PCF with SMF	62
Fig.2.13	Lab image of designed photodetector	64
Fig.2.14	Setup represents pulse compression based on solid core photonic crystal fiber	66
Fig.2.15	Setup represents pulse compression based on hollow core photonic crystal fiber	67

Fig.2.16	Shows setup that used in infiltration process	68
Fig.3.1	Simulated characteristics of laser source a) Optical spectrum, b) Oscilloscope trace	72
Fig.3.2	Characteristics of the pulsed laser source a) Optical spectrum, b) Pulse duration, c) Pulse repetition rate (PRR).	73
Fig.3.3	Compressed signal in frequency and time domains for four lengths of 19 cells PCF a-b) 7 cm length, c-d) 12 cm length, e-f) 20 cm length, g-h) 30 cm length.	75
Fig.3.4	Relationship between length of 19 cells PCF and a) Full width at half maximum (FWHM), b) Compression factor ( $F_c$ ).	79
Fig.3.5	Compressed signal in frequency and time domains for four lengths of 7 cells PCF a-b) 7 cm length, c-d) 12 cm length, e-f) 20 cm length, g-h) 30 cm length.	81
Fig.3.6	Relationship between length of 7 cells PCF and a) Full width at half maximum (FWHM), b) Compression factor ( $F_c$ ).	85
Fig.3.7	Optical spectrum of compressed pulse using Infiltrated sample of 19 cells HC-PCF by Ethanol.	87
Fig.3.8	Optical spectrum of the compressed pulse using Infiltrated 19 cells HC-PCF by Acrylic acid solution.	88
Fig.3.9	Optical spectrum of the compressed pulse using PM-1550-01.	89
Fig.3.10	Optical spectrum of the compressed pulse using ESM.	90
Fig.3.11	Optical spectra of 19 cells HC-PCF infiltrated by a) ethanol b) acrylic acid solution.	91

# **Chapter One**

## **Introduction and Basic Concepts**

## **Chapter One**

### **Introduction and Basic Concepts**

#### **1.1 Introduction**

Over the past decade, a considerable amount of interest in optical properties of multidimensional, periodic structure had arisen. An especially class of such structures in which light propagation for certain range of frequencies is prohibited, are often known in literature as photonic crystals or photonic bandgap materials. The large interest in PCs arises because it offers the possibility of controlling and manipulating light within a given frequency range through photonic bandgap [1]. Among the most interesting aspects of photonic crystals are the possibilities of creating new means of waveguiding [2], the flow of light may be controlled to an extreme degree. An exciting area where 2D photonic crystals could be employed is, optical fibers. The fiber form of these structures, which is attracting a lot of interest because of its unique wave guiding properties unattainable in conventional optical fibers, is known as Photonic Crystal fibers [3]. Thus, photonic crystal fibers (PCFs) are single material optical fiber with a periodic array of air holes running down the length of the fiber, with a central guiding core. PCFs can be divided in two classes according to the mechanisms used to guide light. The newer classes of structures are the Photonic Band gap Fibers, where, the light is guided by photonic band gap effect in low index region (i.e. air). The second class of photonic crystal fiber's guide light by modified Total Internal Reflection, where light is confined to the high index defect introduced at a design state. Photonic crystal fibers show some remarkable properties since they appeared in the mid-1990s [4] like single mode operation in wide wavelength range (337nm-1550nm), large mode area, unique wave guiding and dispersion properties, excitation of non-linear effects at small mode area etc.

The effective index difference between the core and cladding in PCF is a strong function of wavelength, since at longer wavelength the modal fields extend into the air holes, thereby reducing the effective index. This strong wavelength dependence results in a range of unique & potentially useful properties for such fibers. The arrangement and spacing of air holes provide freedom to tailor the dispersion properties for telecom applications. Therefore, these fibers are particularly attractive for Photonic devices because of their optical properties which can be engineered during fabrication process and it is expected that the PCFs will find its place in telecommunications network [5]. The majority of fiber devices, such as optical sources, detectors, switches, interrogation units etc., use standardized telecom fiber connectors. Therefore, most of the practical applications of specialty, including photonic crystal, side-hole, air-clad etc., fibers require a reliable and repeatable low-loss splicing with a standard single mode fiber (SMF) [6]. Low loss splicing a PCF with a single-mode fiber (SMF) remains a key problem that limits the widespread development of PCF devices and sensors. In general the splicing loss is due to two reasons: one is the mode field mismatch between PCFs and SMFs; the other is that the air holes in PCFs at the splice joint are often collapsed during the splicing process, which significantly increases the coupling loss by destroying the light guiding structure of the PCF near the joint interface. There are two methods to make splicing between photonic crystal fibers and single mode fiber either using fusion splicers or CO<sub>2</sub> lasers gradient index fiber lenses splice-free PCF technique tapered PCF and different fiber splicer's. The most suitable and practical method is used a method of arc fusion splicing

## 1.2 Aim of the thesis

The aim of this thesis is to investigate and implement all-fiber pulse compression based on In-Line Fabry-perot and Mach-Zehnder interferometers by using of hollow core photonic crystal fiber (HC-PCF) and solid core photonic crystal fiber (SC-PCF).

## 1.3 Photonic crystal fibers

The Photonic crystal fiber (PCF) is a new class of optical fiber based on the properties of photonic crystal [15]. A defect was created by filling the central air-hole with glass to guide light by modified total internal reflection (MTIR) between the solid core and the cladding region with multiple air holes. These index-guiding PCFs also called MTIR-PCFs. Another PCFs use a perfectly periodic structure exhibiting a photonic band-gap (PBG) effect at the operating wavelength to guide light in a low index core region [16]. A PCF can be described by its cladding structure, the air hole size diameter ( $d$ ), and the distance between neighboring air holes, called the pitch or hole-to-hole spacing,  $\Lambda$ , as illustrated in Figure 1.1. The relative hole size ( $d/\Lambda$ ), defined as the ratio of the air hole size to the hole-to-hole spacing is also a commonly used parameter. Another measure often used to describe PCFs is the air filling fraction, defined as the fraction of the area of the air holes to the area of the silica in the cladding. The core diameter in PCFs is not as clear as that for standard fibers with a circular core. Nonetheless the core diameter of hexagonal PCFs with one air hole defect is often counted for as  $2\Lambda-d$ , also indicated in Figure 1.1 [17].

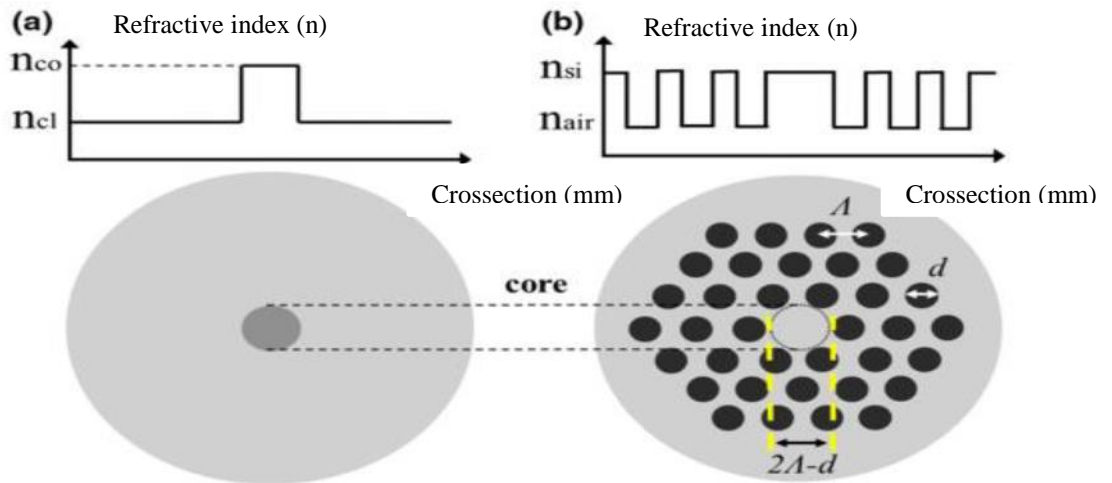


**Fig. 1.1** Cross section and refractive index profiles of a) conventional step-index, b) a solid-core PCF. The gray and black regions correspond to silica material and air, respectively [16].

### 1.3.1 Guiding Mechanism in Photonic Crystal Fiber

In photonic crystal fiber (PCF) there are many designs to confine light to its core. Figure 1.2 shows the three design of PCF: (a) Bragg fiber, (b) Hollow core fiber and (c) Solid core fiber. PCF is constructed of two materials with different refractive indexes, arranged in a periodic structure [16]. Hollow core fibers (HCFs) are built from a periodic lattice of holes in the cladding that run parallel to the propagation axis of the fiber, with a large hole at their center. Both Bragg fibers and HCF utilize a photonic band gap to confine light to their core [17]. Solid core fibers (SCF<sub>s</sub>) have a periodic lattice of holes like hollow cores, but have a silica core which the light propagates down. Like SMF, SCF<sub>s</sub> use total internal reflection to confine light to their cores. SMF is constructed to have a small core, which can only guide one fundamental mode above a cut-off wavelength [15]. SMF used the refractive index contrast between its higher refractive index core and its lower refractive index cladding. Light was confined to the core due to total internal reflection, and propagate along the propagation axis of the fiber due to Snell law which is given by:

$$n_1 \sin(\theta_1) = n_2 \sin(\theta_2) \quad (1.1)$$

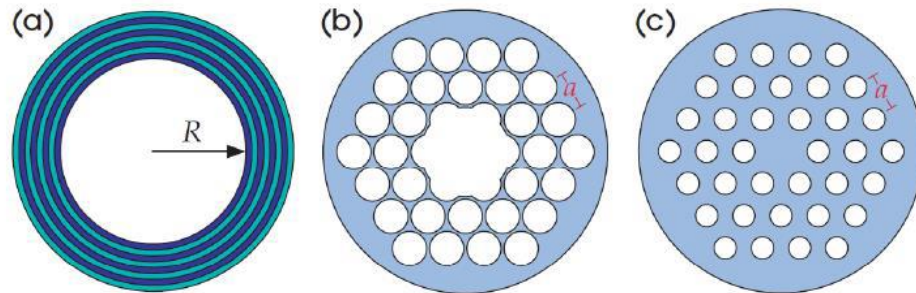


**Fig. 1.2 Photonic Crystal Fiber designs, a) Bragg fiber, b) hollow-core fiber and, c) solid-core fiber. [17]**

Solid core fiber (SCF) provided the contrast in refractive index between the core and cladding by reducing the refractive index of its cladding by inserting the air holes as a periodic lattice around the core. SCF can be constructed that is endlessly single mode [18]. Endlessly single mode fiber doesn't possess a cut-off wavelength, and only guides the fundamental mode regardless of wavelength [16,18]. There are two descriptions of the causes of this endlessly single mode property state that shorter wavelengths penetrate less into the PCF cladding from their core, and therefore experience a higher refractive index of the cladding than for longer wavelengths [18].

As a consequence of this, they experience the lower effective refractive index difference between the cladding and the core will reduce the confinement for shorter wavelengths. Therefore higher order modes are not confined to the core of the PCF [17,19]. The endlessly single mode property is due to the different intensity profiles of higher modes when compared to fundamental mode. Light is evanescent in air that provides a strong barrier for light. The air hole structure can be imagined as a "sieve", with the air holes the "wire mesh". The fundamental mode is a lobe that acts like a "grain of rice", trapped in the mesh. Higher order modes have finer lobes that can escape through the gaps in the mesh. The endlessly single mode property of

the PCFs has been experimentally verified [17], and has provided benefits in high power delivery. Hollow core PCF is also capable of high power delivery since the high power doesn't damage the air in the core of the fiber. The band gap means that the fiber can be filled with air, or other fluids with a refractive index lower than the cladding [20]. This is a very versatile property and has been used for high non-linearity for super continuum generation and even transportation of polystyrene spheres along their length [21].

### **1.3.2 Challenges in Splicing of Photonic Crystal Fiber**

In any splicing operation, the key point is the mode coupling between two fibers. If there is any mismatch during the splicing process, loss will be the cost. Therefore, it is important to ensure that the efficiency of light coupling from a SMF to the PCF is as good as possible, in other words, with the high coupling efficiency. However, the challenge in splicing conventional SMFs with the PCF raises from the fact that the PCF has a periodic number of microstructure air holes surrounding the core. The heating process require for splicing damages the hole structure of PCF. To understand why, an effect called hole collapse and related loss will be explain:

#### **1.3.2.1 Hole Collapse**

When forming a splice between SMF and PCF the two fibers must be heated. The heat caused hole collapse, which is where the light guiding structure of PCF collapses [22, 23].

Regions of PCF where the hole structure has collapsed no longer guide light, which allows light to escape from the core of the fiber and is a source of loss. For SMF- SCPCF type (ESM-12B) the hole collapse region isn't birefringent. To reduce the length of the hole collapse region, and reducing loss caused by it, the heat was applied to the PCF need to be reduce. This can be achieved by reducing the arc power during splice. The hole

collapse was composed of two types which were known as complete hole collapse and partial hole collapse. The complete hole collapse is where the hole structure has collapsed completely and the fiber no longer confines light to the core. The holes in a partial collapse have shrunk in diameter, causing light confinement to be weakened but still present [23].

When PCF is heated during splicing, the air holes collapsed and its rate was determined by two forces: the surface tension of the silica and viscosity of the silica. The surface tension effects on collapsing the air holes and pulls the fiber ends together into a splice, where the viscosity resists the surface tension. When the fiber was not being heated, the viscosity is high enough that the diameters of the holes remained constant. As the fiber was heated towards the melting point of silica 2000°C the viscosity of the silica reduces [23]. There is a threshold point closed to 2000°C where the surface tension overcomes its viscosity, and the holes begin to collapse [24]. The speed of this collapse is given by equation (1.5):

$$V_{collapse} = \gamma / \eta \quad (1.5)$$

where  $\gamma$  is the surface tension of the silica and  $\eta$  is the viscosity of the silica.

The temperature in a region of the PCF experiences decreases as a function of distance of that region from the arc points [24]. This means that when the electrical arc is on, the viscosity of the silica of a region increases the further away from the arc points that region is. This reduces the speed of the collapse, for holes of regions further away from the arc point. The time it takes for a hole structure to collapse is given by

$$T = D_{hole} / V_{collapse} \quad (1.6)$$

where  $V$  is the speed of collapse and  $D_{hole}$  is the diameter of the hole.

As the speed of collapse reduces, it takes longer time for the whole structure to collapse [26]. For some of the fiber far enough away from the arc points, this time is longer than the duration of the electrical arc. This

region of the PCF experiences partial collapse. There is a point along the fiber far enough away from the arc points that the temperature does not reach the threshold value for collapse to begin, which represents the boundary between partial collapse and no collapse [22]. The effect of hole collapse on the loss across the splice is that the mode field diameter (MFD) increases across the hole collapse region. This can cause a mismatch between the MFD of PCF and the fiber to which it is being spliced. If the MFD of the PCF is greater than the fiber to which it is spliced, only the intensity of light within the area of the MFD of the other fiber will be transmitted into its core. The greater the mismatch, the lower the fraction of light that will transmit from the core of the PCF into the core of the other fiber. If the MFD of the PCF is smaller than of the fiber to which it is spliced, all of the light that transmits across the splice will be guided by the core of the other fiber [23]. This means that loss across the splice is described as non-symmetrical, or non-reciprocal. The MFD of both fibers can be chosen to match, but as the MFD of the PCF depends on the length of the hole collapse region, the mismatch is dependent on the nature of the splice [25].

### **1.3.2.2 Splice Loss**

Loss is an important factor for optical fiber technology. But over the last 50 years, losses in standard optical fibers have been reduced. The minimum loss in pure fused silica at 1550 nm wavelength is slightly less than 0.2 dB/km [26].

In photonic crystal fiber light moves away from the core if the confinement provided by the air-holes is not enough. This means that it is important to design such aspects of the PCF structure as air-hole diameter and hole-to-hole spacing, or pitch  $\Lambda$ , in order to realize low-loss PCFs[27].

In general, fiber loss or attenuation can be calculated with attenuation constant,  $\alpha$ , is a measure of energy loss during the transmission in the fiber. This constant is represented by [28]:

$$\text{Loss} = -10 \log (p_{out} / p_{in}) \quad (1.2)$$

where L is the total fusion splice loss in dB,  $p_{in}$  is the input power,  $p_{out}$  is the transmitted power.

The splice loss is generally due to two reasons: one is the mode field diameter (MFD) mismatch between PCFs and SMFs, and the other is that the air holes in PCFs may completely collapse in the vicinity of the splice joint during the splicing process MFD is the characteristics of a fiber which describes the confinement of mode or light in the core part of an optical fiber. The total attenuation or total splice loss between PCF and SMF due to the mode mismatch can be calculated by using the following relations [29]:

$$\text{MFD} = 2w \sqrt{1 + \frac{z\lambda}{\pi n w}} \quad (1.3)$$

$$\alpha_{(dB)} = -20 \log \frac{2w_{PCF} w_{SMF}}{w_{PCF}^2 + w_{SMF}^2} \quad (1.4)$$

where n is the refractive index of the pure silica ( $n_{\text{silica}}=1.45$  at 1550 nm and 20 c°),  $\lambda$  is the light wavelength.

The (dB) is the total fusion splice loss in dB and the  $w_{smf}$  and  $w_{pcf}$  are the mode field diameters of SMF and PCF respectively, the loss mechanism is due to the mode mismatch between PCF and SMF [30].

## 1.4 Interferometers

Interferometers operate according to the principle of grazing incidence of light [6]. Typically an incident light beam of interferometer is split into two or more parts and then recombine together to create an interference pattern. The integer number of wavelength for the optical path difference between the two paths corresponds to constructive points and odd number of half wavelengths corresponds to destructive points of the interference pattern. So, in the output optical spectrum of the optical fiber interferometer (OFI), the position of minimum can be shifted to maximum position if the optical path difference varies by odd number of half wavelengths. At least two optical paths are necessary for an interferometry experiment. These optical paths can be in one optical fiber with two or more different optical fiber modes. Each of modes defines one optical path for the interferometer such as the Sagnac interferometer where the optical paths are defined by the clockwise and counter clockwise modes [6].

There are many interferometers configurations that have been realized with the PCF. To see the principle of their operation, the detail of some interferometers such as Mach-Zehnder, Sagnac, Fabry Perot, and Michelson interferometers are presented [7].

### 1.4.1 In Line Fiber Photonic Crystal Fiber as Michelson Interferometer

A schematic of conventional Michelson Optical Fiber Interferometer (OFI) is depicted in Figure 1.3. The high coherent light beam is split into two different optical paths in the upper and lower photonic crystal fibers by the  $2 \times 2$  optical fiber coupler (OFC). The light reflected back by mirrors  $M_1$ , through  $\emptyset$  for phase shift and  $M_2$  are recombined by the OFC to produce interference pattern at the receiver [8].

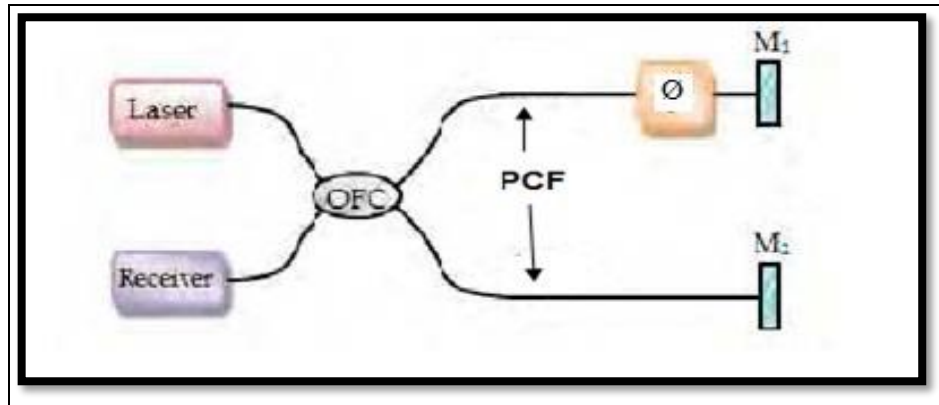


**Fig. 1.3** A schematic configuration of in line PCF as Michelson interferometer [5].

### 1.4.2 In Line Photonic Crystal Fiber as Sagnac Interferometers

The configuration of a Sagnac optical fiber is illustrated by Figure 1.4. The optical source is a single mode stabilized coherent semi-conductor or Erbium doped optical fiber laser. The laser output beam is assumed to be well collimated with uniform phase. The laser beam enters the lossless 3dB Optical Fiber Coupler (OFC). At the OFC the injected light splits into two parts with equal intensity that each of them travels around single mode optical fiber coil in opposite directions. The output of Sagnac coil is guided toward a single detector [8].

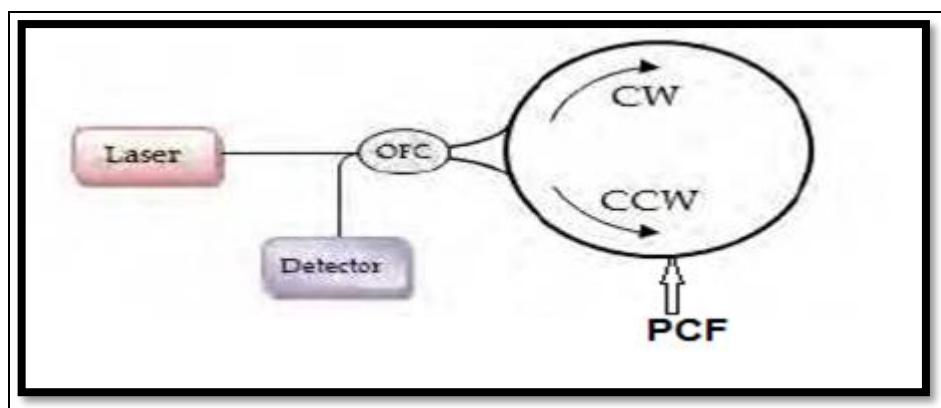


**Fig. 1.4** A schematic configuration of in line PCF as Sagnac interferometer [6].

Due to this specific configuration, fiber Sagnac interferometer has been used for rotation sensing primarily. In a non-rotating Sagnac

interferometer, the clockwise (CW) and counter clockwise (CCW) modes are in phase while for a rotating Sagnac configuration due to the rotating velocity, the optical path of one of the modes is shorten and the other one is lengthen. The Sagnac effect causes the interference spectrum depends on the angular frequency of the setup [9]. Analysis can be based on the Doppler frequency difference between the CW and CCW modes. The detector output frequency is the beating frequency of CW and CCW modes. When rotational axis is oriented along the optical fiber coil axis, the phase difference of CW and CCW modes is:

$$\Delta\varphi = 8 \pi N A \Omega / \lambda_o \quad (1.5)$$

where  $\lambda_o$  is the free space optical wavelength, A is the area of Sagnac coil, N is the number of the coil turn and  $\Omega$  is the angular velocity [10].

The previous equation can be rewritten as:

$$\Delta\varphi = S \Omega \quad (1.6)$$

where  $S = 8 \pi N A / \lambda_o$

S is the sensitivity of Sagnac interferometer.

### **1.4.3 Mach-Zehnder Interferometers (MZI) using Photonic Crystal Fiber**

In the present PCF between two single mode fibers the collapsed region allows the input light to split into the core and the cladding of the PCF, resulting in light propagating as core mode and cladding modes, respectively. Figure 1.5 shows a schematic diagram of the in-fiber PCF MZI. The first collapsed region acts as a beam splitter coupler where the core and cladding modes are excited in PCF simultaneously while the second collapsed region acts as combiner coupler. The core mode and cladding modes travel along the PCF length (L) with different speeds. Since these modes are characterized by their effective refractive indices ( $n_{\text{core}}$  and  $n_{\text{clad}}$ )

therefore, a relative group delay is developed after the propagation. They (core mode and the cladding modes) recombine at the second collapsed region of PCF output end [11].

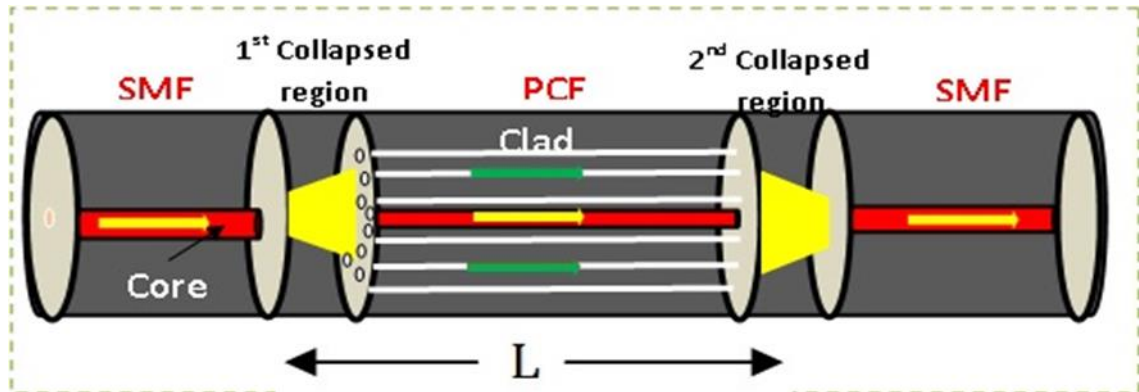


Fig. 1.5 A schematic configuration of in line PCF as MZI interferometer [11].

#### 1.4.3.1 Mach-Zehnder Interferometer based on Mode Mismatch

This technique is done by a small lateral offset when the two fibers are spliced because of the offset in the point of core mismatch, a part of core mode is coupled to cladding mode [12]. Three pieces of PCF were spliced with a minute lateral offset as shown in Figure 1.6, this process is done by a fusion splicer.

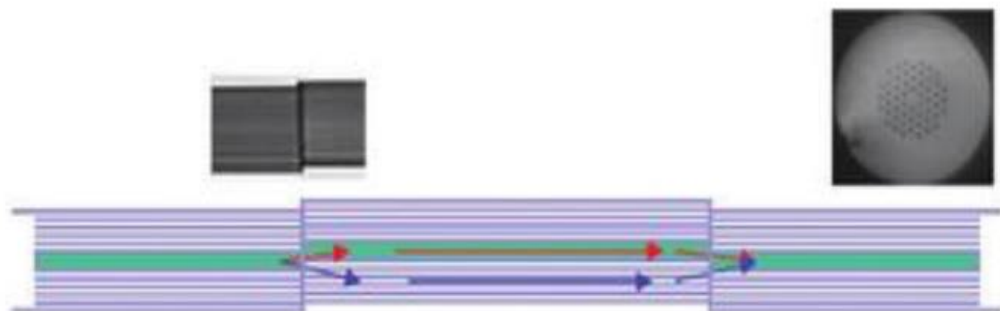


Fig. 1.6 Schematic of the interferometer based on core mismatch Technique [8].

At the spliced point of the middle PCF, the core mode is coupling with the cladding mode, and then at the other splice point, the coupled mode recombines to the core mode. This technique can be formed by fusion

splicing which is a piece of photonic crystal fiber (PCF) in between two conventional fibers with a small lateral offset. This method is fast and has an effective cost and insertion loss can be controlled [12].

#### 1.4.4 Hollow Core Photonic Crystal Fiber as Fabry-Perot Interferometer

A Fabry-Perot (FPI) consists of two optically parallel reflectors with reflectance  $R_1(W)$  and  $R_2(W)$  separated by a cavity of length  $L$ . Reflectors can be mirrors, interface of two dielectrics or fiber Bragg gratings. The cavity may be an optical fiber or any other optical medium. Two different optical fiber Fabry-Perot interferometers are shown in Figure 1.7 (a,b).

Interferometer is based on the light transmission through a Fabry-Perot, and interferometer based on the reflection. Due to multiple reflections, the reflected and transmitted spectrums are functions of cavity length, medium index of refraction and mirrors reflectivity because of energy conservation law, the transmitted spectrum is opposite to the reflected spectrum [7].

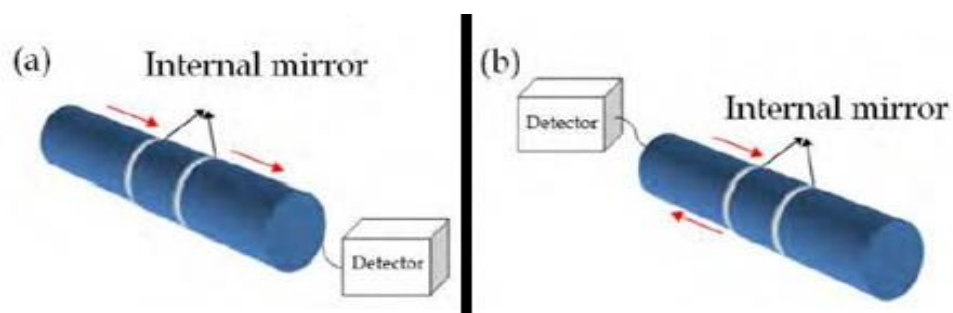


**Fig. 1.7 a) Fabry-Perot based on the light transmission, b) Fabry-Perot based on the light reflection [7].**

Optical fiber Fabry-Perots are classified as intrinsic and extrinsic types. In the intrinsic fiber FP interferometer (IFFPI), the two mirrors are

separated by a single mode fiber, while in the extrinsic fiber FP interferometer (EFFPI), the two mirrors are separated by an air gap or by some solid material other than fiber. In both IFFPI and EFFPI, light from emitter to the FP and from FP to the detector are transmitted by a single mode fiber. Figure 1.8 (a,b,c) shows schematic configurations of three IFFPI [13].

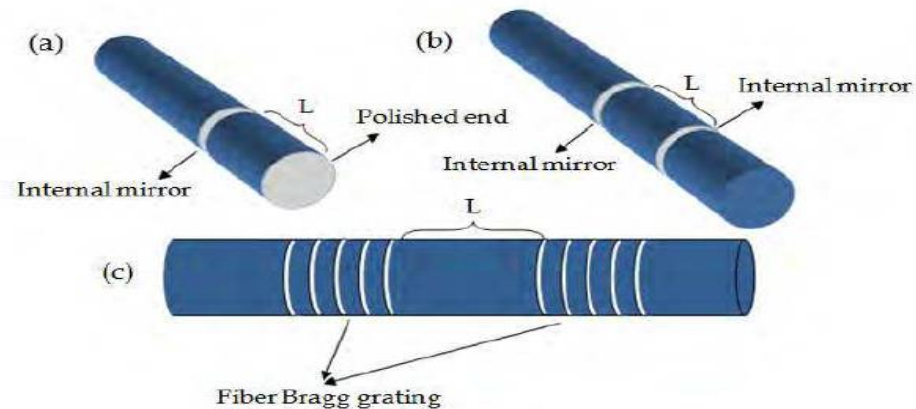


**Fig. 1.8 Schematic configurations of three IFFPI [7].**

While four different EFFPI configurations are shown in Fig.1.9 (a,b,c,d) [13].

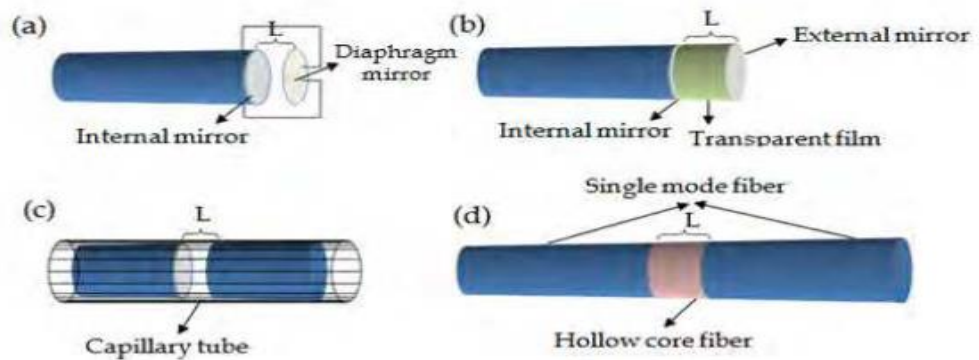


**Fig. 1.9 Schematic configurations of four EFFPI [7].**

The structure shown in Figure 1.9 (d) is called the in-line fiber etalon (ILFE) which will be explained in next subsection. The diffraction loss causes to limit the practical length of EFFPI to a few hundred of microns [13]. Fabry-Perot interferometer can be classified into two parts these are:

#### 1.4.4.1 In Line Photonic Crystal Fiber Fabry-Perot interferometers

A Fabry-Perot (FP) consists of two optically parallel reflectors separated by a cavity of length  $L$ . Reflectors used mirrors; these mirrors can be mechanically varied this type of Fabry-Perot called interferometers.

#### 1.4.4.2 In Line Hollow Core Photonic Crystal Fabry-Perot Interferometer

The in-line fiber etalon (ILFE) uses a short segment of silica hollow-core fiber spliced between two cleaved sections of single-mode fiber to form a mechanically robust in-line cavity. In making the interferometer, a portion of a protective coating is removed from one end of each of the two cleaved sections of the single-mode fiber to form a bare portion adjacent to a partially reflective end face on each fiber section. The silica hollow core fiber is fabricated to have the same outside diameter as each of the bare portions of the fiber sections. One end of the silica hollow core fiber is then fusion spliced in-line with the partially reflective end face of one of the fiber sections, before the other end of the silica core fiber is fusion spliced in line with the partially reflective end face of the other fiber section to form a cavity within the silica hollow core fiber that is bounded by the two partially reflective end faces as shown in Figure 1.10. Operation of the in-line fiber etalon is based on interference between the Fresnel reflections from the two glass/air interfaces formed by the cleaved surfaces of the single mode fibers at each end of the hollow core fiber [14].

The phase difference between the reflecting modes and transmission modes is given by:

$$\Delta\varphi = \frac{4\pi}{\lambda} nl \cos\theta \quad (1.7)$$

Where  $\Delta\varphi$ : the phase different between modes.

$\lambda$  : the wavelength.

- $n$  : the refractive index of the air.  
 $l$  : the length of HC-PCF.  
 $\theta$  : the angle for reflected modes.

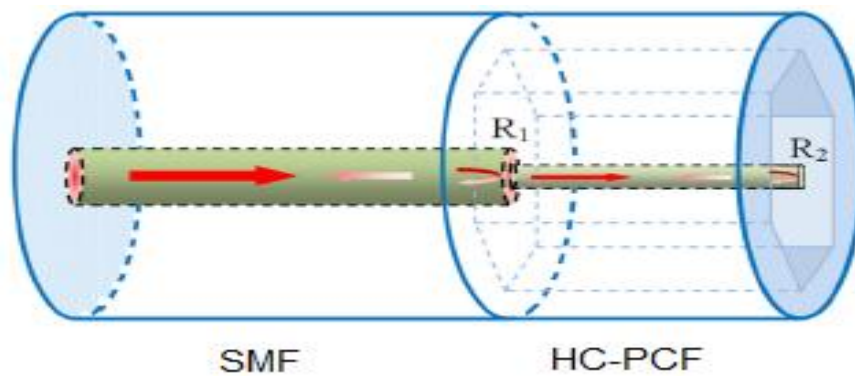


**Fig. 1.10** A schematic configuration of fiber in line HC-PCF as etalon interferometer [14].

## 1.5 Degradation of the Propagated Signals in Optical Fibers

Microstructure fibers have received significant attention due to their unique optical properties. More specifically, such fibers can provide special dispersion properties, enhanced nonlinearity and higher birefringence compared with conventional optical fibers. Furthermore, the possibility of guiding light in air makes PBFs attractive for many sensing applications [31]. The main reasons for degradation of optical signals after propagated HC-PCFs are shortly described in the following sub-sections:

### 1.5.1 Transmission Loss of Optical Fiber

The most important factor in any communication system is the losses of the optical signals that are transmitted through the optical fiber [31]. The minimum loss in fused silica, which is around 1550 nm is slightly less than 0.2 dB/km as it is shown in Figure (1.11). This limit is important, since it sets the amplifier spacing in communications systems, and thus is a major cost of a transmission system.

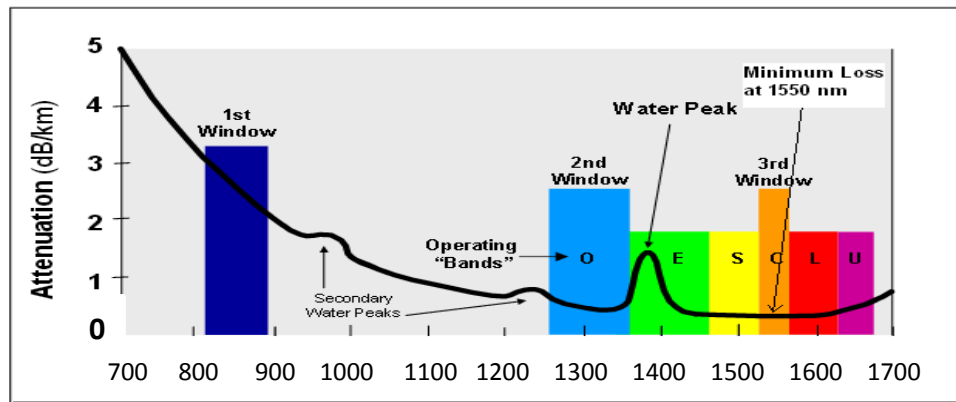


**Fig. 1.11 Attenuation spectrum of optical fiber [32].**

So that the loss or the attenuation ( $\alpha$ ) represent energy loss during the transmission of the data in the fiber as in equation (1.2).

The Photonic crystal fiber (PCFs) have many types of losses like absorption, scattering, bend loss and confinement loss, but since the pure silica that are used in PCFs has a lower Rayleigh scattering loss than standard germanium-doped fibers, Air guiding PBFs have potential to exhibit even lower losses than SMFs as most of the light is guided in an air core, therefore, losses are not limited by Rayleigh scattering and silica absorption in the same way as in conventional optical fibers [34]. A loss of 9 dB/km at 1550 nm has been reported for a 19 cell PBF [35] and a loss of 16 dB/km at 1550 nm for a 7 cell photonic bandgap fiber (PBF) [36] as shown in Figures 1.12, 1.13. Although, the loss is still much higher when compared with the loss of SMFs, the pace of the loss reduction has been very fast for PBFs. In PBFs, losses are mainly caused by leakage loss, light scattering and coupling to surface and cladding modes while the limiting loss mechanism is surface capillary waves. In addition to optical communications, the relatively low loss of PBFs could be beneficial in sensing applications requiring long optical path lengths [37].

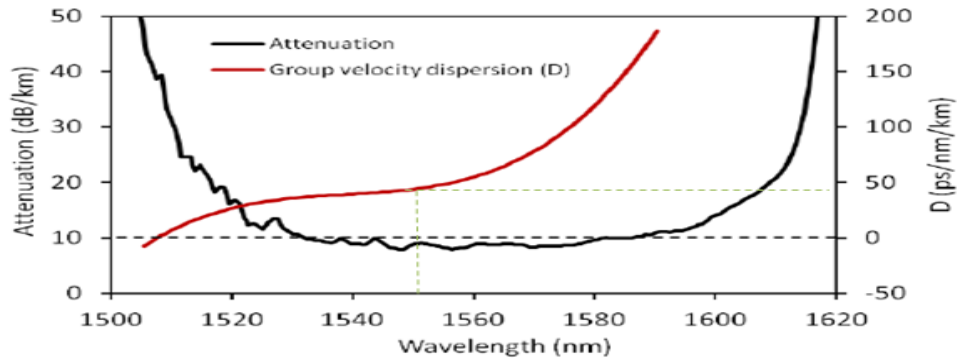


**Fig. 1.12 Attenuation and group velocity dispersion spectra of photonic crystal fiber 19 cells [35].**

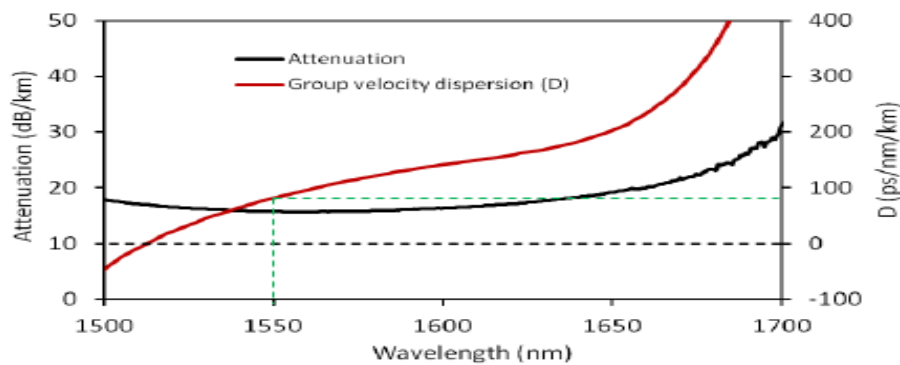


**Fig. 1.13 Attenuation and group velocity dispersion spectra of photonic crystal fiber 7 cells [36].**

### 1.5.2 Confinement loss

Confinement loss originates by the infinite number of air-holes in the cladding. So that to obtain a low confinement loss, the core of the PCFs must be small and the number of the rings of the air holes must be at least 6 rings [38]. So that to reduce the confinement loss, the number of the air holes rings must increase and be careful of the selection of dimension of air holes and spacing between adjacent air holes.

The confinement loss (CL) can be calculated from attenuation constant as it is shown in equation (1.8) [39]:

$$CL = 8.886 \alpha \quad (\text{dB/m}) \quad (1.8)$$

where  $\alpha$  : attenuation constant.

### 1.5.3 Bending loss

PCFs have a complex cladding structure, they have bending loss at short and long wavelengths unlike conventional fibers where only the long wavelength bend edge exists [40]. The macro bend loss is expressed as [41]:

$$\alpha_{\text{mac}} = -10 \log \left( 1 - \left\{ \frac{1}{2\Delta} \left[ \frac{2r}{R} + \left( \frac{2}{2nkR} \right)^{\frac{2}{3}} \right] \right\} \right) \quad (1.9)$$

And the micro bend loss is given as [41]:

$$\alpha_{\text{mic}} = 0.05 \alpha_m \frac{k^4 w^6 NA^4}{r^2} \quad (1.10)$$

where  $\Delta$ : is the difference between core and cladding refractive indices.

$r$ : core radius.

$R$ : radius of curvature of bends with proportional to  $\frac{\Lambda^3}{\lambda^2}$ .

$k$ : wave vector =  $2\pi/\lambda$ ,  $NA$ : numerical aperture.

$\alpha_m$ : attenuation constant,  $W$ : mode field diameters.

### 1.5.4 Dispersion

In telecommunication systems, information is transmitted as binary data, taking the form of light pulses in optical fibers. In the field of optical waveguides, dispersion is a generic term referring to all phenomena causing these pulses to spread while propagating and they eventually overlap and light pulses could not be distinguished by the receiver [42]. There are essentially three causes of dispersion.

#### 1.5.4.1 Chromatic Dispersion

Chromatic intramodal dispersion is an important phenomenon in the propagation of short pulses in optical fibers. Temporally short pulses have a large spectral bandwidth. The different spectral components of the pulse travel through the medium at slightly different group velocities

because of chromatic dispersion, which can result in a temporal broadening of the light pulses with no effect on their spectral compositions. This phenomenon is referred to as group velocity dispersion (GVD), [42].

#### 1.5.4.1.1 Material Dispersion

Material dispersion is an important effect because when a short pulse propagates through an optical fiber its width gets broaden. The effects arise from the variation of the refractive index of the material as a function of wavelength. This causes a wavelength dependence of the group velocity of any given mode, that is, pulse spreading occurs even when different wavelengths follow the same path [42]. This phenomena can be understood by expanding the mode-propagation constant  $\beta$  in a Taylor series about the frequency  $\omega_o$  at which the pulse spectrum is centered, [43]

$$\beta(\omega) = n_{eff}(\omega) \frac{\omega}{c} = \beta_o + (\omega - \omega_o) \beta_1 + \frac{1}{2} (\omega - \omega_o)^2 \beta_2 + \frac{1}{6} (\omega - \omega_o)^3 \beta_3 + \dots \quad (1.11)$$

where:

$$\beta_m = \left( \frac{d^m \beta}{d\omega^m} \right)_{\omega=\omega_o} \quad (m = 1, 2, \dots) \quad (1.12)$$

$$\beta_o = n_{eff}(\omega_o) \frac{\omega_o}{c} \quad (1.13)$$

$$\beta_1 = \frac{1}{c} \left( n_{eff} + \omega \frac{dn_{eff}}{d\omega} \right) = \frac{1}{v_g} = \frac{n_g}{c} \quad (1.14)$$

$$\beta_2 = \frac{1}{c} \left( 2 \frac{dn_{eff}}{d\omega} + \omega \frac{d^2 n_{eff}}{d\omega^2} \right) = \frac{d}{d\omega} \left( \frac{1}{v_g} \right) \quad (1.15)$$

where  $\beta_o$  is the mode-propagation constant of frequency  $\omega_o$ ,  $v_g$  is the group velocity, and  $n_g$  is the group index.

The group velocity is the speed of the envelope of an optical pulse propagating in a fiber. The coefficient  $\beta_2$  determines the changes in the group velocity of an optical pulse as a function of optical frequency. This

phenomenon is known as group velocity dispersion (GVD) and is responsible for pulse broadening. Thus,  $\beta_2$  is called the GVD parameter. In general, we must retain terms up to the second-order dispersion  $\beta_2$  to describe pulse propagation in dispersive media, and for ultrashort pulses or those with a wide frequency spectrum it may sometimes be necessary to also include higher order terms.

The dispersion parameter  $D$  is commonly used in place of  $\beta_2$  to describe the total dispersion of a single mode fiber. It is related to  $\beta_2$  by the relation

$$D \cong \frac{d\beta_1}{d\lambda} = -\frac{2\pi}{\lambda^2} \beta_2 \quad (1.16)$$

And is expressed in unit of ps/(km.nm).

Since GVD mainly comes from the combined effects of material and waveguide dispersion,  $D$  can be written as the sum of two terms, as:

$$D_{\text{intra}} = D_M + D_W \quad (1.17)$$

where  $D_M$  is the material dispersion and  $D_W$  is the waveguide dispersion.

$$D_M = \frac{-\lambda}{c} \frac{d^2 n_{\text{eff}}}{d\lambda^2} \quad (1.18)$$

where  $n_{\text{eff}}$  is the effective refractive index given by [44]

$$n_{\text{eff}} = \sqrt{fn_{\text{air}}^2 + (1-f)n_{\text{silica}}^2} \quad (1.19)$$

where  $f$  is the air filling fraction,  $n_{\text{air}}$  obtained from the following equation [45]:

$$n_{\text{air}} = 1 + 0.0472326(173.3 - \frac{1}{\lambda^2})^{-1} \quad (1.20)$$

But When the holes of the hollow core photonic crystal bandgap fiber filled with materials other than air specially the  $n_{\text{air}}$  in equation (1.20) replaced by  $n_m$  that obtained by the following Cauchy formula[46]

$$n_m = ac + \frac{bc}{\lambda^2} + \frac{cc}{\lambda^4} \quad (1.21)$$

where  $ac$ ,  $bc$ ,  $cc$  are the Cauchy coefficients and  $n_{\text{silica}}$  in equation (1.17) is the refractive index of silica that get from the following Sellmeier equation[47]:

$$n_{\text{silica}}(\omega) = 1 + \sum_{j=1}^m \frac{B_{sj} \omega_j^2}{\omega_{sj}^2 - \omega^2} \quad (1.22)$$

where  $\omega_{sj}$  the resonance frequency and  $B_{sj}$  is the strength of  $j^{\text{th}}$  resonance. In the case of bulk-fused silica, these parameters are obtained empirically with  $m = 3$  to the measured refractive index, and they are found to be:

$$\begin{aligned} B_{s1} = 0.6961663 & , & B_{s2} = 0.4079426 \\ B_{s3} = 0.8974794 & , & \lambda_1 = 0.0684043 \mu\text{m} \\ \lambda_2 = 0.1162414 \mu\text{m} & , & \lambda_3 = 9.896161 \mu\text{m} \end{aligned}$$

where  $\lambda_j = \frac{2\pi c}{\omega_{sj}}$  [48].

#### 1.5.4.1.2 Waveguide Dispersion

The group velocity of guided optical pulses depends on the wavelength even if material dispersion is negligible. This dependence is known as the waveguide dispersion [47]. The contribution of waveguide dispersion  $D_w$  to the dispersion parameter  $D$  is given by the equation (1.20).  $D_w$  depends on the difference in the index  $\Delta$  which was given by the following equation (1.23):

$$\Delta = (n_{\text{co}} - n_{\text{cl}}) / n_{\text{co}} \quad (1.23)$$

#### 1.5.4.2 Intermodal Dispersion

It results from the propagation delay differences between modes within a multimode fiber. As the different modes that constitute a pulse in a

multimode fiber travel along the channel at different group velocities, the pulse width ( $D$ ) at the output is dependent upon the transmission time of the lowest and fastest modes as expressed by 1.24 [42]:

$$D_{\text{total}}^2 = (D_{\text{material}} + D_{\text{waveguide}})^2 \Delta \lambda^2 + D_{\text{modal}}^2 \quad (1.24)$$

### 1.5.4.3 Polarization Mode Dispersion

A fundamental property of an optical signal is its polarization state. Polarization refers to the electric-field orientation of a light signal, which can vary significantly along the length of a fiber. As shown in Figure 1.14, signal energy at a given wavelength occupies two orthogonal polarization modes. A varying birefringence along its length will cause each polarization mode to travel at a slightly different velocity and the polarization orientation will rotate with distance. The resulting different in propagation modes will result in pulse spreading that called polarization mode dispersion (PMD) [48].

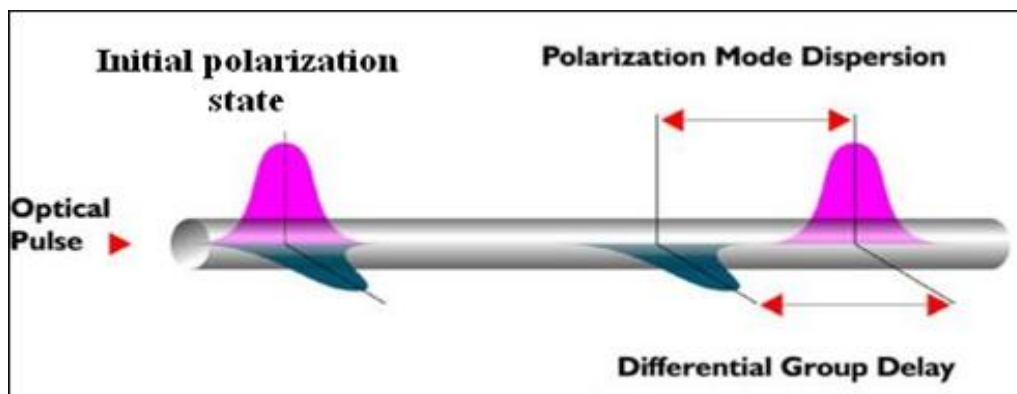


Fig. 1.14 Variation in polarization states of an optical pulse as it passes through a fiber [48].

### 1.5.5 Nonlinearities phenomena

When an intense electromagnetic field is applied to a material, the response of the material depends in a nonlinear manner upon the strength of the applied optical field. The polarization  $P$  induced by the electric dipoles

does not depend linearly on the electric field  $E$ , but satisfies the more general relation by expressing  $P$  as a power series in  $E$  as in equation 1.25 [42]:

$$P = \varepsilon_o (\chi^{(1)} \cdot E + \chi^{(2)} : EE + \chi^{(3)} \vdash EEE + \dots) \quad (1.25)$$

where  $\varepsilon_o$  is the permittivity of free space, and  $\chi^{(j)}$  ( $j = 1, 2, \dots$ ) is the  $j$ th order susceptibility and a tensor of rank  $j + 1$  of the medium. The linear susceptibility  $\chi^{(1)}$  is the dominant contribution to  $P$ . The linear refractive index,  $n$ , and the attenuation coefficient,  $\alpha$  are related to  $\chi^{(1)}$  by the relations:

$$n(\omega) = \sqrt{1 + \Re [\chi^{(1)}(\omega)]} \quad (1.26)$$

$$\alpha(\omega) = \frac{\omega}{nc} \Im [\chi^{(1)}(\omega)] \quad (1.27)$$

where  $\Re$  and  $\Im$  stand for the real and imaginary parts, respectively. The second-order susceptibility  $\chi^{(2)}$  gives rise to nonlinear effects such as sum and difference frequency generation and second-harmonic generation. The term  $\chi^{(3)}$  is responsible for nonlinear effects such as third-harmonic generation, four-wave mixing, two-photon absorption and nonlinear refractive index [32]. As the higher order terms in the power series become smaller and smaller, the only nonlinear term that is important for us is  $\chi^{(3)}$ . In the following subsections, it will explain briefly the different effects like intensity dependent refractive index, self-phase modulation (SPM) effective length and cross section area of the PCF stimulated Raman scattering (SRS) and cross phase modulation (XPM or CPM) caused by  $\chi^{(3)}$  [42,49].

### 1.5.5.1 Intensity-Dependent Refractive Index

The intensity-dependent refractive index in the presence of this type of nonlinearity can be described as

$$\bar{n}(\omega, |E|^2) = n(\omega) + n_2(\omega) |E|^2 \quad (1.28a)$$

where  $n(\omega)$  is the linear, weak-field refractive index given by equation (1.26) and  $n_2(\omega)$  is the nonlinear refraction coefficient. A bar over the refractive index  $n$  to prevent confusion with the usual, weak field refractive index. The nonlinear refraction coefficient  $n_2(\omega)$  is related to  $\chi^{(3)}$  by [42]:

$$n_2(\omega) = \frac{3}{8n(\omega)} \Re[\chi_{xxxx}^{(3)}] \quad (1.28b)$$

Where the optical field is assumed to maintain it's linearly polarization to the  $x$  axis along the fiber length so that only one component  $\chi_{xxxx}^{(3)}$  of the fourth rank tensor contributes to the refractive index.

The change in refractive index described by equation (1.28 a,b) is also known as the optical Kerr effect (OKE), by analogy with the electro-optic Kerr (or d.c. Kerr) effect, in which the changes in the refractive index of a material are proportional to the square of the strength of an applied static field [42].

### 1.5.5.2 Self-Phase Modulation

Self-phase modulation (SPM) is a nonlinear effect of light-matter interaction. An ultrashort pulse of light, when traveling in medium, will induce a varying refractive index of the medium due to optical Kerr effect. This variation in refractive index will produce a phase shift in the pulse, leading to a change of the pulse's spectrum [50].

The refractive index  $n$  of many optical materials has a weak dependence on optical intensity  $I_{\text{eff}}$  (equal to the optical power per effective area in the fiber) given by [42]:

$$n = n_0 + n_2 I_{\text{eff}} = n_0 + \frac{n_2 P}{A_{\text{eff}}} \quad (1.29)$$

where  $n_0$  is the ordinary refractive index of the material and  $n_2$  is the nonlinear refractive index. In silica, the factor ( $n_2$ ) varies from 2.2 to  $3.4 \times 10^{-20}$

$m^2/W$  and  $24 \times 10^{-21} m^2/W$  for air [51]. SPM is described as the intensity of an optical field modulates the phase of optical field, where an optical field modifies its own phase [50].

The nonlinear phase shift of the pulse  $\varphi_{NL}$  is given by the following equation:

$$\varphi_{NL} = n_2 \frac{P}{A_{eff}} \frac{2\pi}{\lambda} L_{eff} \quad (1.30)$$

where  $L_{eff}$  is the fiber effective length.

The total phase shift  $\varphi$  experienced by the optical field is therefore [48]:

$$\varphi = \left( n_0 + n_2 I_{eff} \right) \frac{2\pi L_{eff}}{\lambda} = \varphi_L + \varphi_{NL} \quad (1.31)$$

This phase shift varies with time for pulses and each optical pulse become chirped, which means a pulse propagates along the fiber, its spectrum changes because of SPM as shown in Figure 1.15 [54].

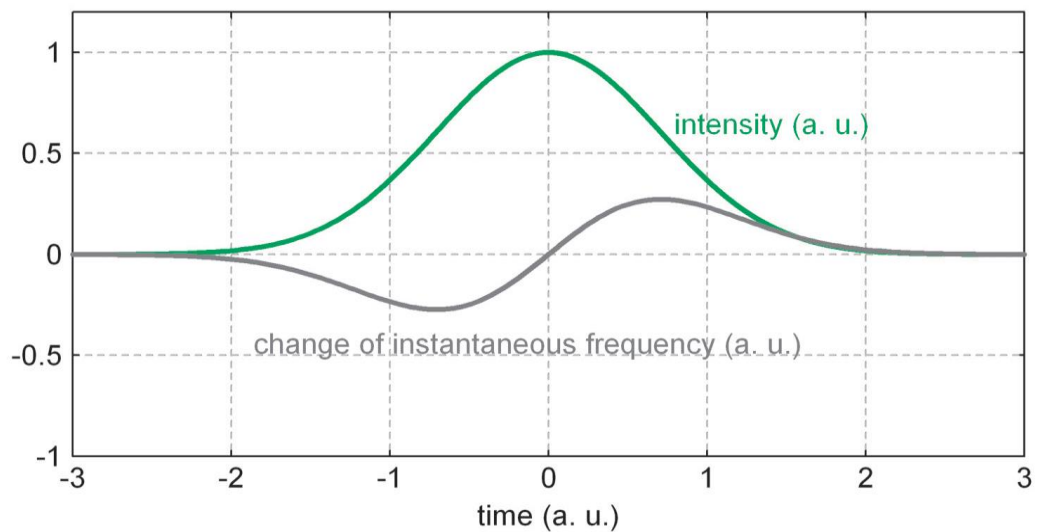


**Fig. 1.15 The effect of SPM on un-chirped pulse [52].**

When SPM effects are strong, a pulse will be spectrally broadened. Typically, if SPM is the dominating effect, the spectrum develops strong wiggles as shown in the Figure 1.16. The spectral broadening effect may be used for nonlinear pulse compression [52].

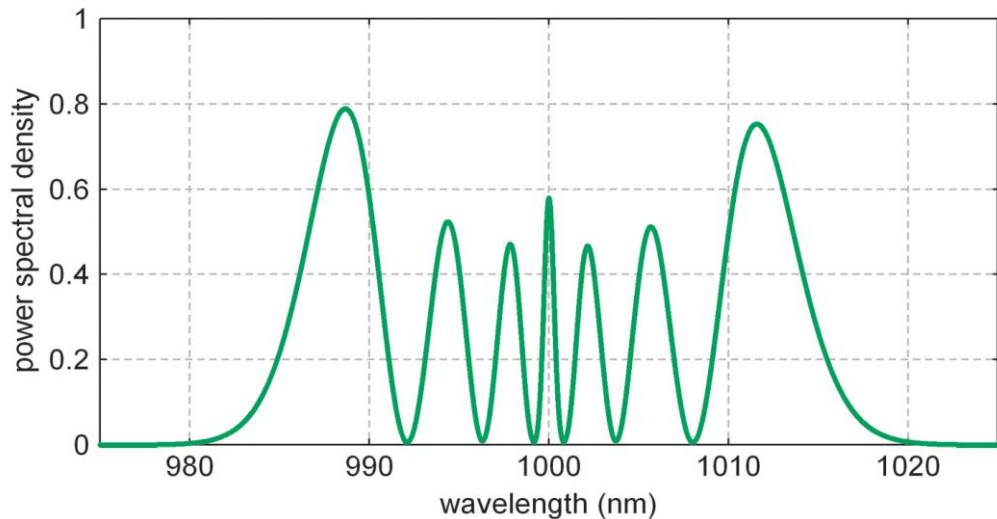


**Fig. 1.16** The effect of SPM on the spectrum [52].

### 1.5.5.3 Cross phase modulation

Cross-phase modulation (XPM) refers to the nonlinear phase shift of an optical field induced by the intensity of other co-propagating optical fields. XPM is always accompanied by SPM and occurs because the effective refractive index seen by an optical beam in a nonlinear medium depends not only on the intensity of that beam but also on the intensity of other co-propagating beams [42].

### 1.5.5.4 Stimulated Raman Scattering

Stimulated Raman scattering (SRS) is an important nonlinear phenomenon that can lead to the generation of new spectral lines. SRS is governed by the third-order susceptibility  $\chi^{(3)}$ . It results from stimulated inelastic scattering process in which the optical field transfers part of its energy to the medium generating a photon [53]. The Spontaneous Raman effect can be observed when a beam of light illuminates any molecular medium and the scattered light is observed spectroscopically. The energy levels of this process shown in Figure 1.17.

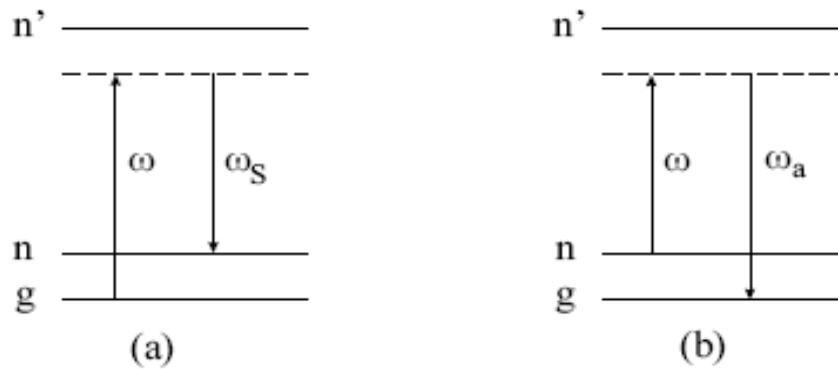


**Fig. 1.17** Energy level diagrams describing, a) Raman Stokes scattering and b) Raman anti-Stokes scattering [42].

The Raman Effect scatters only a small fraction of the incident optical field into other fields. Those new frequency components shifted to lower frequencies are called the Stokes lines and those shifted to higher frequencies are called the anti-Stokes lines. The amount of frequency shift is determined by the vibrational modes of molecules [42].

#### 1.5.5.5 Effective length

The nonlinear interaction depends on the transmission length and the cross-sectional area of the fiber. The longer the link length is the more the interaction and the worse the effect of the nonlinearity. However, as the signal propagates along the link, its power decreases because of fiber attenuation. Thus most of the nonlinear effects occur early in the fiber span and diminish as the signal propagates. A simple model assumes that the power is constant over a certain effective length  $L_{\text{eff}}$  has proved to be quite sufficient in understanding the effect of nonlinearities. Suppose  $P_0$  denotes the power transmitted into the fiber and  $p(z) = p_0 \exp(-\alpha z)$  denotes the link, with  $\alpha$  being the fiber attenuation [47,54].

The effective length described in Figure 1.18 is defined as the length  $L_{\text{eff}}$  such that [55]:

$$P_0 L_{\text{eff}} = \int_{z=0}^L P(z) dz \quad (1.32)$$

where  $L_{eff}$  is:

$$L_{eff} = \frac{1 - \exp(-\alpha L)}{\alpha} \quad (1.33)$$

where  $L$  denote the actual link length of the fiber.

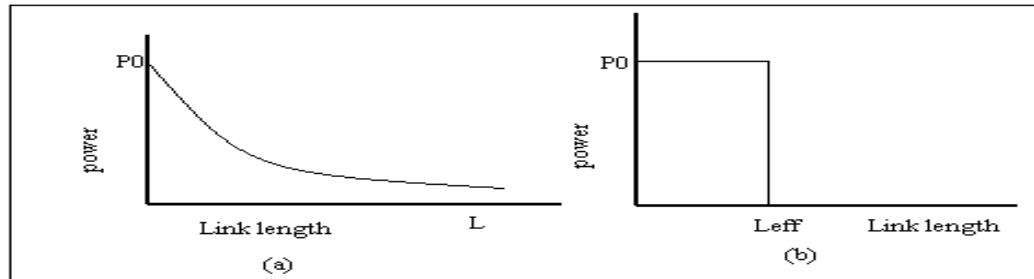


**Fig. 1.18 Effective transmission length calculation, a) A typical distribution of the power along the length  $L$  of a link. The peak power is  $p_0$ , b) A hypothetical uniform distribution of the power along a link up to the effective length  $L_{eff}$ . This length  $L_{eff}$  is chosen such that the area under the curves (a) and (b) is equal [55].**

## 1.6 All-Fiber Pulse Compression

Optical fibers can be used in various ways for pulse compression. In general, pulse compression in optical media is classified into two types: linear pulse compression and nonlinear pulse compression [56].

### 1.6.1 Linear Pulse Compression

Linear compression techniques are based purely on the chromatic dispersion of fibers. They are applied to pulses that are initially chirped, not bandwidth limited. A reduction of pulse duration results from the removal of the chirp, whereas the pulse bandwidth stays more or less unchanged. Normal chromatic dispersion can compensate a down-chirp, whereas anomalous dispersion may remove an up-chirp, but note that higher-order dispersion may also have to be considered [55]. The linear pulse compression can be implemented with fiber-based by using different techniques these are

### 1.6.1.1 Linear pulse compression based Fibers Dispersion

For a wide range of wavelengths, fibers with either normal or anomalous chromatic dispersion are available, for anomalous dispersion at relatively short wavelengths, for example, in the visible spectral region, photonic crystal designs are required. One may, however, require relatively long lengths of fibers. Strong nonlinear effects, pulse distortion or prohibition of compression may then be avoided only for rather low peak power levels. Large mode area fibers can somewhat mitigate this problem, but their chromatic dispersion can hardly be tailored via the fiber design [58].

### 1.6.1.2 Linear Pulse Compression based Fiber Bragg Grating

Much stronger group delay dispersion within a short length can be obtained with fiber Bragg gratings. Accordingly, shorter fibers can be used, and higher peak powers are possible, although nonlinear self-focusing may set a limit to that. Additionally, the grating design gives more freedom for tailoring the higher-order dispersion as shown in Figure 1.19 [58,59].

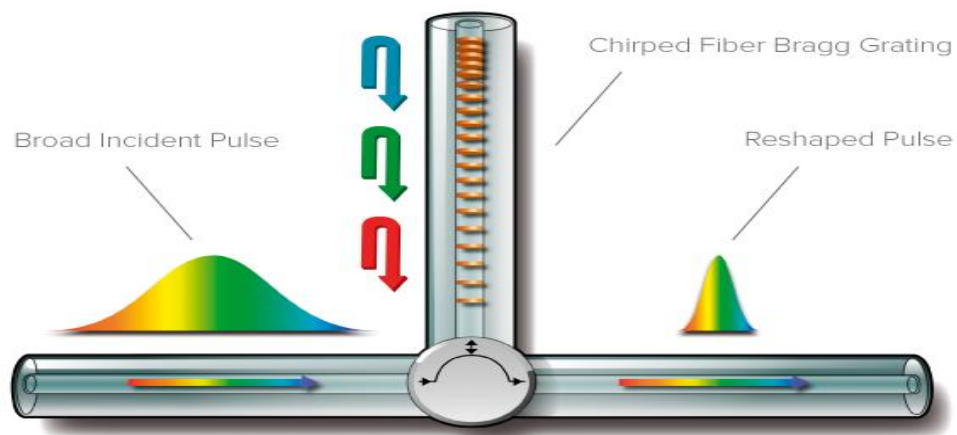


Fig. 1.19 Re-shaped the pulse by using chirped Fiber Bragg Grating [59].

## 1.6.2 Fiber Nonlinear Pulse Compression

There are nonlinear compression techniques, where typically the Kerr nonlinearity is used for increasing the spectral width, and a suitable amount of chromatic dispersion (inside or outside the nonlinear device) removes the pulse chirp, thus minimizing the pulse duration [60]. There are variants of this technique can be implemented with fibers these are:

### 1.6.2.1 Nonlinear Pulse Compression using Dispersive Compressor

Pulses that are originally un-chirped can be spectrally broadened in a normally dispersive optical fiber and then dispersively compressed in a fiber with anomalous dispersion or in some other optical element, such as a pair of diffraction gratings as shown in Figure 1.20.

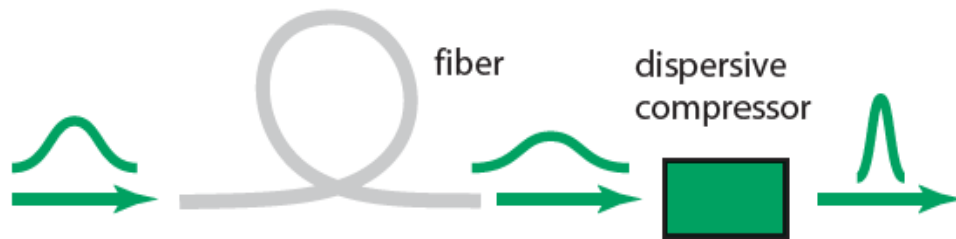


Fig. 1.20 Compression using dispersive compressor [61].

The useful fiber length is limited by the temporal pulse broadening, which leads to a reduction in peak power. Substantial pulse compression requires a sufficiently high peak power of the input pulses.

### 1.6.2.2 Nonlinear Pulse Compression using Hollow Core Photonic Crystal Fiber

A variant of that technique for high-intensity femtosecond pulses is based on spectral broadening in a gas filled hollow fiber. Here, most of the optical power propagates in the gas, where self-phase modulation occurs.

Despite the low nonlinearity of gases, a moderate length of hollow fiber is sufficient due to the very high peak intensity [61].

### 1.6.2.3 Nonlinear Pulse Compression using Higher-Order Soliton

Pulse compression is also possible with a single fiber with anomalous dispersion. The most common variant is higher-order soliton compression, where a pulse with energy far above the fundamental soliton energy is injected into the fiber [62]. After a certain propagation distance, a strongly compressed pulse can be obtained, but the choice of propagation distance can be critical Figure 1.21.



**Fig. 1.21** A schematic configuration for high order soliton compression [62].

For deviations from the optimal fiber length or pulse energy, strong pulse distortions can result. The pulse energy can be roughly one to two orders of magnitude above that of a fundamental soliton. Higher compression ratios imply a more critical adjustment of parameters [63].

### 1.6.2.4 Nonlinear Pulse Compression using Adiabatic Soliton

Another variant requiring only a fiber is adiabatic soliton compression. Here, a soliton pulse is compressed during propagation in a fiber where the anomalous dispersion becomes weaker and weaker along the propagation direction [61]. Alternatively, the pulse energy can be increased by amplification in a doped fiber with constant dispersion properties. If the dispersion (or pulse energy) varies sufficiently slowly, the soliton will adiabatically adapt to the changing conditions by continuously reducing its

duration. The pulse quality can be very high with adiabatic soliton compression. The pulse energy, however, is fairly limited due to the small soliton pulse energies of typical fibers. Also, a very long length of fiber may be required if the input pulses are not rather short already. Therefore, initial pulse durations below 1ps are desirable [63].

### 1.6.2.5 Nonlinear Pulse Compression using Self-Similar Technique

In a fiber amplifier with normal dispersion, one may exploit self-similar parabolic pulse evolution. Here, the nonlinearity, dispersion, and laser gain act together such that the pulse duration and spectral width increase together with the pulse energy, but the parabolic pulse shape is preserved. The input pulses do not need to be parabolic pulses, as the parabolic shape is automatically more and more approximated during propagation Figure 1.22 [64].

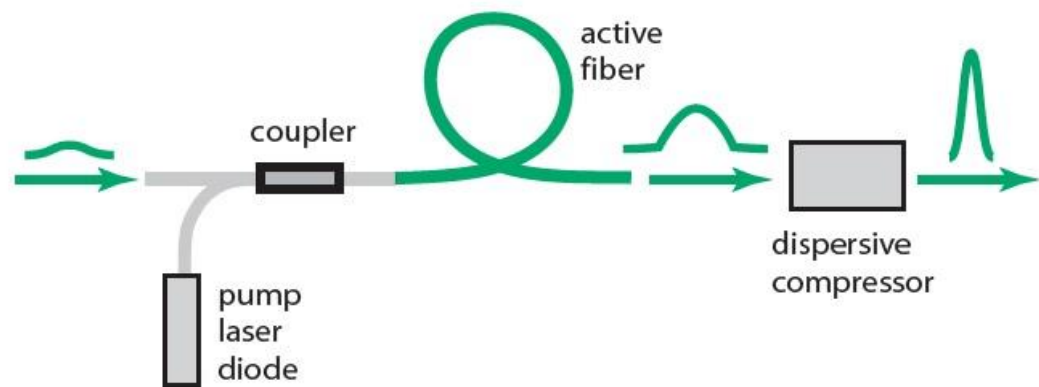


**Fig. 1.22 A schematic configuration for pulse compression by using self-similar technique [64].**

The parameters of the input pulses are fairly uncritical, as the pulses automatically evolve towards the asymptotic solution. High pulse energies (far above typical soliton pulse energies) are possible. The resulting chirp is linear, which makes it relatively easy to obtain strong temporal compression in a subsequent dispersive optical element, such as a pair of diffraction gratings.

### 1.7 Compression factor ( $F_c$ )

The compression factor ( $F_c$ ) is a good indication for obtaining a narrow laser pulse with different technique of compression. This factor explained by the relation between input and output pulses for the system of compression as shown in equation 1.37 [65]:

$$F_c = \frac{\text{FWHM}_{i/p}}{\text{FWHM}_{o/p}} \quad (1.34)$$

where FWHM (i/p) is pulse duration of input pulse. And FWHM (o/p) is pulse duration of output pulse of the system.

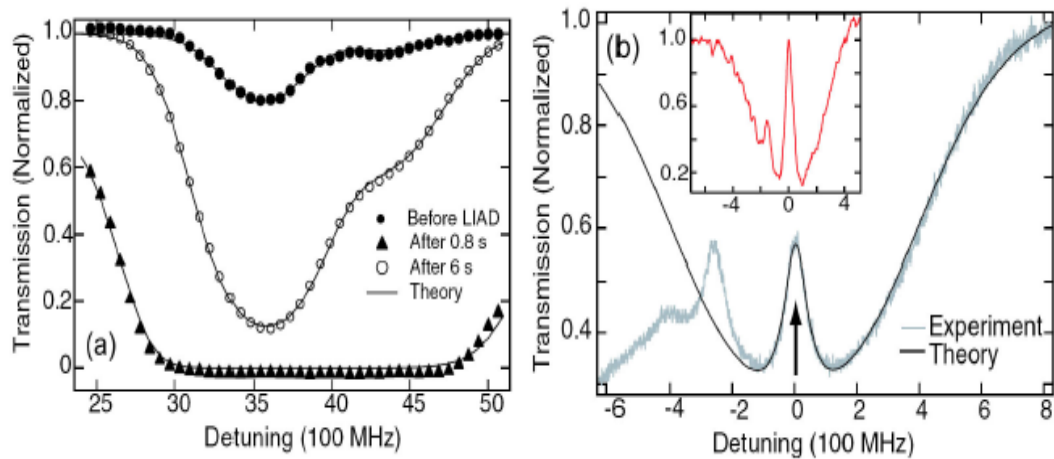
### 1.8 Literature survey

Silica photonic crystal fiber (PCF) is a type of fiber that has an array of microscopic air holes running along its length. Splicing PCF to standard single-mode fiber (SMF) is a challenging task, and it is also important because of the potential broad applications. Proper splicing of SMF to PCF is imperative in order to avoid collapsing of the PCF on the air holes; however, the two types of fiber require different powers for melting. A fusion splicing system is developed to demonstrate its effectiveness at splicing between the PCF and SMF with low splice loss. An important application of photonic crystal fibers is pulse compression. Many research groups around the world have investigated different schemes to get the minimum loss between PCFs and SMF. Many researches were published about the photonic crystal fiber as pulse compression. They will summarize as most important published work related to the SMF and PCF splice loss and photonic crystal fiber as a pulse compression.

**(1) (2008) Nonlinear optics in hollow-core photonic bandgap fibers**

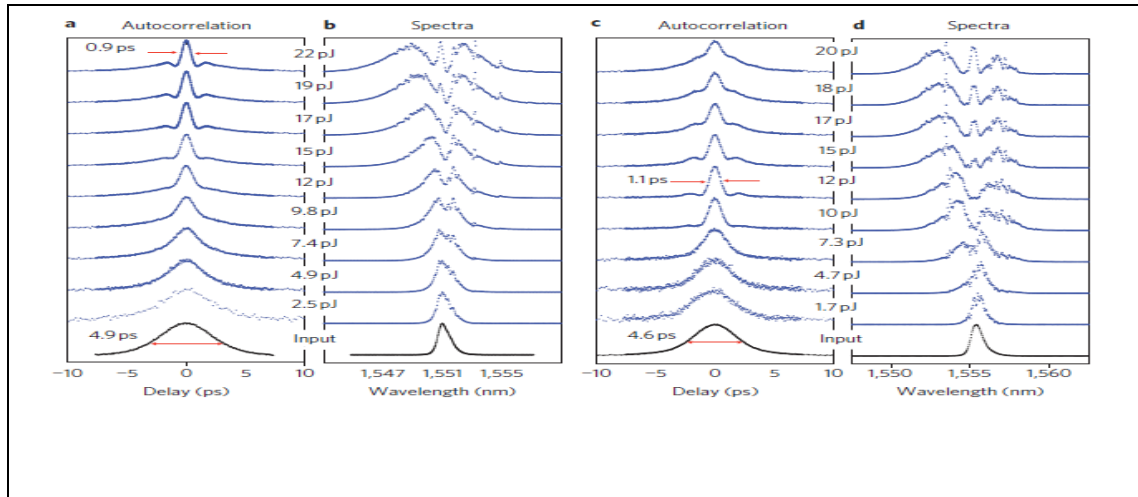
**(Amar R. Bhagwat and Alexander L. Gaeta)**

- ✓ Technique used (HC-PCF filled with Xe).
- ✓ Wavelength (514) nm.
- ✓ Input pulse width 15.4 ps.
- ✓ Output pulse width 213 fs.
- ✓ Compression factor 72.3.
- ✓ Theoretical work.



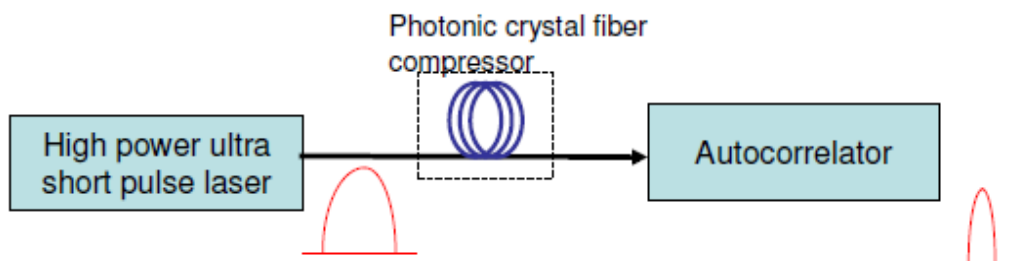
**(2) (2010) Temporal solitons and pulse compression in photonic crystal waveguides (P. Colman, C. Husko, S. Combrie, I. Sagnes, C. W. Wong and A. De Rossi).**

- ✓ Technique used (Decreasing Energy for pulse that inject in solid core PCF).
- ✓ Wavelength (1.555) nm.
- ✓ Input pulse width 3 ps.
- ✓ Output pulse width 580 fs.
- ✓ Compression factor 5.17.
- ✓ Theoretical work.



**(3) (2011) One stage pulse compression at 1554nm through highly anomalous dispersive photonic crystal fiber (Maggie Yihong Chen, Harish Subbaraman and Ray T. Chen).**

- ✓ Technique used (Compression by using highly anomalous dispersive PCF).
- ✓ Wavelength (1554 nm) nm.
- ✓ Input pulse width 2898 fs.
- ✓ Output pulse width 630 fs.
- ✓ Compression factor 4.6.
- ✓ Experimental work



**(4) (2012) Two Models of Optical Pulse Self-Compressor Combined the Nonlinear Coupler with Backward Raman Fiber Amplifier, (Quang Quy Ho, Van Bien Chu).**

- ✓ Technique used: (nonlinear optical coupler (NOC) and the amplifying capacity of the backward Raman fiber amplifier (PBRFA)).
- ✓ Wavelength used: (1500) nm.
- ✓ Input pulse width: 1 ns.
- ✓ Output pulse width: 0.5 ns.

- ✓ Compression factor: 2.
- ✓ Experimental work.

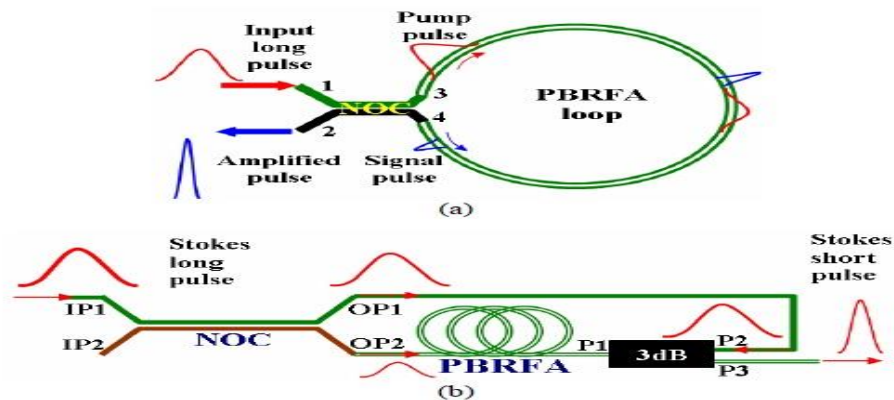


Figure 4. Set-up of OPSC. (a) OPSC consist of the NOC and PBRFA loop; (b) OPSC consist of the NOC and PBRFA and 3 dB.

(5) (2012) Femtosecond pulse compression in a hollow-core photonic bandgap fiber by tuning its cross section, (N. González-Baquedano, N. Arzate, I. Torres-Gómez, A. Ferrando, D.E. Ceballos-Herrera, C. Miliañ).

- ✓ Technique used: (Tuning the cross section of HCPCF).
- ✓ Wavelength used (800) nm.
- ✓ Input pulse width 5 ps.
- ✓ Output pulse width 1.56 ps.
- ✓ Compression factor theoretically 5.7, experimentally 3.2.
- ✓ Experimental work.

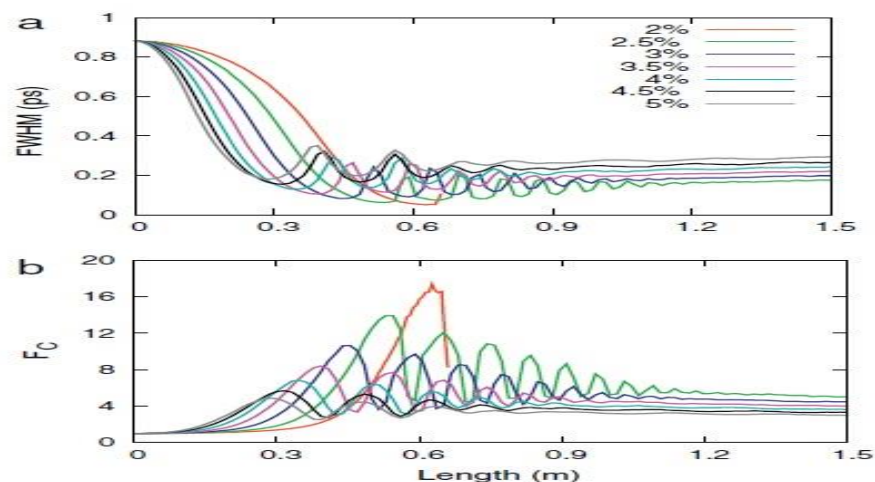
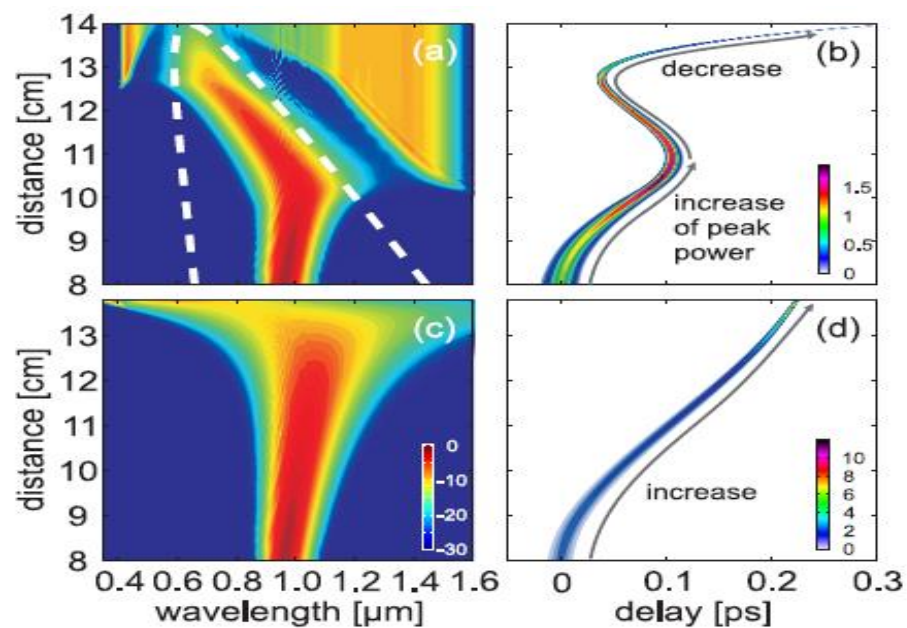


Fig. 5. Full width at half maximum (a), FWHM, and compression factor (b) as a function of the propagation length of a pulse and for different tapering factors.

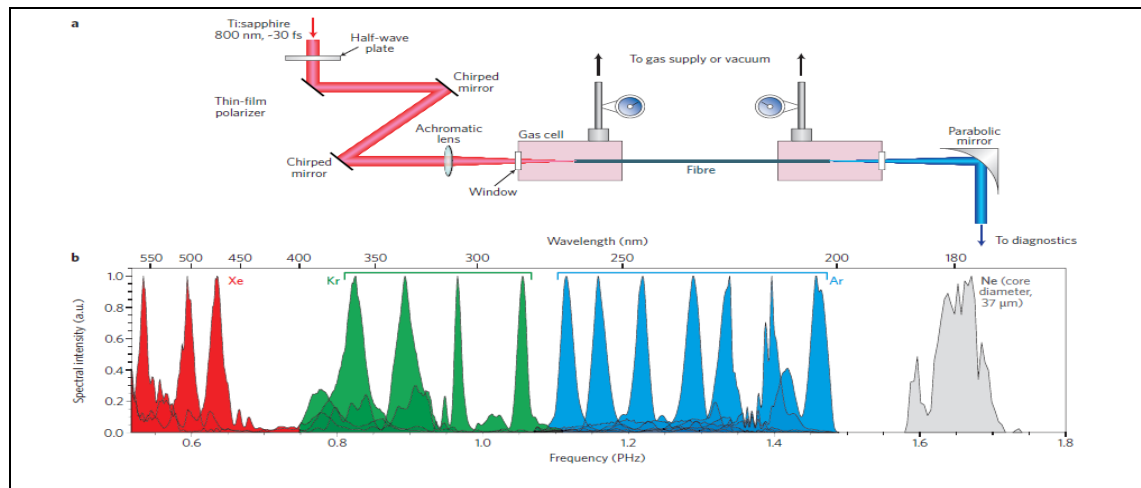
**(6) (2012) Soliton blue-shift in tapered photonic crystal fiber (S. P. Stark, A. Podlipensky and P. St.J. Russell).**

- ✓ Technique used / Tapered solid core PCF.
- ✓ Wavelength (735) nm.
- ✓ Input pulse width 130 fs.
- ✓ Output pulse width 17 fs.
- ✓ Compression factor 7.65.
- ✓ Theoretical work.



**(7) (2014) Hollow-core photonic crystal fibers for gas-based nonlinear optics (P. St. J. Russell, P. Holzer, W. Chang, A. Abdolvand and J. C. Travers).**

- ✓ Technique used: (Applied pressure on the cross section of HC-PCF).
- ✓ Wavelength (800) nm.
- ✓ Input pulse width 30 fs.
- ✓ Output pulse width 3 fs.
- ✓ Compression factor 10.
- ✓ Experimental work.



**(8) (2015) Linear compression of chirped pulses in optical fiber with large step-index mode area, (S. V. Smirnov, S. M. Kobtsev, S. V. Kukarin).**

- ✓ Technique used: (Step-Index Large Mode Area Fiber (LMA)).
- ✓ Wavelength used (1560) nm.
- ✓ Input pulse width 5 ps.
- ✓ Output pulse width 3.2 ps.
- ✓ Compression factor 1.56.
- ✓ Experimental work.

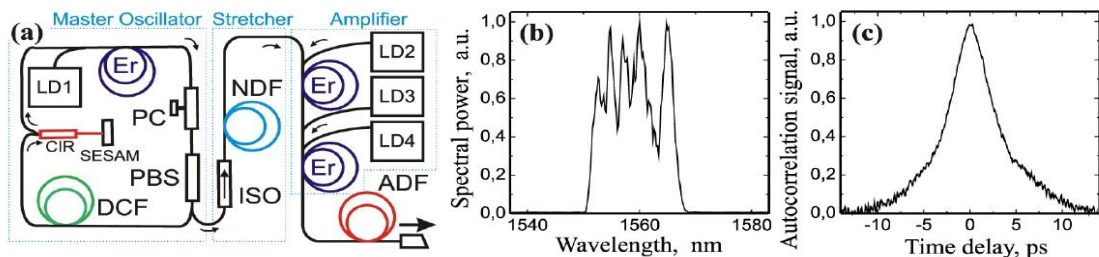
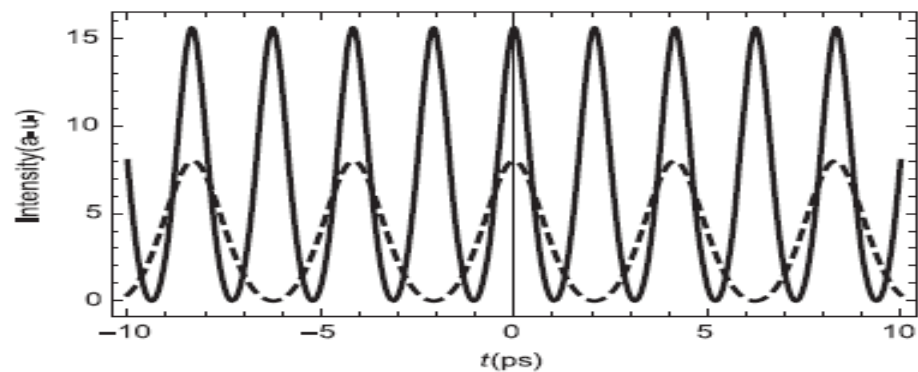


Fig. 1. (a) All-fibre laser system schematic diagram. LD – laser diode pump, Er – Er-doped active fibre, PC – polarisation controller, PBS – polarisation beam splitter, CIR – 3-port circulator, SESAM – semiconductor saturable absorber, ISO – optical isolator, DCF – passive double-clad fibre, NDF – normal-dispersion fibre, ADF – anomalous-dispersion fibre (LIEKKI Passive-25/250); (b), (c) Spectrum and auto-correlation function of pulses at the output of the master oscillator.

**(9) (2016) Generation of a train of ultrashort pulses using periodic waves in tapered photonic crystal fibers, (S. O. Atuba, K. Nakkeeran, K. W. Chow, P. Ramesh Babu, A. Manimegalai & K. Senthilnathan).**

- ✓ Technique used: (tapering solid core PCF).
- ✓ Wavelength (1550) nm.
- ✓ Input pulse width 0.8 ps.
- ✓ Output pulse width 0.15 ps.

- ✓ Compression factor 5.3.
- ✓ Theoretical work.



**(10) (2016) Tapering photonic crystal fibers for generating self-similar ultrashort pulses at 1550 nm, (Annamalai Manimegalai, Krishnamoorthy Senthilnathan, Kaliyaperumal Nakkeeran, and Padmanabhan Ramesh Babu).**

- ✓ Technique used / Tapering PCF through self-similar.
- ✓ Wavelength (1550) nm.
- ✓ Input pulse width 800 fs.
- ✓ Output pulse width 201 fs.
- ✓ Compression factor 3.998.
- ✓ Theoretical work.

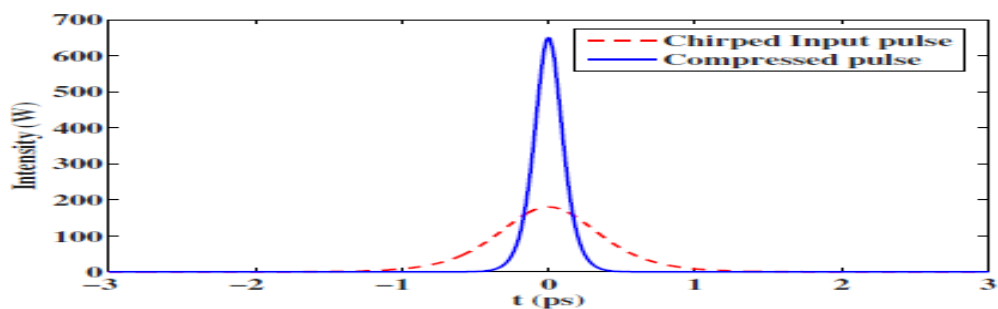


**Table (1.1) compare experimental results of literature survey and this thesis**

<b>No.</b>	<b>Compression Factor</b>	<b>Year of the work</b>	<b>Notes</b>
<b>1</b>	<b>72.3</b>	<b>2008</b>	Theoretical work
<b>2</b>	<b>5.17</b>	<b>2010</b>	Theoretical work
<b>3</b>	<b>4.6</b>	<b>2011</b>	<b>Experimental work</b>
<b>4</b>	<b>2</b>	<b>2012</b>	<b>Experimental work</b>
<b>5</b>	<b>3.2</b>	<b>2012</b>	<b>Experimental work</b>
<b>6</b>	<b>7.65</b>	<b>2012</b>	Theoretical work
<b>7</b>	<b>10</b>	<b>2014</b>	<b>Experimental work</b>
<b>8</b>	<b>1.56</b>	<b>2015</b>	<b>Experimental work</b>
<b>9</b>	<b>5.3</b>	<b>2016</b>	Theoretical work
<b>10</b>	<b>3.998</b>	<b>2016</b>	Theoretical work
<b>This Thesis</b>	<b>4.9</b>	<b>2019</b>	<b>Experimental work</b>

### **1.9 Thesis layout**

This thesis contains three chapters and is organized as follows:

**Chapter one** gives a general introduction about, all-fiber pulse compression and the optical interferometers that are based on PCF. Then a brief literature survey related to optical pulse compression introduced. Finally, the aim of the work is presented in this chapter.

**Chapter two** presents the experimental setups and explained the entire component and the equipment are used in experimental work. Then explained how to design and construct inline interferometers, and using them for all- fiber pulse compression.

**Chapter three** illustrates and discuss the experimental results. Next, summarizes the main conclusions drawn from this study followed by suggests some points which need further investigation as a future work.

# **Chapter Two**

## **Experimental Setups**

## Chapter Two

### Experimental Setups

#### 2.1 Introduction

In this chapter, the pulse compression setups using hollow core photonic crystal fiber (HC-PCF) and solid core photonic crystal fiber (SC-PCF) are demonstrated. Two techniques of the pulse compression are introduced. The first is in line PCF interferometer without infiltration, and study effect of length of PCF on pulse compression and the second one was achieved by infiltrated of the PCF with different chemical compounds. Figure 2.1 presents a flow chart of the work's procedure for pulse compression that implemented with and without infiltration using HC-PCF and SC-PCF and controlling the length of fiber.

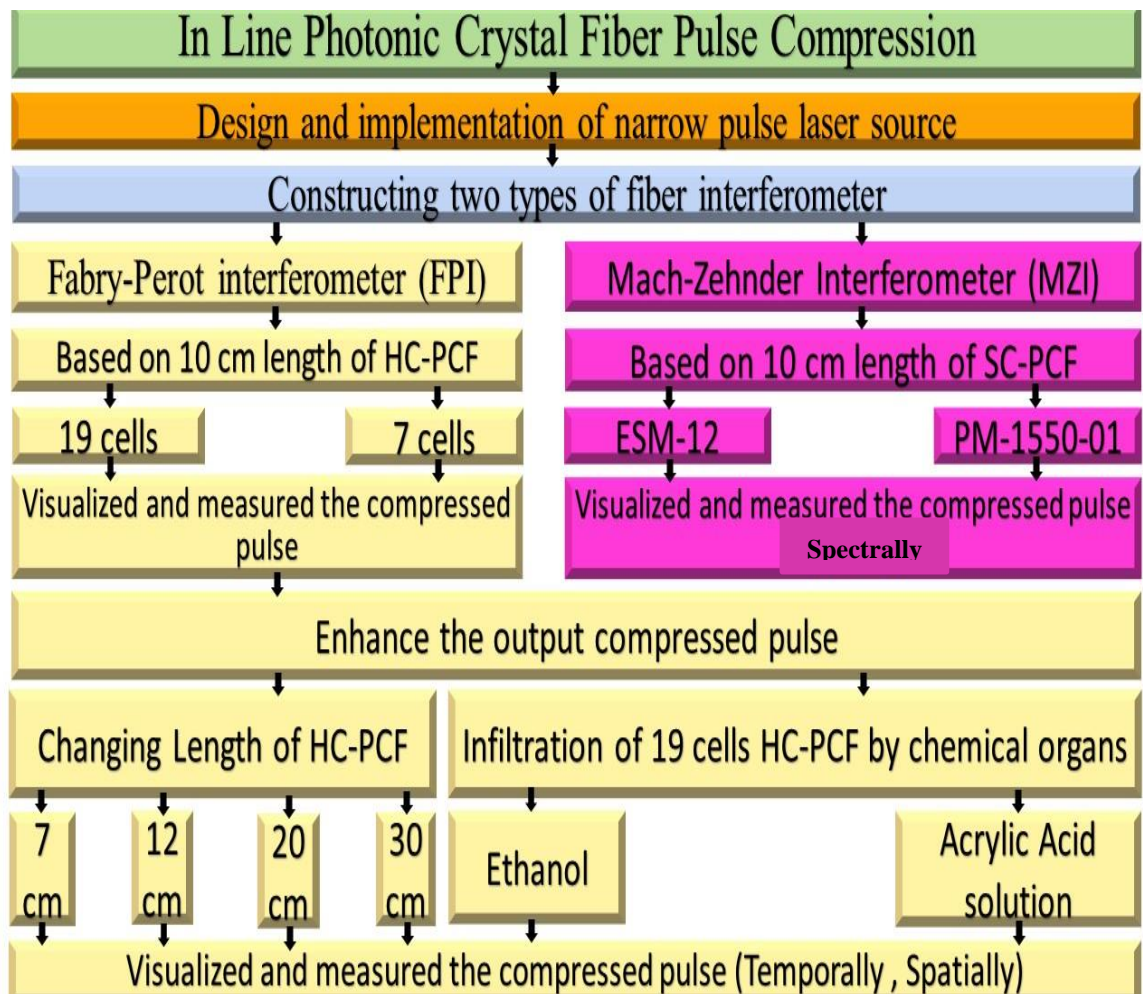
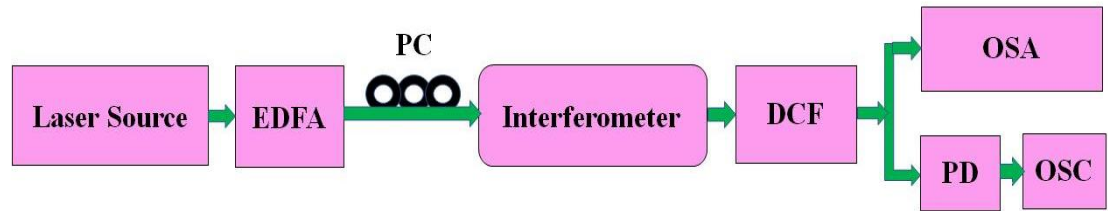


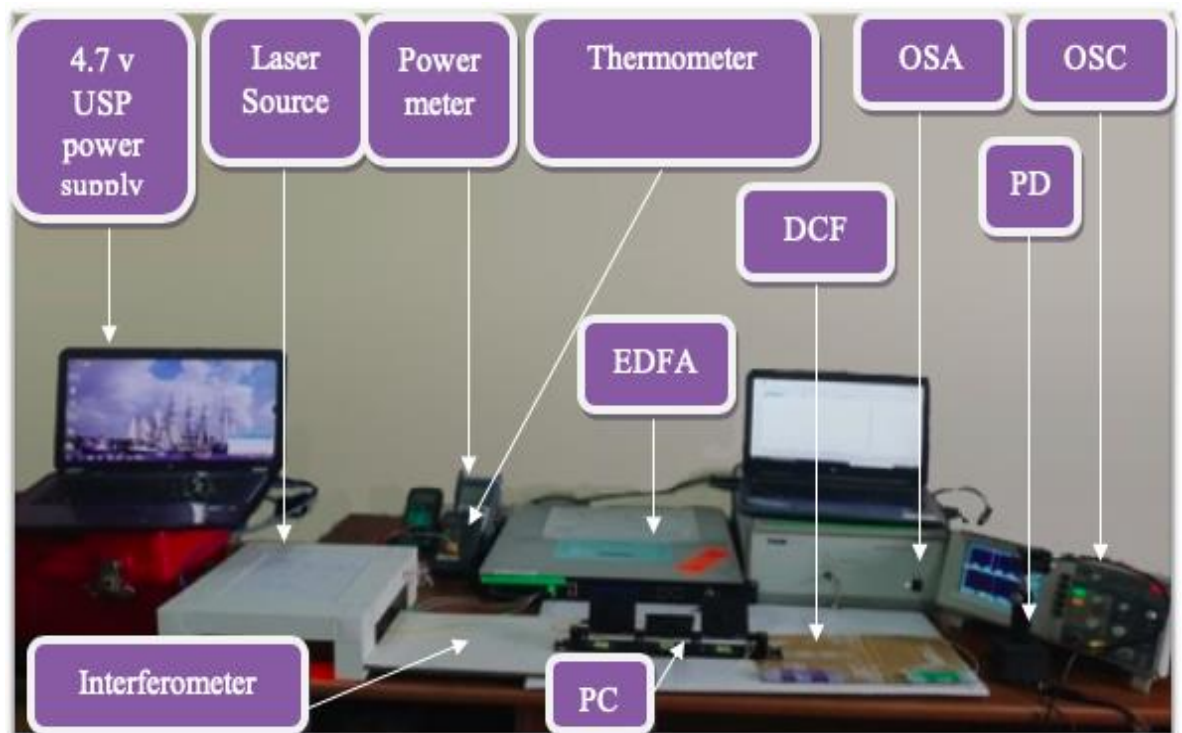
Fig. 2.1 Flow chart of the work's steps.

## 2.2 key Components and Equipment

The main schematic and experimental setup of the pulse compression is shown in Figure 2.2. This figure shows the main components that used in setups, it consists of pulsed laser source, Erbium-doped fiber amplifier, interferometer, polarization controller, and visualizers.



(a)



(b)

**Fig. 2.2 Pulse compression, a) Schematic diagram, b) experimental setup.**

## **2.2.1 Laser Source**

In the experiments, continuous laser diode source were used. This source from Wuhan Shengshi Optical Technology with electronic chopping circuit with controllable output power to study the increasing in the power density on the nonlinearity because the increasing in the power cause increasing the power density with remain the area of the cross section for fibers constant. This source described as follow:

### **2.2.1.1 CW Laser Source**

Laser diode MLD-C55D2-1A05P2 is CW source having parameters listing in appendix B9. In this work the CW source has to chop by an electronic circuit to get optical pulse signal with suitable duration for interaction. This source to operate and supplied the suitable pulse can be connecting to two circuits these circuits are:

A- Laser diode controller (driver circuit).

B- Electronic chopping circuits.

#### **2.2.1.1. A Laser diode controller (driver circuit)**

The control circuit design must consider several points to provide power to the laser diode in the specified laser mode and it has threshold current to start lasing. Thus current should be above this threshold to ensure lasing. Also protecting the laser diode from over current is of a prime concerns to the designer. Thus the driver circuit used with this laser diode is programmable micro-controller circuit Arduino-mega (see appendix C1) which is programmed to give pulse signal with 4.7 volt and 15 kHz frequency, this circuit consists of programmable micro-controller with standard (C) programming language as an interface programming language and reaches maximum frequency of 30 KHz.

### 2.2.1.1. B Electronic Chopping Circuit

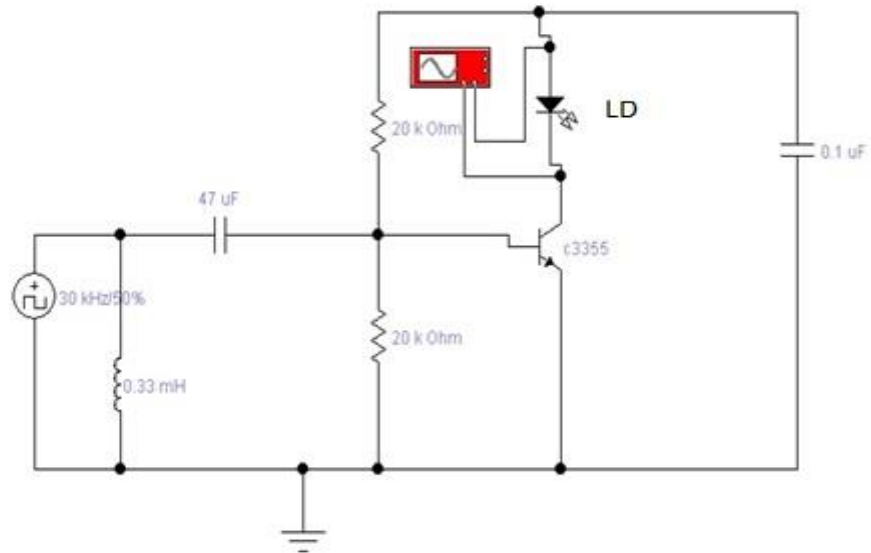
A cheap, simply and easy to implement low signal amplifier electronic circuit can convert the incoming pulse duration from 66  $\mu\text{s}$  to 10 ns, narrow pulse generation could be achieved by controlling the voltage level above and below the lasing threshold of it, the biasing resistor are used for that controlling to electronically chop a CW laser diode. After chopping this signal, the laser began having properties illustrate in table 2.1 bellow.

**Table 2.1 Parameters of chopped laser source.**

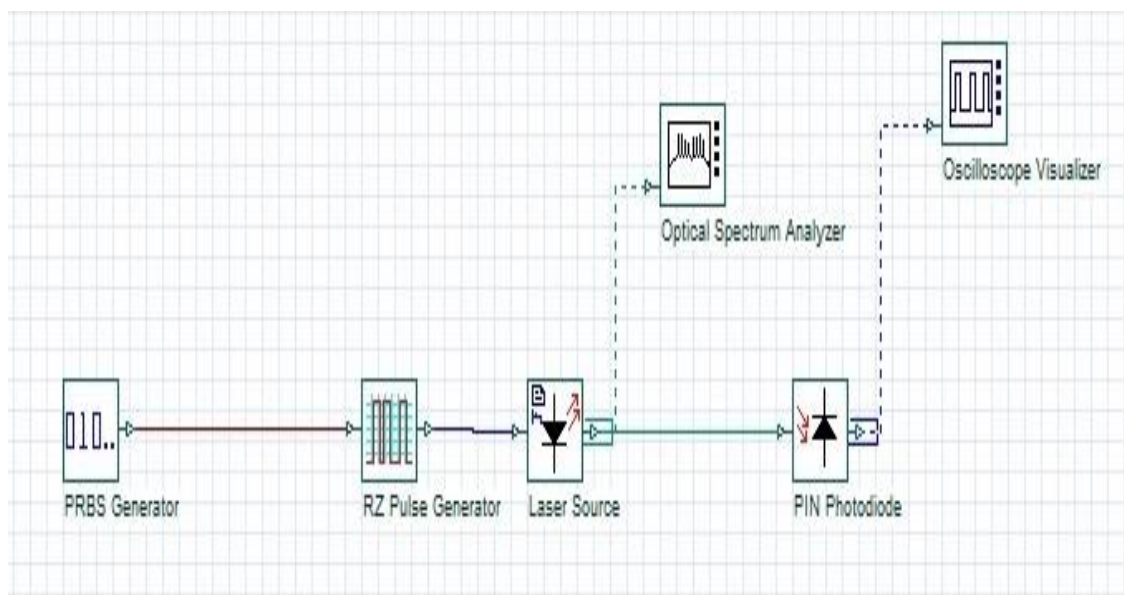
Parameter	Value	Unit
Central wavelength	1546.74	nm
Peak Power	1229.271	$\mu\text{W}$
Energy	0.0123	nJ
Full Width at Half Maximum	10	ns
Full Width at Half Maximum	286	pm
Pulse Repetition Rate	30	kHz
Duty-cycle	90%	—
Voltage	2	mV

The high speed electrical switching that used for chopping is a small signal amplifier supported by (transistor: C3355) with 5 GHz switching frequency (see appendix C2), this circuit needs 4.7 volt power source to energize the device and a non-return to zero input signal wither a positive or negative edge going provided by Arduino. The transistor can be set using a pair of a variable resistor for biasing transistor and a capacitor for smoothing. The value of the inductor sets the time duration of the output signal. By controlling the value of the biasing resistors of the transistor we control the level of the delivered voltage to the laser diode above and below the lasing threshold of it for switching on and off. Finally, this circuit has been designed

and implemented in simulation by Optisystem software (version 14.0), Electronic workbench software to explore the internal structure of it, and experimentally as shown in Figures 2.3 (a-c), respectively.



(a)



(b)

**Fig. 2.3 Electronic Chopping Circuit, a) Schematic diagram b) simulation by Optisystem, c) experimental image.**

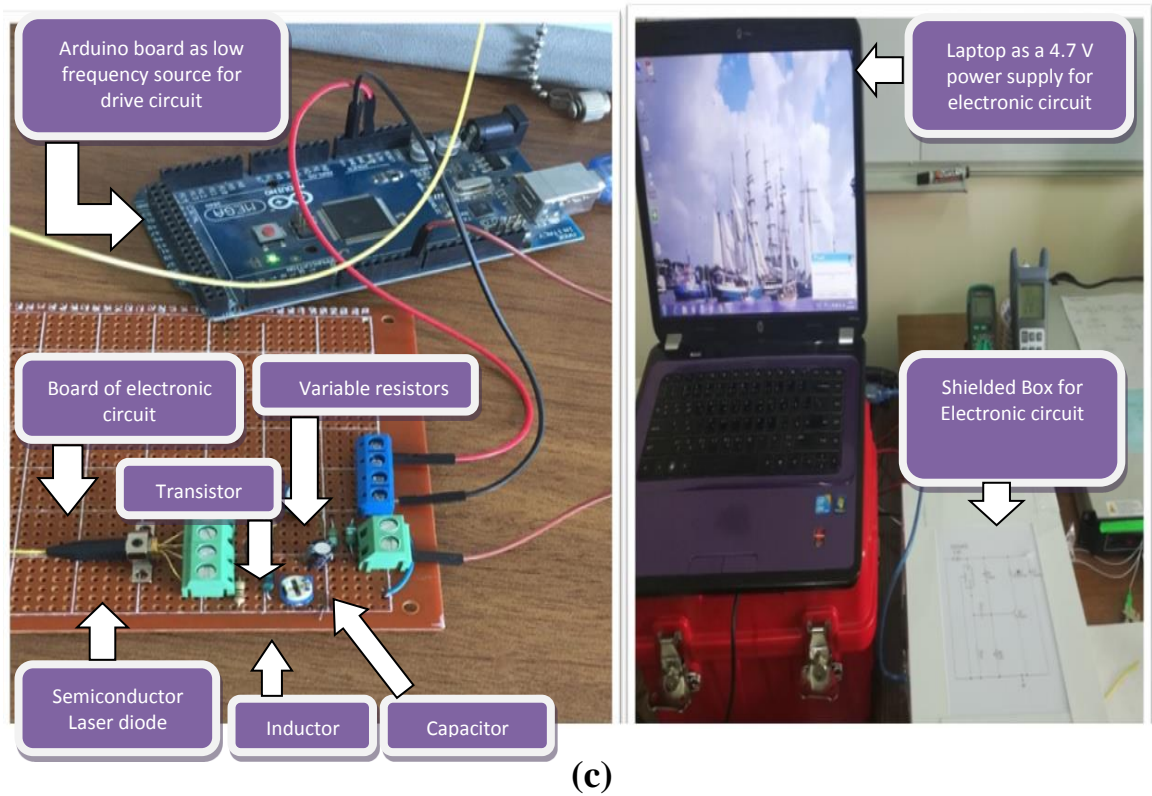


**Fig. 2.3 (Continued)**

### 2.2.2 Erbium-Doped Fiber Amplifier

Erbium-doped fiber amplifier (EDFA) is an important optical component, since it supports low power optical signals and elevates it to the level where it is possible to stimulate Kerr effect. EDFA is an optical amplifier, gives 18 dBm gain for each of its four channels which is in fact, generates a laser pumped by another laser with Erbium-doped fiber. Optical amplifiers work optically without converting from optical to electrical signals and back again. For more information see appendix B1.

### 2.2.3 Interferometer

It is a device that separates a beam of light into two ray beams, usually by means of reflection, and that brings the rays together to produce interference, used to measure wavelength, index of refraction, and astronomical distances.

### 2.2.3.1 Fiber

In these experiments, it has been used different types of fibers and these fibers are listing in subsections below.

#### 2.2.3.1.1 Single Mode Fibers

Single mode fiber (SMF-28) is considered as the "standard" optical fiber for telephony, cable television, submarine, and private network applications in the transmission of data, voice and \ or video services. SMF-28 fiber is optimized for use in the 1310 nm wavelength region the information-carrying capacity of the fiber is at its highest in this transmission window, and it has lowest dispersion. SMF-28 fiber also can be used effectively in the 1550 nm wavelength region. Corning SMF-28 fiber has consistent geometric properties; high strength and low attenuation .Corning SMF-28 fiber can be counted on to deliver excellent performance and high reliability. The single mode fiber with core diameter 9  $\mu\text{m}$  and mode field diameter 10.4  $\mu\text{m}$  at 1550 nm was used in our experiments (see appendix A1). Corning single mode fiber can be used for excellent deliver performance and high precision. The corning SMF examined under the microscope to make sure that there are no damages during cleaving Process as shown in Figure 2.4.

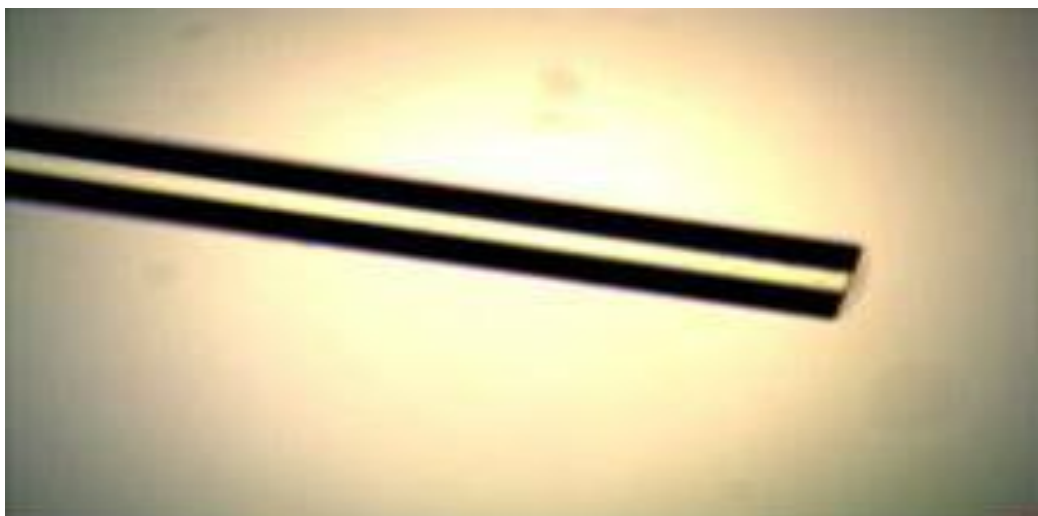


**Fig. 2.4 Side view for the SMF fiber under microscope.**

### **2.2.3.1.2 Photonic Crystal Fibers (PCF)**

Photonic-crystal fiber (PCF) is a class of optical fiber based on the properties of photonic crystals. It was first explored in 1996 at University of Bath, UK. Because of its ability to confine light in hollow cores or with confinement characteristics not possible in conventional optical fiber, PCF is now finding applications in fiber-optic communications, fiber lasers, nonlinear devices, high-power transmission, highly sensitive gas sensors, and other areas. In this work, two types of (PCF) are used which are:

#### **1-Hollow Core-Photonic Crystal Fiber (HC19-1550)**

The second fiber used in the experiments was a hollow core PCF (HC19-1550) manufactured by Thorlab (see appendix A5). It has been based on the 19 cell design core formed by omitting 19 central capillaries from the stack when it performs is being built by extrusion with negative pressure. The fiber must be testing under the microscope to obtain many of physical properties. The microscope that used for such purpose is a transmission Microscope, it has been used to view cross sections of these fibers and it is from (Euromex Company) which has many focusing lenses (4 X, 10 X, 40 X and 50 X), the lens which used for view images was (40 X) to enlarge the picture that was appeared to get the optimum Clarity for the picture. The testing of the cross section for HC-PCF 19 cells under the microscope obtained many of result for physical properties listing in table 2.2. The images of the physical properties for HC-PCF 19 cells which have been checked under microscope are illustrated in Figure 2.5 (a-f).

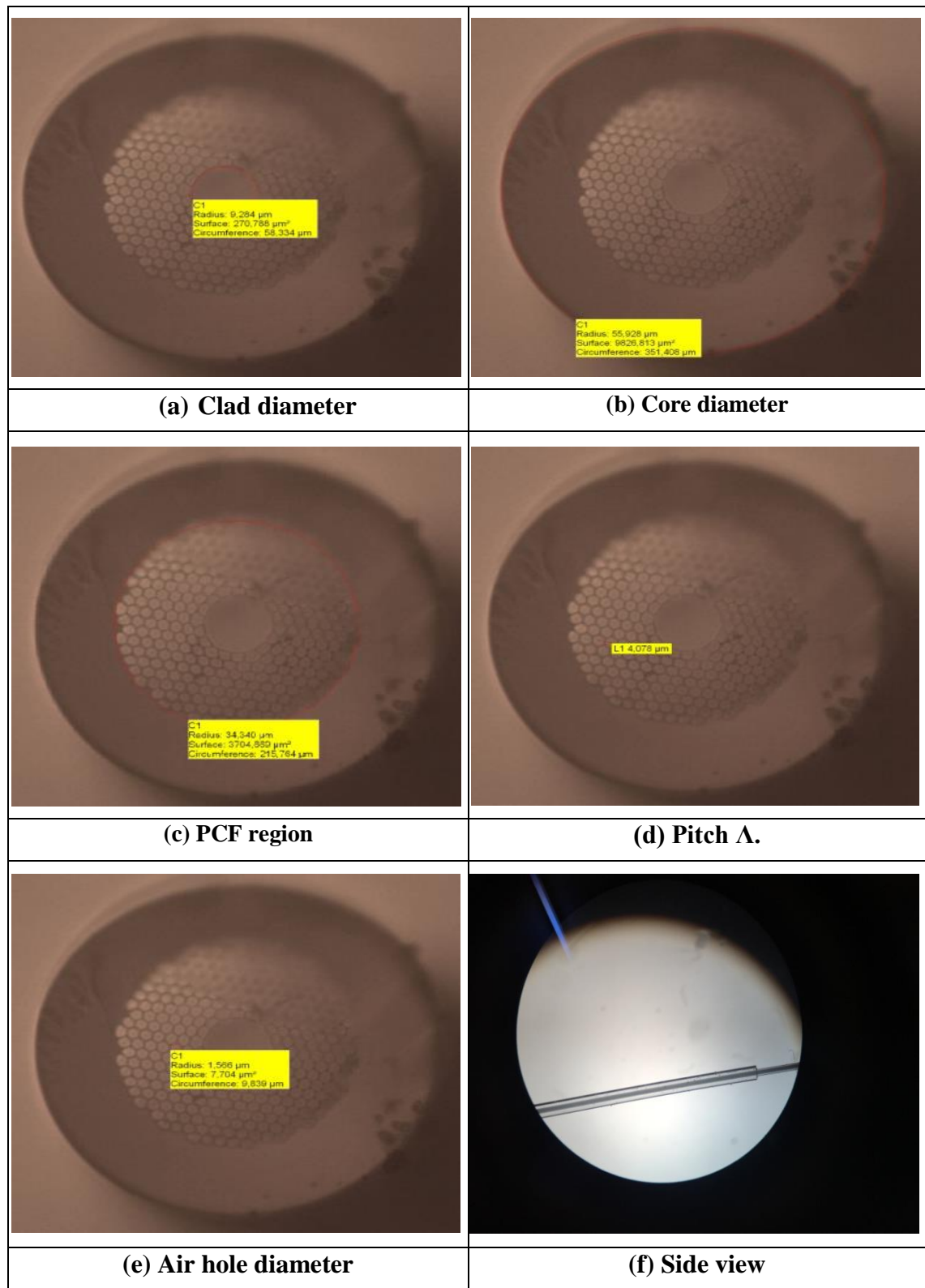


**Fig. 2.5** Cross section of top view and side view for the 19 cells under microscope  
(a,b,c,d,e) top view, and (f) side view.

**Table 2.2 Geometrical properties for 19 cell HC-PCF (HC19-1550) obtained from microscope.**

<b>Geometrical properties</b>	<b>Value</b>
Core diameter ( $\mu\text{ m}$ )	21
Pitch ( $\Lambda$ ) ( $\mu\text{ m}$ )	4
Air hole diameter ( $\mu\text{ m}$ )	3.2
Diameter of holey region ( $\mu\text{ m}$ )	68.68
Cladding diameter ( $\mu\text{ m}$ )	115
Coating diameter ( $\mu\text{ m}$ )	220

Although the parameters of HC-PCF 19 cells that are calculated by different equation are illustrate in table 2.3.

**Table 2.3 Optical parameters of HC-PCF (19 cells HC19-1550).**

<b>Parameters of 19 cells</b>	<b>Value</b>
nonlinear index coefficient for the core ( $n_2$ ) ( $\text{m}^2/\text{W}$ )	$24 \times 10^{-21}$
$A_{\text{eff}}$ ( $\text{m}^2$ )	$223.93 \times 10^{-12}$
$L_{\text{eff}}$ (mm)	1.5
nonlinear coefficient( $\gamma$ ) ( $\text{W}^{-1}\text{m}^{-1}$ )	$4.35 \times 10^{-4}$
$\beta_2$ ( $\text{ps}^2/\text{km}$ )	-38.1
$\Phi_{\text{NL}}$	$6.2 \pi$

## **2-Hollow Core-Photonic Crystal Fiber 7 cell HC-PCF (HC-1550-02)**

Third fiber was used in the experiments was hollow core PCF (HC-1550-02) from Thorlab (see appendix A6). This fiber has been based on the 7 cells design core formed by omitting 7 central capillaries from the stack when it performs is being built. The testing of the cross section for HC-PCF 7 cells under the microscope obtained many result for physical properties listing in

table 2.4. The images of the physical properties for HC-PCF 7 cells which have been checked under microscope are illustrated in Figure 2.6 (a-f).

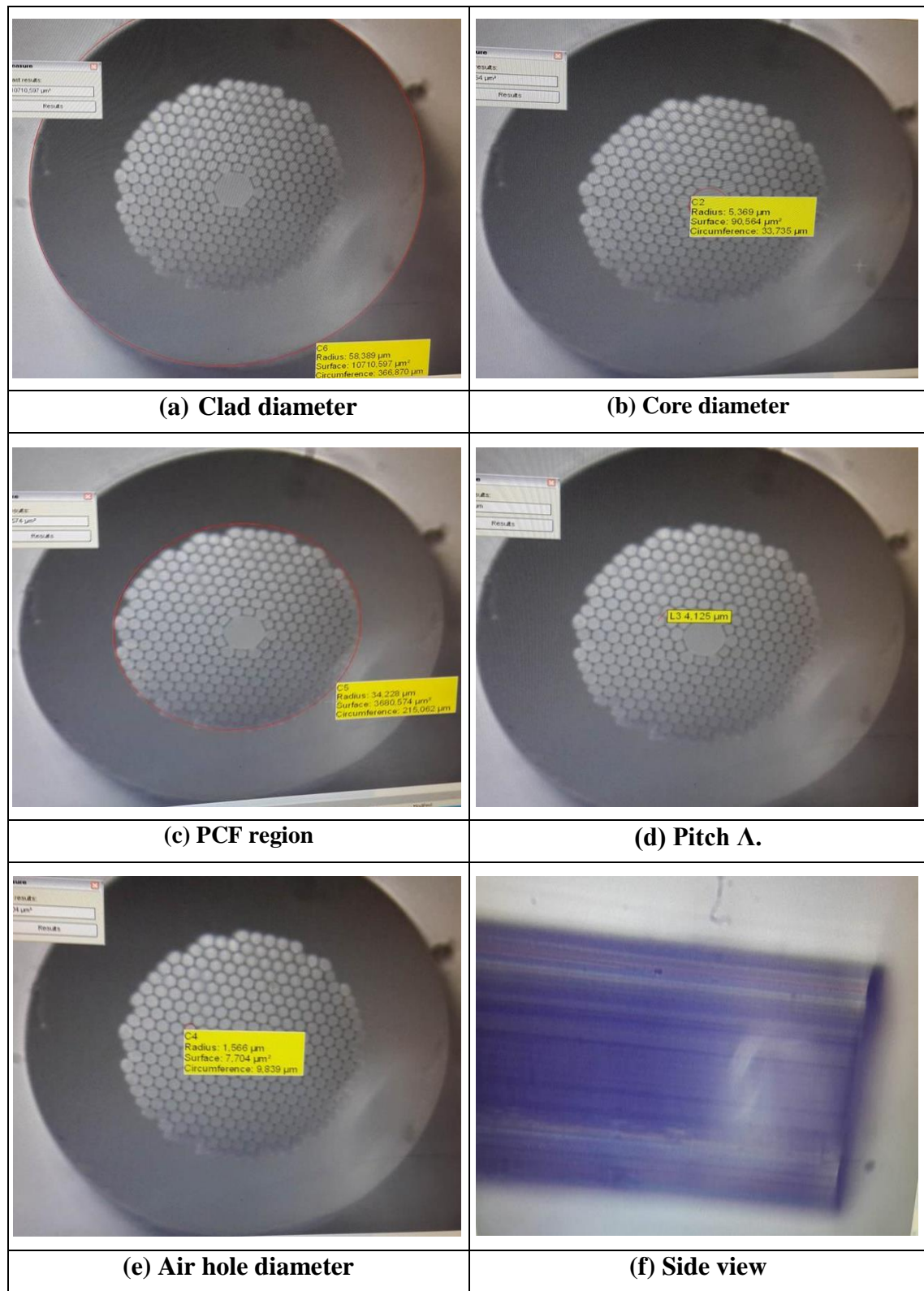


**Fig. 2.6** Cross section of top view and side view for the 7 cells under microscope (a,b,c,d,e) top view, and (f) side view.

**Table 2.4 Geometrical properties for 7 cell HC-PCF (HC-1550-02) obtained from microscope**

<b>Geometrical properties</b>	<b>Value</b>
Core diameter ( $\mu\text{ m}$ )	10
Pitch ( $\Lambda$ ) ( $\mu\text{ m}$ )	4
Air hole diameter ( $\mu\text{ m}$ )	3.2
Diameter of holey region ( $\mu\text{ m}$ )	68.46
Cladding diameter ( $\mu\text{ m}$ )	120
Coating diameter ( $\mu\text{ m}$ )	220

Although the parameters of HC-PCF (HC-1550-02) that are calculated by different equation are illustrate in table 2.5.

**Table 2.5 Optical parameters of HC-PCF (7 cell HC-1550-02).**

<b>Parameters of 7 cells</b>	<b>Value</b>
nonlinear index coefficient for the core ( $n_2$ ) ( $\text{m}^2/\text{W}$ )	$24 \times 10^{-21}$
$A_{\text{eff}}$ ( $\text{m}^2$ )	$74.898 \times 10^{-12}$
$L_{\text{eff}}$ (mm)	1.5
nonlinear coefficient( $\gamma$ ) ( $\text{W}^{-1}\text{m}^{-1}$ )	$13 \times 10^{-4}$
$\beta_2$ ( $\text{ps}^2/\text{km}$ )	-114.29
$\varphi_{\text{NL}}$	$18.6 \pi$

### **3-Polarization Maintaining Solid Core Photonic Crystal Fiber (SC-PCF: PM)**

In fiber optics, polarization-maintaining optical fiber (PMF or PM fiber) is a single-mode optical fiber in which linearly polarized light, if properly launched into the fiber, maintains a linear polarization during propagation (see appendix A7), exiting the fiber in a specific linear polarization state; there is little or no cross-coupling of optical power between the two polarization modes. Such fiber is used in special applications where preserving polarization is essential. Table 2.6 contains

general properties of the fiber. And Figure 2.7 shows a cross sectional view of PM fiber.

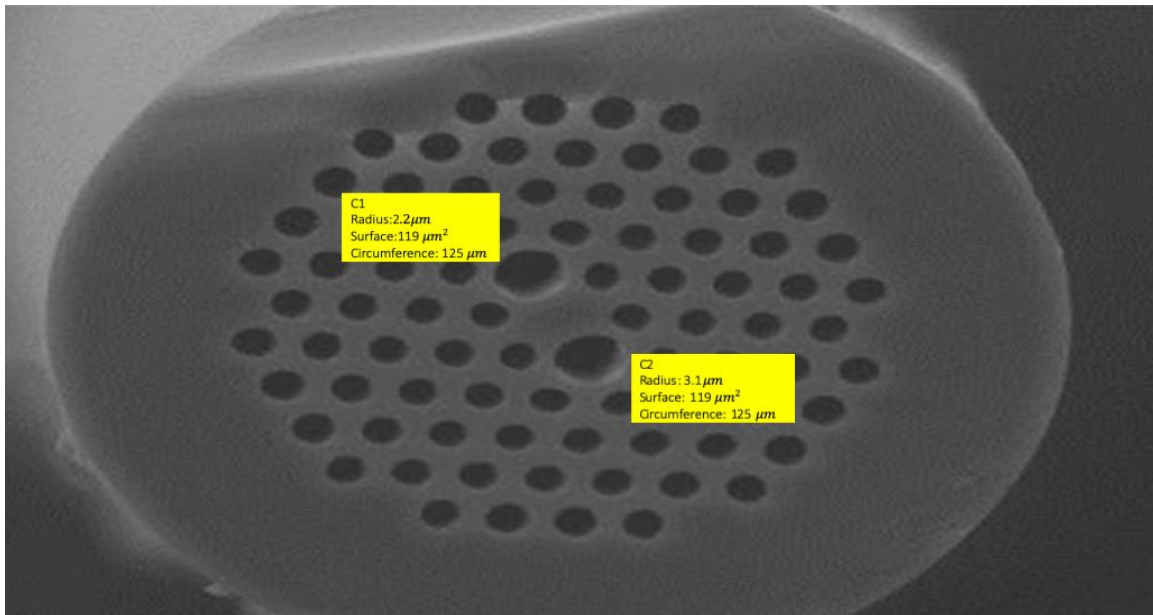


**Fig. 2.7 Shows a cross sectional view of PM-1550-01 fiber.**

**Table 2.6 General properties of PM-1550-01 fiber.**

General Specifications	Value
Core diameter ( $\mu\text{m}$ )	6.6/4.3
Outer cladding diameter, OD ( $\mu\text{m}$ )	125
Coating diameter ( $\mu\text{m}$ )	230
Pitch ( $\mu\text{m}$ )	4.17

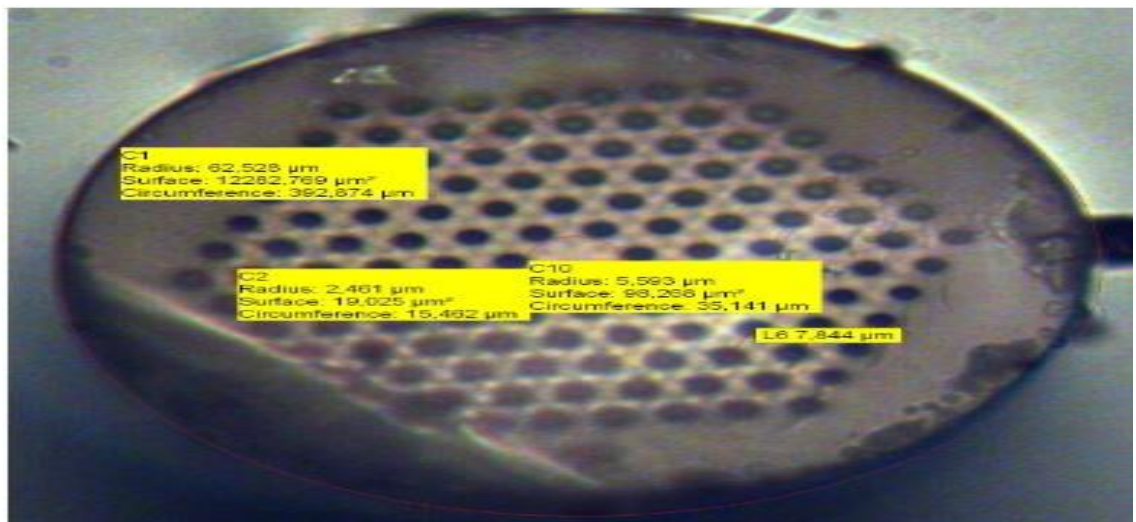
#### **4-Solid Core Photonic Crystal Endless Single Mode Fiber (SC-PCF: ESM-12)**

One of the attractive properties of the photonic crystal fiber (PCF) is their possibility to be single- mode over a wide wavelength range, surpassing the ordinary single mode fibers which become multi-mode for wavelength below their single-mode cut-off wavelength. PCFs which are specially designed with this property are called the endlessly single mode fiber (ESM) PCF [65] (see appendix A8). For PCF a value of the effective refractive index of photonic cladding depends strongly on wavelength, while

in classical fibers it was almost constant. The normalized frequency tends to a stationary value for short wavelengths. A refractive index of photonic cladding and therefore stationary value of normalized frequency is defined by the cladding structure, namely by the all factor (the ratio of the hole diameter  $d$  to the period of the lattice  $\Lambda$ ). With a proper design it is possible to keep normalized frequency ( $V$ ) below a cut-off normalized frequency for any wavelength range. A side and cross-sectional view are shown in Figure 2.8 (a-b), respectively. And table 2.7 explores the general properties of ESM fiber.



(a) Side view



(b) Cross sectional

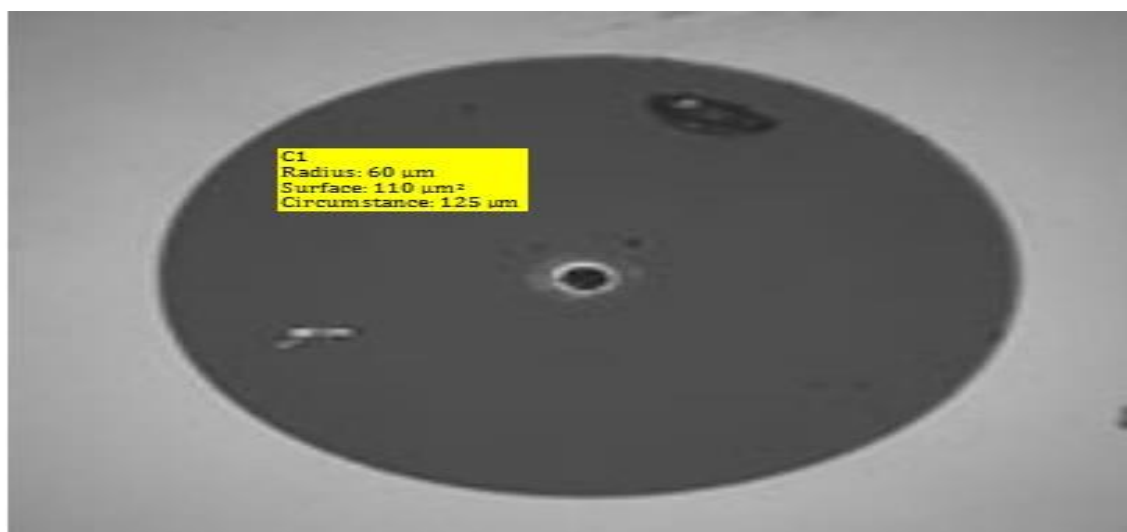
Fig. 2.8 a) side view of ESM, b) cross sectional view of ESM.

**Table 2.7 Shows general properties of the ESM fiber.**

Parameter	Value
Core diameter ( $\mu\text{m}$ )	11.186
Outer cladding diameter (OD) ( $\mu\text{m}$ )	125
Coating diameter ( $\mu\text{m}$ )	245
Mode field diameter ( $\mu\text{m}$ ) at 1550 nm	10.5
relative hole size ( $d/\Lambda$ )	0.46
Pith ( $\Lambda$ ) ( $\mu\text{m}$ )	7.844
Numerical aperture (NA)	0.14

### 2.2.3.1.3 Dispersion Compensation Fiber

A dispersion compensation fiber (DCF38) is used to compensate the cumulative dispersion in a single mode fiber and a dispersion coefficient is used to characterize the dispersion value. The value for regular SMF is around +16~17 ps/(nm.km) at 1550 nm. To properly manage this, it has a negative value of dispersion coefficient, ranging from -30 to -300 ps/(nm.km). Figure 2.9 shows a cross-sectional view of it, and table 2.8 lists its general properties, for more information (see appendix A9).

**Fig. 2.9 Cross sectional view of DCF38.**

**Table 2.8 General properties of fiber**

Parameter	Value
Mode Field Diameter ( $\mu\text{m}$ ) at 1550 nm	6.01
Numerical Aperture ( $\mu\text{m}$ ) at 1550 nm	0.14
Cladding Diameter ( $\mu\text{m}$ )	125.0
Coating Diameter ( $\mu\text{m}$ )	250
Attenuation (dB/km)	$\leq 0.265$

### 2.2.3.2 Procedures of Constructing Interferometers

There are many steps have been achieved for constructing these interferometers as follows:

#### 2.2.3.2.1 Fibers Stripping

First of all, the fibers must be stripped according to the required length that was needed in the experiment. This process is started by removing the protective polymer coating around PCF to prepare it for the next step. The stripping machine that used in this experiment was the (JIC – 375 Tri – Hole). It had three holes to perform all common fiber stripping functions. This fiber optic stripper strips the (1.6 - 3) mm fiber jacket down to the (600-900) micron buffer coating. The second hole strips the (600-900) micron buffer coating down to the (250) micron coating and the third hole is used to strip the (250) micron cable down to the (125) micron glass fiber without nicks or scratches.

#### 2.2.3.2.2 Fibers Cleaving

The cleaving is the process to scribe and break the fiber optic end face. The goal for this process is to produce a mirror like fiber end face. Incorrect cleaving techniques will result in lips and hackles which makes not good fiber for the working in the experiment. The tools needed for fiber

cleaving are called fiber optic cleavers. In this experiment; six types of optical fiber have been used, the single mode fiber (SMF-28), HC-PCF (19-1550 and 1550-02), DCF38 and SC-PCF (ESM-12B, PM-1550-01). For the single mode fiber (SMF-28) there is no too much restrictions like PCF, just cleaning the fiber with lint-free wipes moistened with isopropyl alcohol and place the stripped and cleaned bare fiber (SMF-28) into the fiber cleaver and then breaks the fiber (SMF-28) with the built-in mechanism on the cleaver. The PCF has a special procedure due to its structures. There is no solvent to be used for cleaning the PCF after the cleaving because this will lead the solvent to infiltrate inside the air holes of the PCF, dry wiping was used to remove remains coating after cleaving. A fiber optic cleaver has been used for cleaving the optical fibers.

#### **2.2.3.2.3 Fibers Splicing**

Fusion splicing is the technique that used in the experiments for joining two pieces of fiber and it is the process of applying heat to fuse together optical fibers, which minimizes insertion loss and back reflections in the fused component. It is a good fixing for the fibers will guarantee that the breaking of the fibers during the work and the misalignment between the tips (core) of the fiber during the focusing of the laser from the (SMF-28) to the HC-PCF and SC-PCF are limited. A commercial arc fusion splicer (DVP-740, see appendix B11) was employed to splice a PCF and a conventional SMF. Manual operation mode was available for the arc Fusion Splicer as shown in Figure 2.17. In these experiments, the splicing of PCF with SMF is achieved by arc fusion splicer. Splicer may be fused using either automatic or manual operation modes. The splicer setup list contains the functions of the arc fusion splicer which used in these experiments which they are given in table 2.9.

**Table 2.9 Setting parameters of the arc fusion splicer for HC-PCF, SC- PCF, DCF38.**

Fiber		Arc Time(ms)	Pre Arc Time(s)	Arc Power (mW)	Pre Arc power (W)	Gap (Length) ( $\mu\text{m}$ )	overlap (width) ( $\mu\text{m}$ )	Re-arc Time (ms)
HC-PCF	HC19-1550	2	0.25	280	60	18.0	20.0	2.5
	HC-1550-02	0.5	0.2	180	50	12.0	8.0	1.5
SC-PCF	ESM-12B	0.36	0.18	40	Stander	15.0	10	3.6
	PM-1550-01	1	0.9	70	78	08	10	3
DCF38		1.5	0.17	250	40	15.0	15.0	2

Firstly, the PCF (HC19-1550) was spliced to SMF as shown in Figure 2.10 (a). Then; the cleaved PCF and SMF were manually aligned via motors to reduce the butt-coupling loss as low as possible. In the second step, the splicing region for 30 cm PCF length resulting very good fusion with the splicing loss of 0.07 dB. Then, the splicing arc was repeated in the second PCF length with 20 cm as shown in Figure 2.10 (b). The splice loss reduced to 0.01 dB, the 12 cm and 7 cm PCF pieces were spliced with same procedure with splicing losses of 0.2 dB and 0.6 dB, respectively. Then, using the same splicing procedure, the PCF (HC-1550) and SMF were spliced. Figure 2.11 (a) shows the splicing region for seven cells at 30 cm length of PCF with splicing loss of 0.6 dB. Figure 2.11 (b) shows the splicing of same fiber but different length of 20 cm with splicing loss of 0.33 dB by the parameters mentioned in the table 2.8. A 12 cm and 7 cm of PCF pieces were spliced at the same procedure with splicing loss of 0.4 dB and 0.32 dB, respectively.

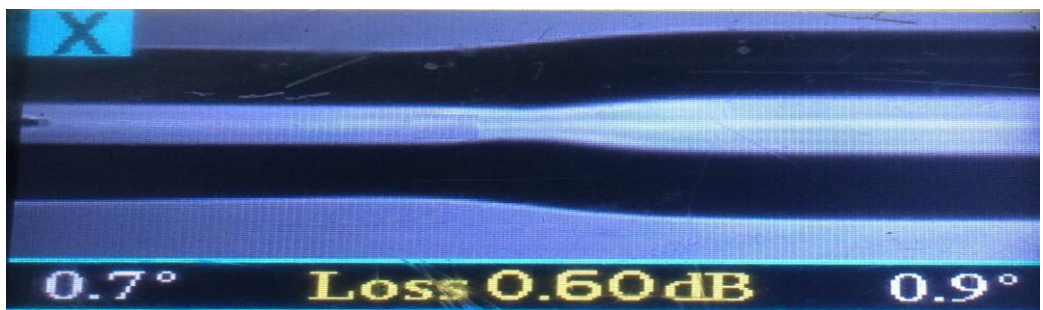


(a)

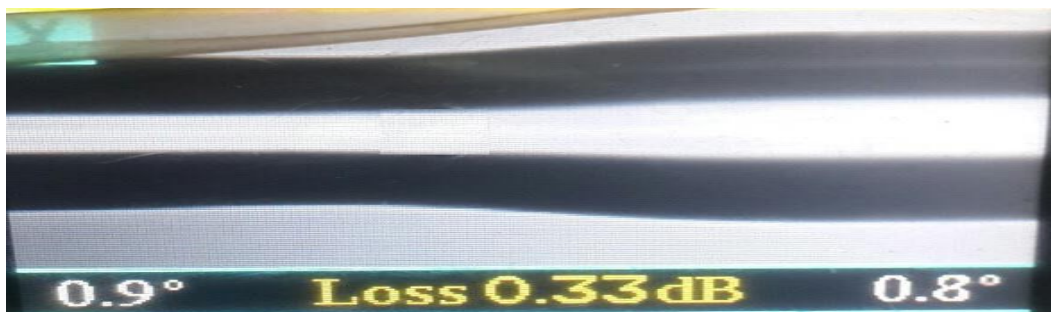


(b)

Fig. 2.10 procedure of the splicing HC-PCF with SMF, a) splicing region for 30 cm, b) splicing region for 20 cm during arcing.



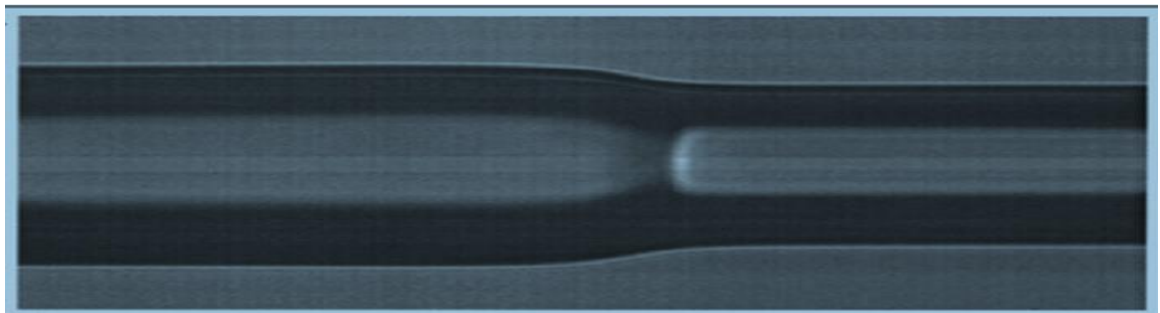
(a)



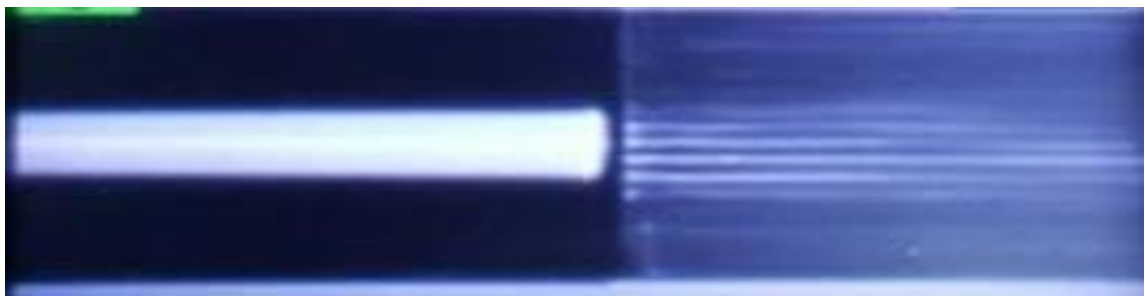
(b)

Fig. 2.11 Images show splicing joints during the splicing of seven cells with SMF, a) splicing region for seven cells at 30 cm length of PCF, b) splicing of same fiber but different length of 20 cm.

when splicing the SC-PCF (ESM12B, PM-1550-01) , DCF38, the splicing parameter also listed in the Table 2.8, these types of fiber should be treated individually in splicing process because the core of such fibers is solid not like hollow fiber. Figure 2.12 (a) shows splicing of endless single mode Fiber ESM12B with resultant splicing loss of 0.02 dB and length of ESM fiber was 7 cm, and Figure 2.12 (b) shows the splicing of Polarization maintaining fiber (PM-1550-01) with resultant splicing loss of 0.01 dB and length of PM fiber was 7 cm with single mode fiber from both ends, the 3.5 m DCF fiber is also spliced with 0.0 dB loss.



(a)



(b)

**Fig. 2.12** Images show the splicing joints during the splicing of SC-PCF with SMF.

### 2.2.3.3 Coupling Laser to Interferometers

After preparing interferometers by splicing two sides of HC-PCF, SC-PCF with SMF then they are connected with pulsed laser source by ferrule connector (FC) connectors and visualized the outputs in both frequency and time domains.

### **2.2.4 Polarization Controller (PC)**

Polarization controller is used to ensure an efficient performance of the pulse compression process by changing an arbitrary polarization to linear one and this is achieved by the stress which induced birefringence produced by wrapping the fiber around three paddles to generate independent wave plates that will alter the polarization of the passing light in a single mode fiber. The fast axis of the fiber is in the plane of the spool, allowing an arbitrary input polarization state to be adjusted by rotating the paddles. This polarization controller is connected with single mode optical fibers by FC connectors. For more information see appendix B4.

### **2.2.5 System Visualizers**

The optical signal that emerged from the optical source and propagated through interferometers, then this signal will be received by two types of visualizer. These visualizers give the output signal in both spatial and temporal domain. In addition, thermometer and power meter are also used to visualize environment temperature during experiment and optical power of the signal, respectively.

#### **2.2.5.1 Optically Visualizers**

The optical signal was visualized by optical spectrum analyzer (OSA), it is a device that designed to measure and displays the distribution of power of an optical signal over specified wavelength span. The measuring parameters of this device are the detection window from 600 nm to 1700 nm, wide level range: +10dBm to -70dBm, high wavelength accuracy:  $\pm 0.01$ nm and allowed for single-mode, multimode and PCF fibers. For more information about the optical spectrum analyzer (202 THORLABS, see appendix B6). OSA was used to monitor the interference spectra.

### 2.2.5.2 Temporally visualization

The output of the Fabry-Perot etalon and Mach-Zender interferometers were delivered to an optical spectrum analyzer for frequency domain results and to observe and analyze the obtained output pulse pattern, the designed photodetector was connected to 200 MHz digital storage oscilloscope (OSC: UNI-T: UTD2000m, see appendix B12) via Bayonet Neill–Concelman (BNC) adapter for time domain measurement thus for time domain results, the output was connected to OSC through designed photodetector (PD), as shown in Figure 2.13. A photodetector device has been designed experimentally, to convert the incident light signal to electrical signal, a photo diode should be connected in reverse and a resistor in series, as the intensity of the incident light increased as the band gab of photo detector decrease to allow more current from the source to pass through it. Operational amplifier amplifies the electrical signal in accordance with the delivered signal from the photodiode.

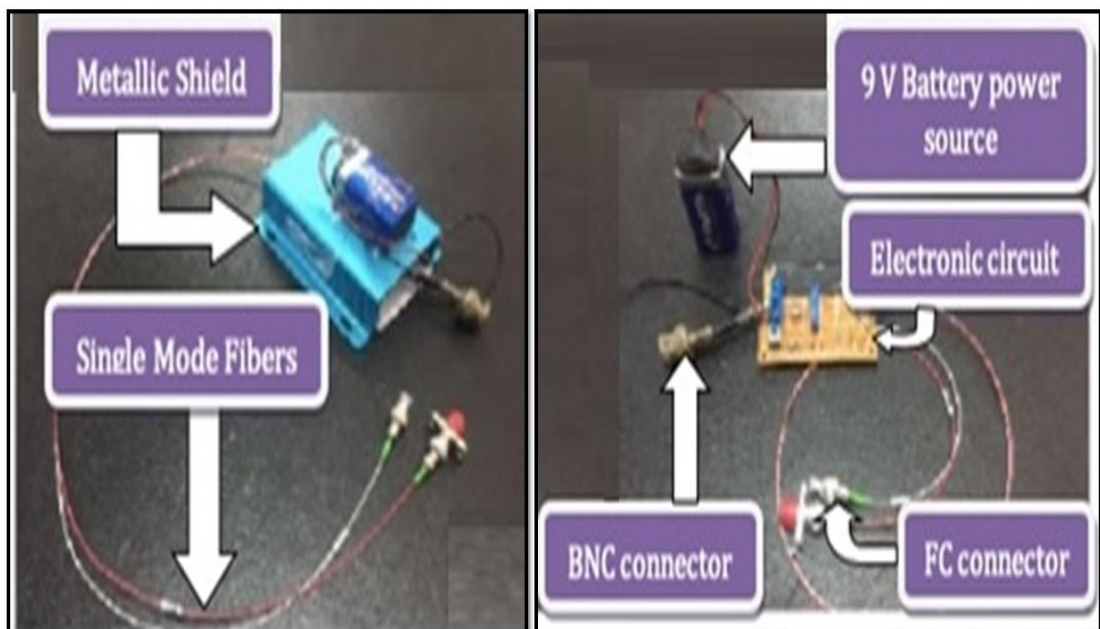


**Fig. 2.13** Lab image of designed photodetector.

### **2.2.5.3 Power Meter**

The power meter (FPM-300\FLS-300\FOT-300: see appendix B14) that is used to detect the light source of 1550 nm wavelength, which is used for transmitter power measurements in dB and watt.

### **2.2.5.4 Thermometer**

To measure the temperature of the environment during the experimental work (TES 1310 TYPE-K) thermometer was used. It was vary in range of (18-23) C°. Temperature is an important parameter should be consider in such works because when temperature vary a lot of results will change specially in filled of semiconductors, changing in the energy gab is a good example for that.

## **2.3 In Line Pulse Compression Techniques**

Two techniques of pulse compression are applied to improve the pulse compression in this work represented by using solid core photonic crystal fiber and HC-PCF.

### **2.3.1 Pulse Compression Based on Solid Core Photonic Crystal Fiber**

This type of optical pulse compression is achieved by the SC-PCF. The fibers used are ESM-12B and PM-1550-01; these fibers have the property of optical pulse compression by their manufacturer design due to their physical structure and optical properties. Laser source generate an optical pulse to be amplified by EDFA and then pass through PC, the PC control the polarization of the optical signal before it pass through interferometer. The interferometer based on these SC-PCF is MZI, to enhance the performance of compression, DCF38 is connected with SC-PCF

interferometer, and the out enhanced and compressed pulse then is visualized by OSA for frequency domain result as explained in Figure 2.14.

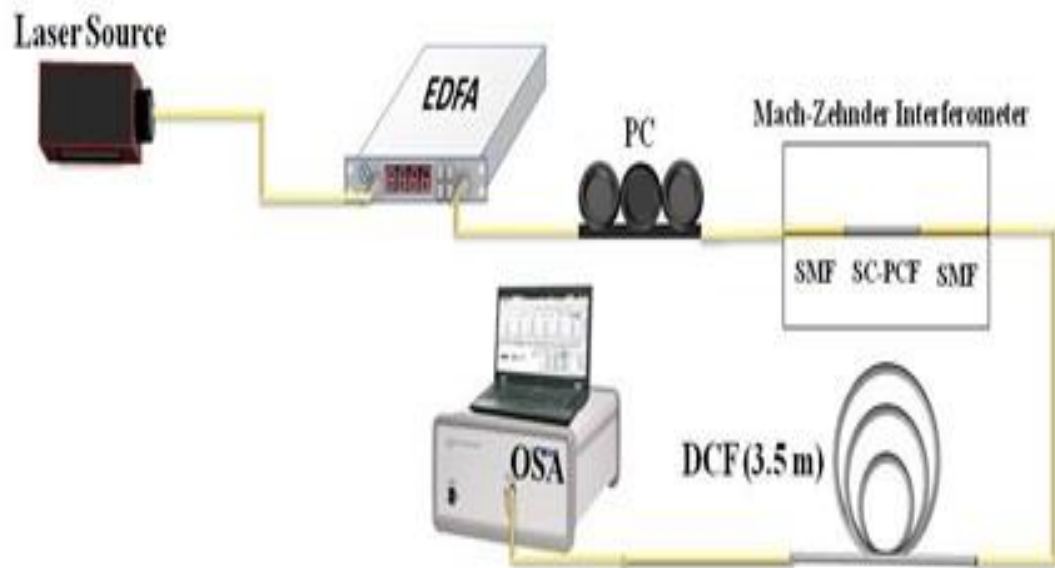


**Fig. 2.14** Setup represents pulse compression based on solid core photonic crystal fiber.

### 2.3.2 Pulse Compression Based on Hollow Core Photonic Crystal Fiber

This type of optical pulse compression was achieved by the HC-PCF; the fibers used were (HC-PCF 19 cell, HC-PCF 7 cell). These fibers had the property of optical pulse compression by their manufacturer design due to their physical structure and optical properties. These fibers guide light in a hollow core, surrounded by a micro-structured cladding of air holes and silica. Since only a small fraction of the light propagates in silica, the effect of material nonlinearities is insignificant and the fibers do not suffer from the same limitations on loss as conventional fibers made from solid material alone. The source emerge an optical pulse to be amplified by EDFA and then pass through PC, the PC control the polarization of the optical signal before it pass through interferometer. The interferometer based on these HC-PCF is FPI, to enhance the performance of compression, DCF38 is connected with HC-PCF interferometer, and the out enhanced and compressed pulse then is

visualized by OSA for frequency domain result and by OSC through PD for time domain result as explained in Figure 2.15.

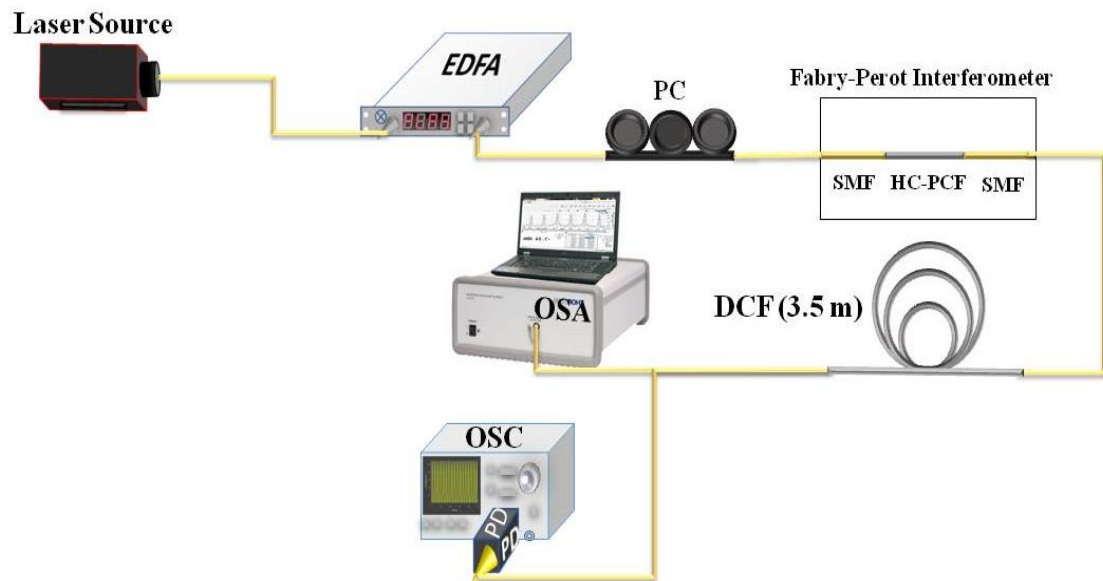


**Fig. 2.15 Setup represents pulse compression based on hollow core photonic crystal fiber.**

### **2.3.2.1 Pulse Compression Based on Infiltration of 19 cells Hollow Core Photonic Crystal Fiber**

In order to enhance the compression factor achieved in techniques discussed before, HC-PCF 19 cell is infiltrated by two chemical materials, optical pulse compression could be also achieved through the process of infiltration by injecting liquids that used in the experiment in both core and cladding of the interferometer. This leads to modify the refractive index of the holes which become approximately equal to the refractive index of the infiltrated material, the modified refractive index causes the pulse compression and same setup was used in this experiment was demonstrated in Figure 2.27. The infiltration process can be summarized by applying negative and positive pressure to the PCF by special types of injectors (small size of diabetes ampoules) as represented in Figure 2.16. The most important part of the process is using special type of epoxy surrounding the interface

region between the needles and PCF in order to prevent leaking during applying positive pressure and injecting the chemical compounds.

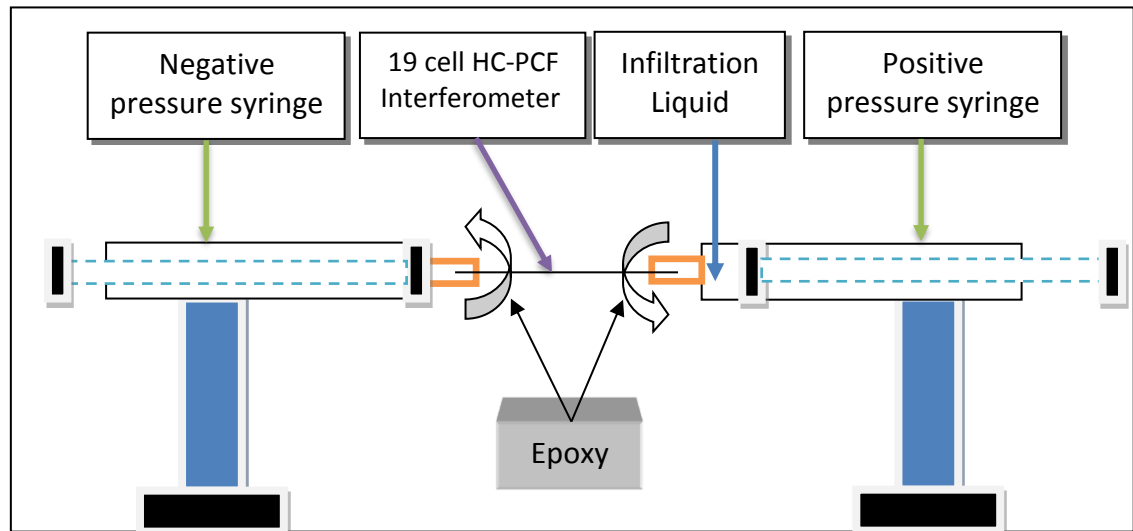


**Fig. 2.16 Shows setup that used in infiltration process.**

Two chemical liquids are used to infiltrate the HC-PCF in this work. These liquids explained briefly in the following subsections.

### 2.3.2.1.1 Ethanol

Ethanol is also called ethyl alcohol, defines as a chemical compound, a simple alcohol with the chemical formula  $C_2H_6O$  (an ethyl group linked to a hydroxyl group), and is often abbreviated as (EtOH). Ethanol is a volatile, flammable, colorless liquid with a slight characteristic odor. It is a psychoactive substance and is the principal type of alcohol found in alcoholic drinks [65]. Ethanol properties are listed in table 2.10.

**Table 2.10 Ethanol properties [65]**

property	Value
Density	0.7893 g/cm <sup>3</sup> at 20 °C
Boiling point	78.24 ± 0.09°C
Refractive index (n) at 1550 nm	1.353 at 20 °C
Viscosity	1.2 mPa·s (at 20 °C)
Chromatic Dispersion (dn/dλ)	-0.010906 μm <sup>-1</sup>
Group Velocity Dispersion	GVD = 40.409 ps/(nm km)
Dispersion Formula	$n = 1.349 + 0.00306\lambda^{-2} + 0.00006\lambda^{-3}$

### 2.3.2.1.2 Acrylic Acid

Acrylic acid (IUPAC: propenoic acid), is an organic compound with the formula  $C_3H_4O_2$ . It is the simplest unsaturated carboxylic acid, consisting of a vinyl group connected directly to a carboxylic acid terminus. This colorless liquid has a characteristic acid or tart smell. It is miscible with water, alcohols, ethers, and chloroform [66]. Table 2.11 represents liquid properties.

**Table 2.11 Acrylic Acid properties [66]**

<b>property</b>	<b>Values</b>
Density	1.03 g/mL
Boiling Point	141 °C (286 °F; 414 K)
Viscosity	1.3 cP at 20 °C (68 °F)
Refractive index at 1550 nm	1.5 at 20 °C

As listed in table 2.11, it seems that this liquid is very viscous, that means it was almost impossible to infiltrate it inside the 19 cell PCF fiber, thus, it should be mixed with suitable low viscosity solvent liquid that has ability to dissolve acrylic acid, infiltrate in fiber and work in between the operation wavelengths of the source that used during experiments, the solution sonicated for 30 min., the refractive index of the acrylic acid duo to mixing process with ethanol will be changed. Thus, a refractometer should be used to ensure the new refractive index. Refractometer was used to find new refractive index after mixture. For more information see appendix B16.

# **Chapter Three**

## **Results and Discussions**

## **Chapter Three**

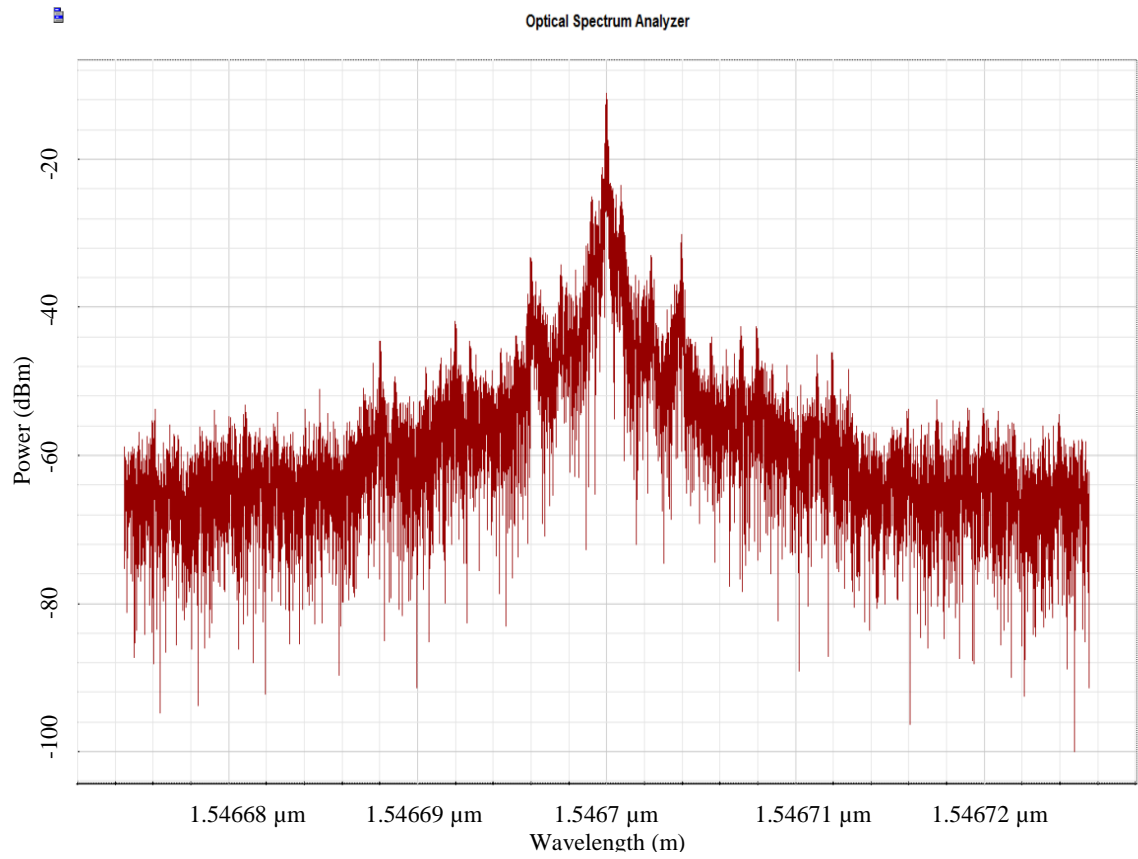
### **Results and Discussions**

#### **3.1 Introduction**

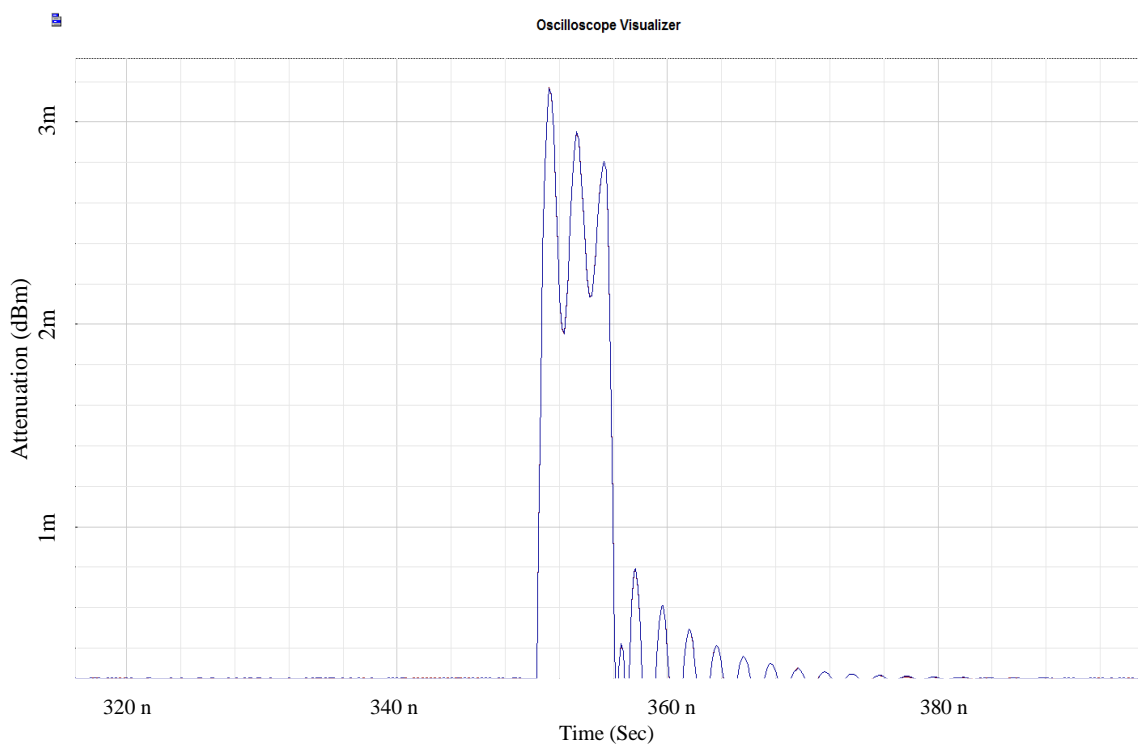
In this chapter, the experimental results of all-fiber pulse compression using in-line fiber interferometers-based photonic crystal fiber (PCF) are introduced and discussed. This chapter can be divided as: the characterizations of the designed pulsed laser source are presented in section 3.2. The results of pulse compression using Fabry-Perot etalon interferometers based on hollow core PCF (7 & 19 cells) are introduced in 3.3. Moreover, infiltrated the 19 cell-PCF by chemical liquids to enhance the compression of the signal. Section 3.4 gives the outcomes of compressed pulse using Mach-Zehnder interferometers-based solid core PCF (i.e., polarization maintaining fiber and endless single mode fiber). Section 3.6 summarizes the main points are concluded from this work followed by some suggestions for future work

#### **3.2 Characterization of the Pulsed Laser Source**

The pulsed laser source that depicted in Figure 2.3 was simulated by Optisystem (version.14) and experimentally implemented. Figure 3.1 (a-b) shows the simulated output of the pulsed laser source. From this figure, it can be seen that the power of 3.15 mW at the central wavelength of 1546.7 nm is achieved. Figure 3.2 depicts the experimental results of the pulse laser source. Figure 3.2 (a) shows the output spectrum of the pulsed laser source, where the central wavelength of 1546.74 nm, full width at half maximum (FWHM) equals to 286.292 pm. This pulsed laser source is designed to operate at pulse duration of 10 ns with pulse repetition rate (PRR) of 100 MHz, as shown in Figure 3.2 (b-c), respectively.

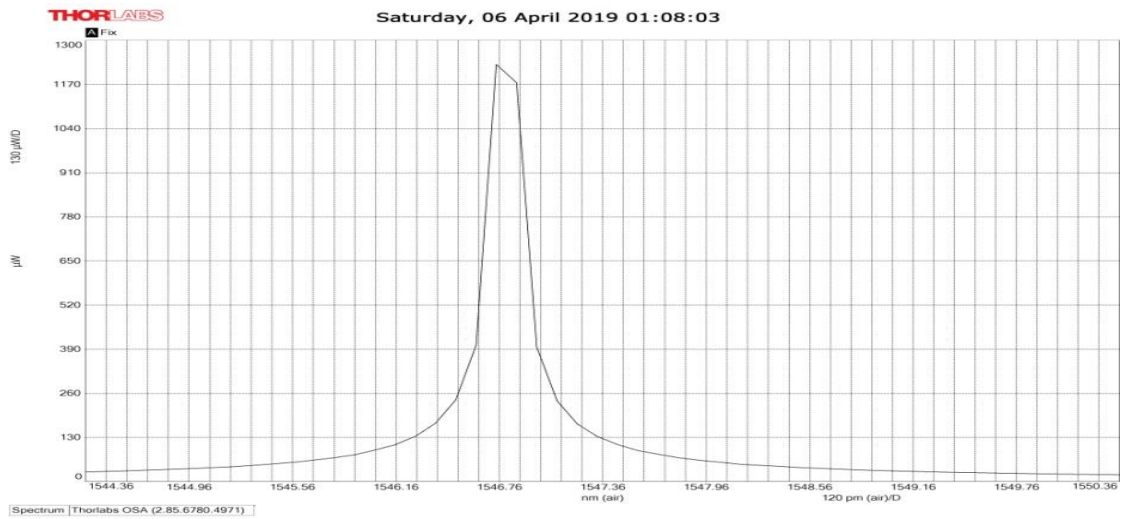


(a)

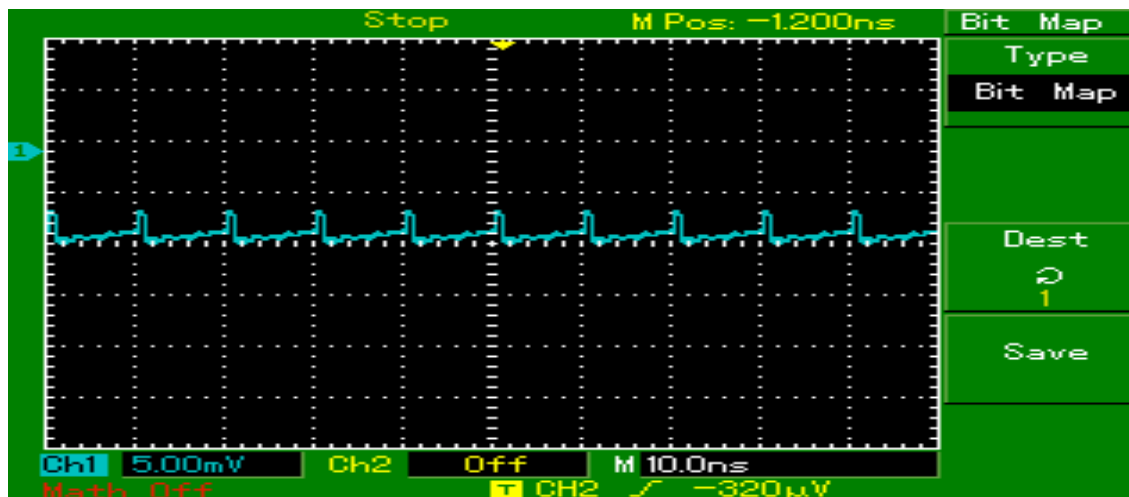


(b)

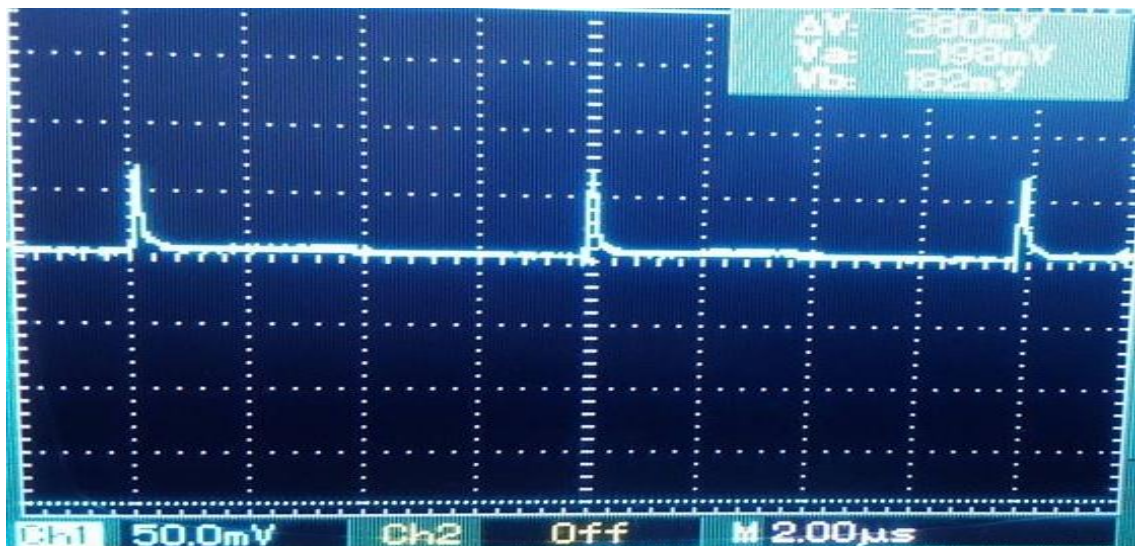
**Fig. 3.1 Output spectrum of simulated pulsed laser source a) Spectrally, b) Temporally**



(a)



(b)



(c)

**Fig. 3.2** Characteristics of the pulsed laser source a) Optical spectrum, b) Pulse duration, c) Pulse repetition rate (PRR).

### **3.3 Pulse Compression Using Fabry-Perot Etalon Interferometers**

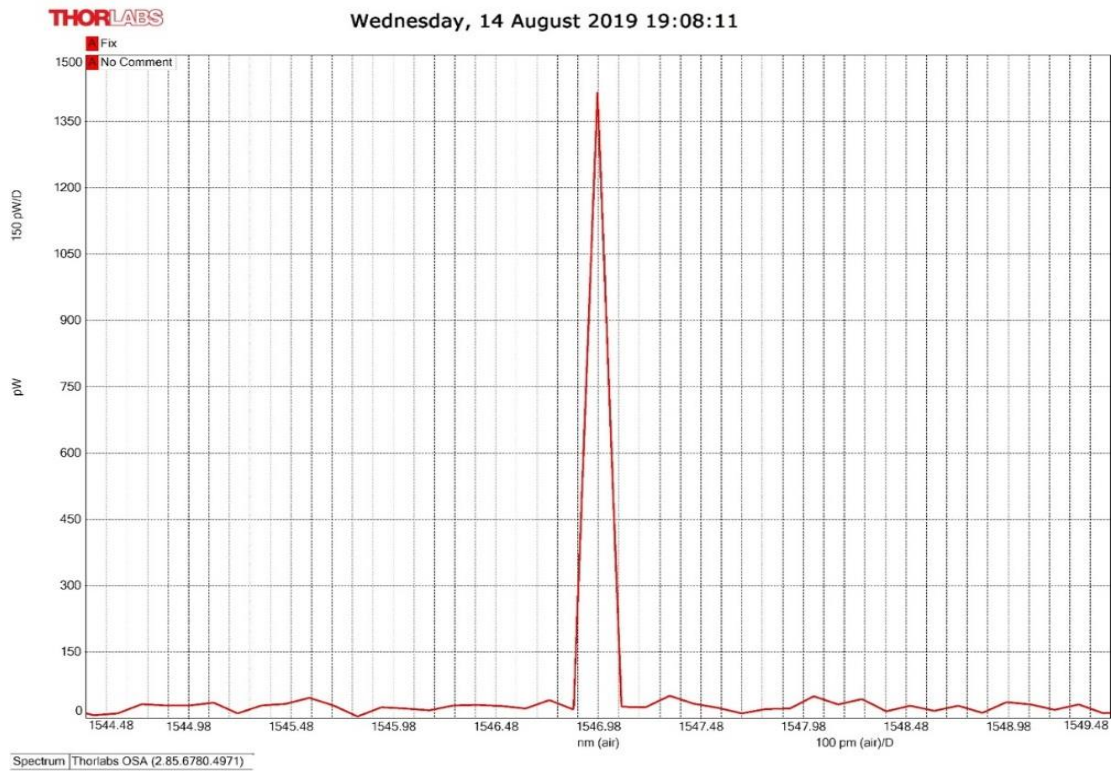
In this section, the results of pulse compression based on Fabry-Perot etalon interferometers are reported. These interferometers were constructed using hollow core PCF (7 and 19 cells) as explained in section 2.3.2. Additionally, 19 cell HC-PCF is infiltrated by organic compounds (i.e., ethanol, and a solution of acrylic acid diluted with ethanol) to enhance the compressed pulse.

#### **3.3.1 Pulse Compression Based on Hollow Core Photonic Crystal Fiber without infiltration**

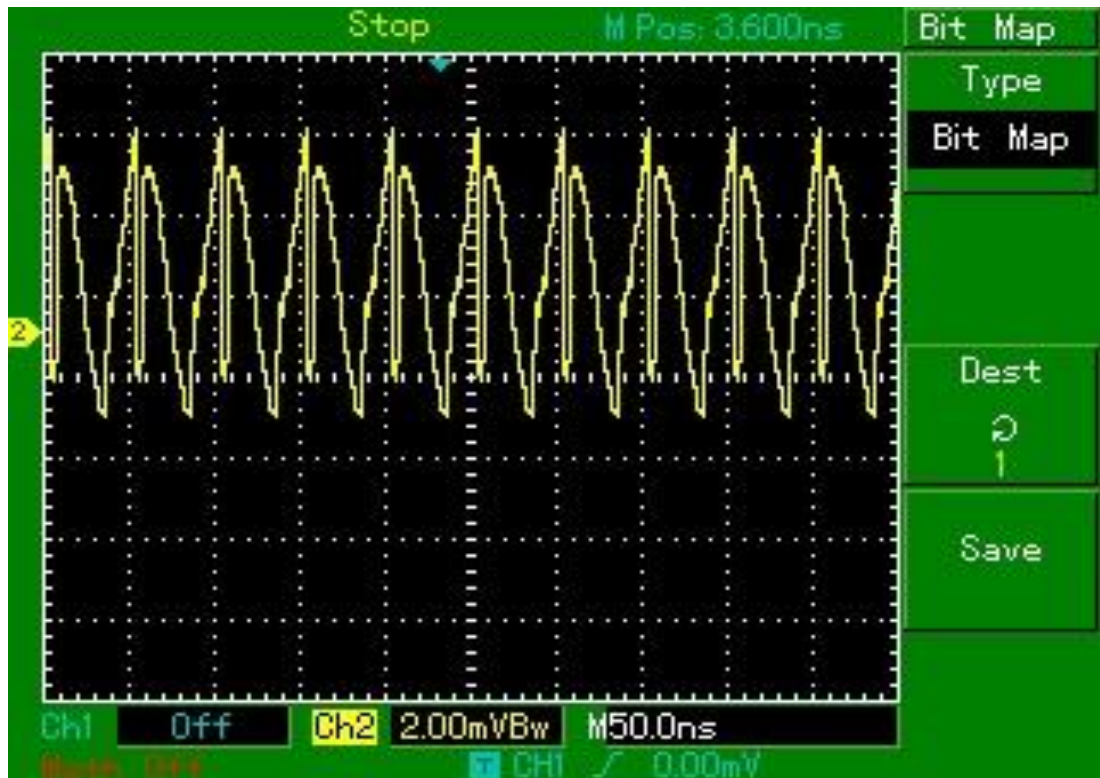
Pulse compression was experimentally achieved using different types of photonic crystal fiber with different setups, Erbium-doped fiber amplifier (EDFA) was connecting to rise the power for the optical pulse when the power level was below the threshold level of the designed photodetector, optical power dropped in some experiments due to splicing between PCF and single mode fiber (SMF).

##### **3.3.1.1 Pulse Compression Based on 19 cells Hollow Core Photonic Crystal Fiber**

The experimental results of the pulse compression setup that illustrated in Figure 2.26 are depicted in Figure 3.3. Figure 3.3 (a-b) shows the compressed pulse using 7 cm long of 19 cells PCF (HC 19-1550) in spatial and temporal domains, respectively. The FWHM of compressed pulse of 117.26 pm was obtained. The compressed pulse with FWHM of 149.511 pm was achieved using 12 cm of PCF, as displayed in Figure 3.3 (c-d). When 20 cm and 30 cm long of PCF were used, 209.27 pm and 117.78 pm, FWHM of the compressed pulse were obtained as shown in Figure 3.3 (e-f) and (g-h), respectively.

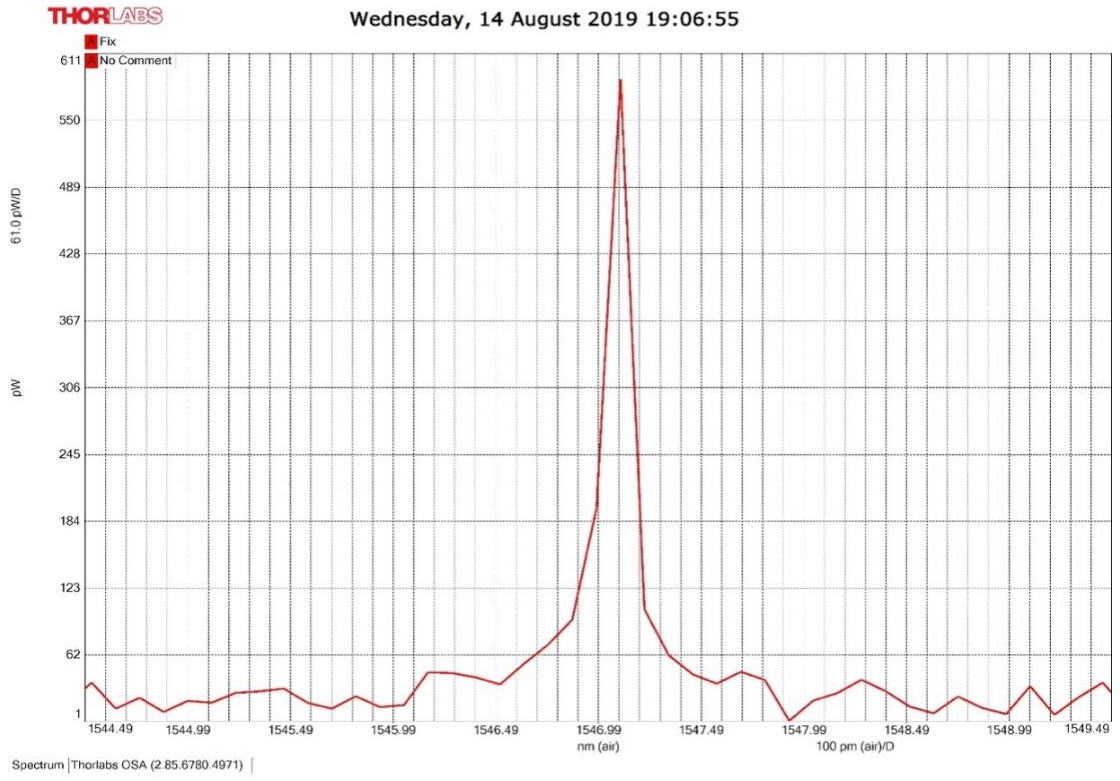


(a)

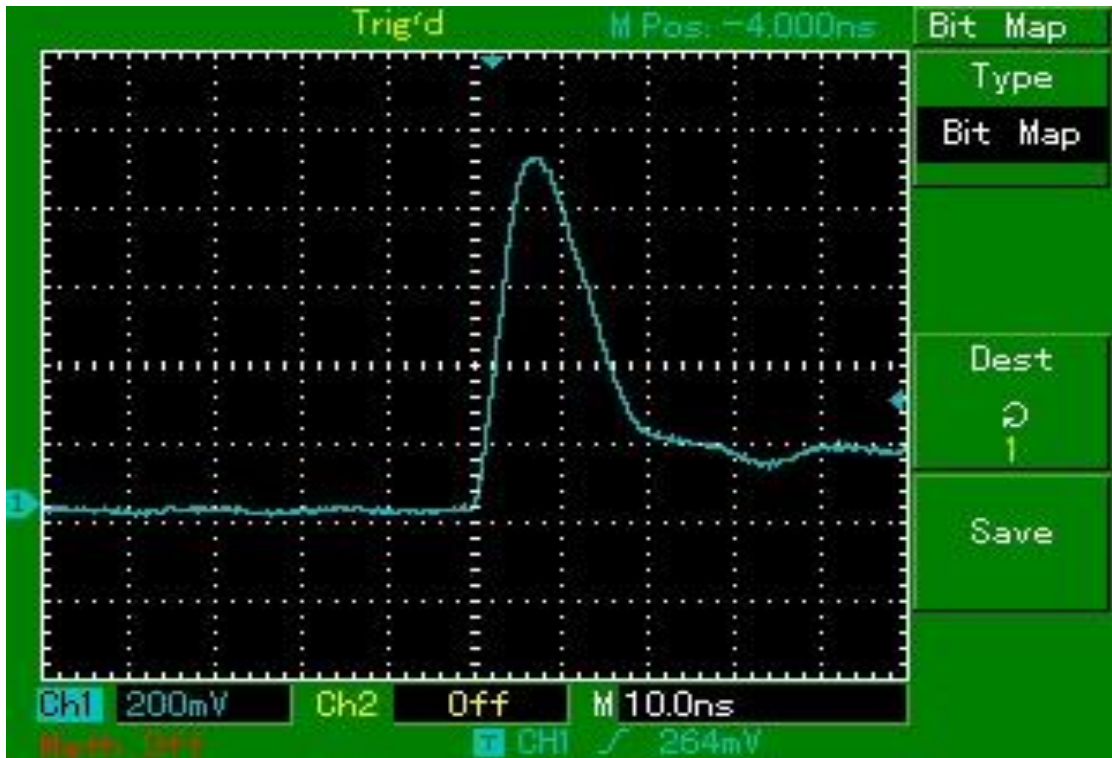


(b)

**Fig. 3.3 Compressed signal in frequency and time domains for four lengths of 19 cells PCF a-b) 7 cm length, c-d) 12 cm length, e-f) 20 cm length, g-h) 30 cm length.**

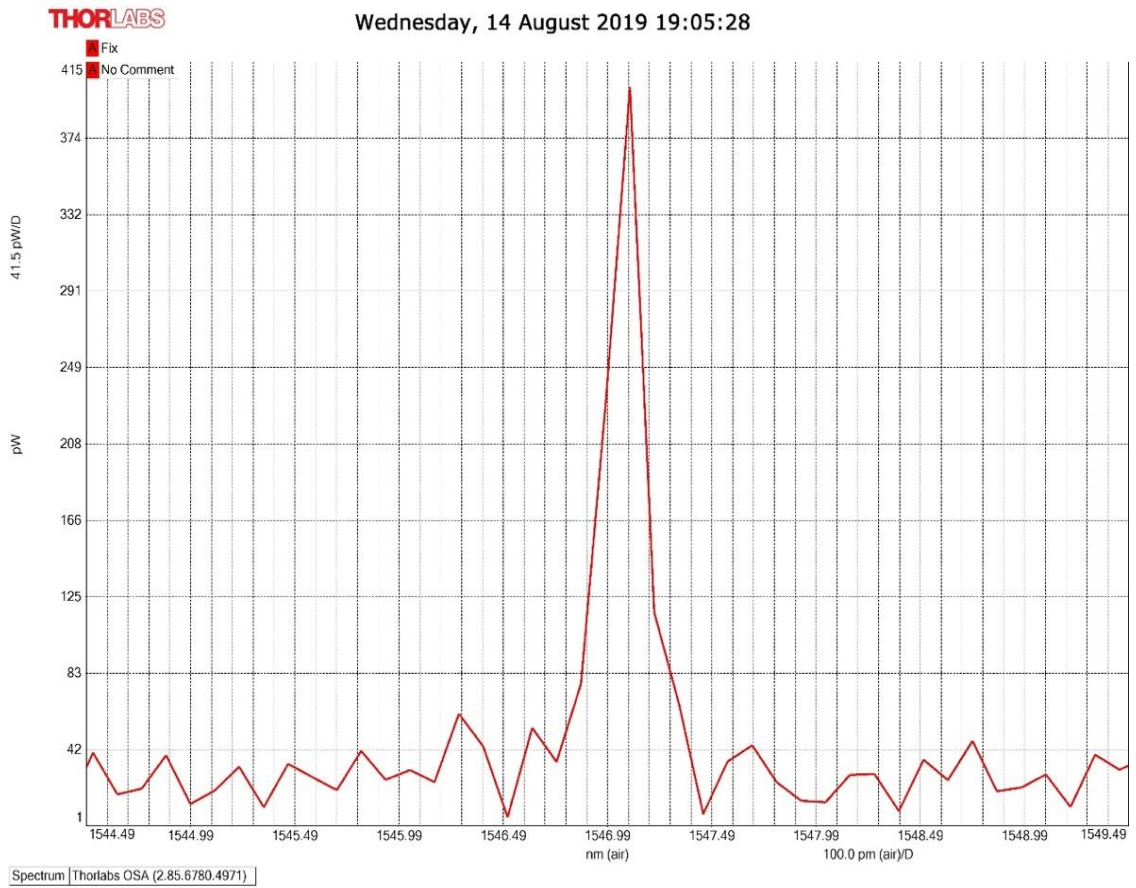


(c)

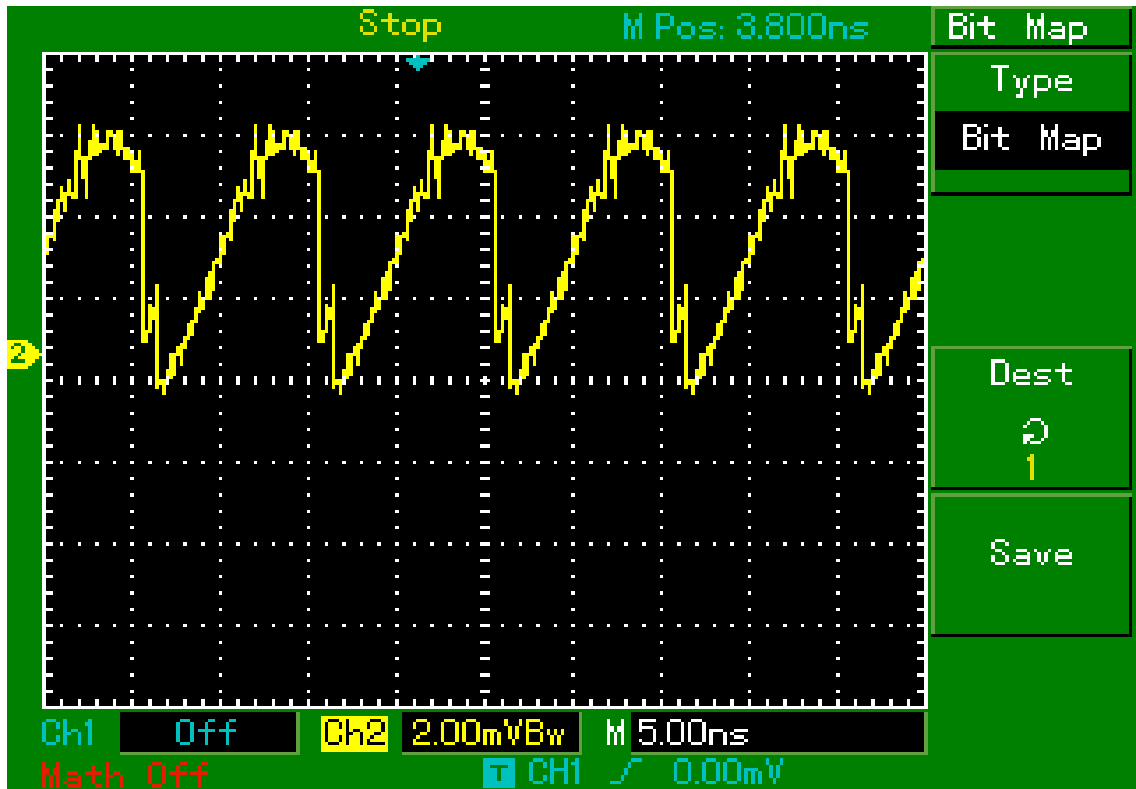


(d)

Fig. 3.3 (continued)

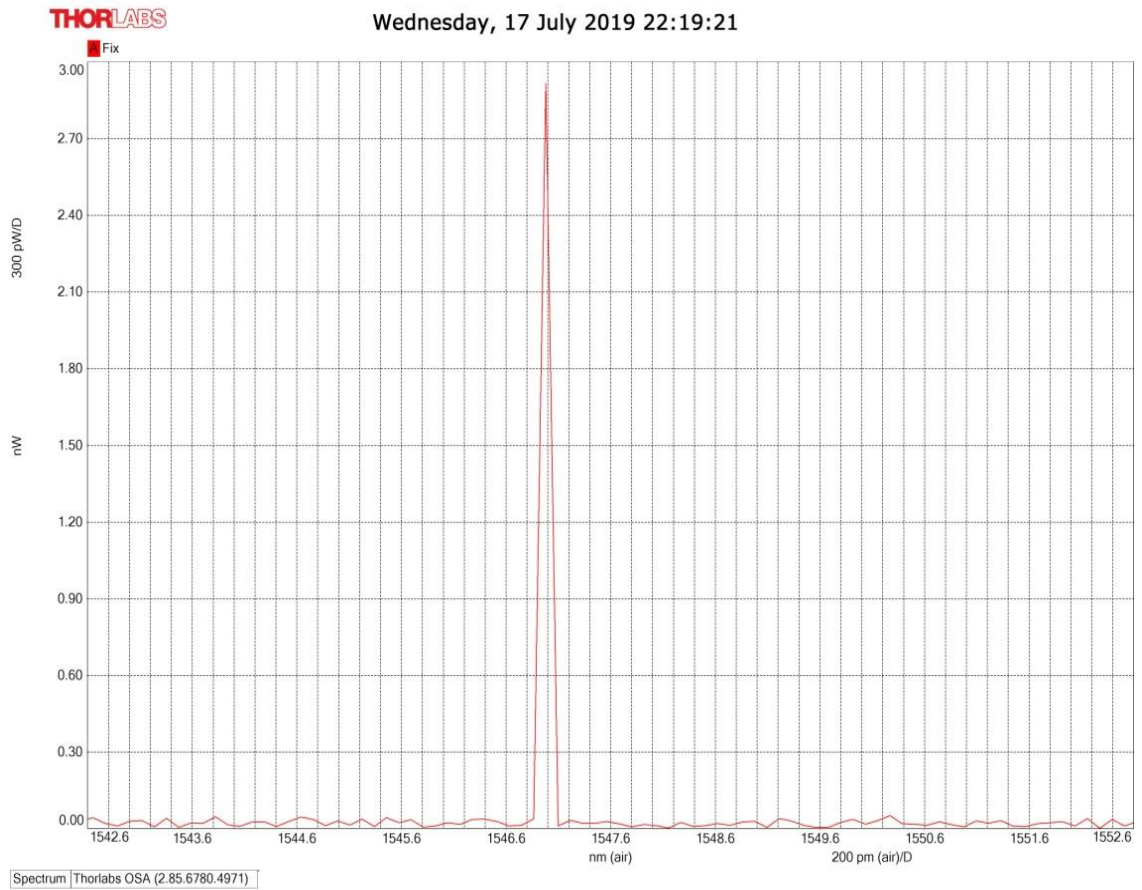


(e)

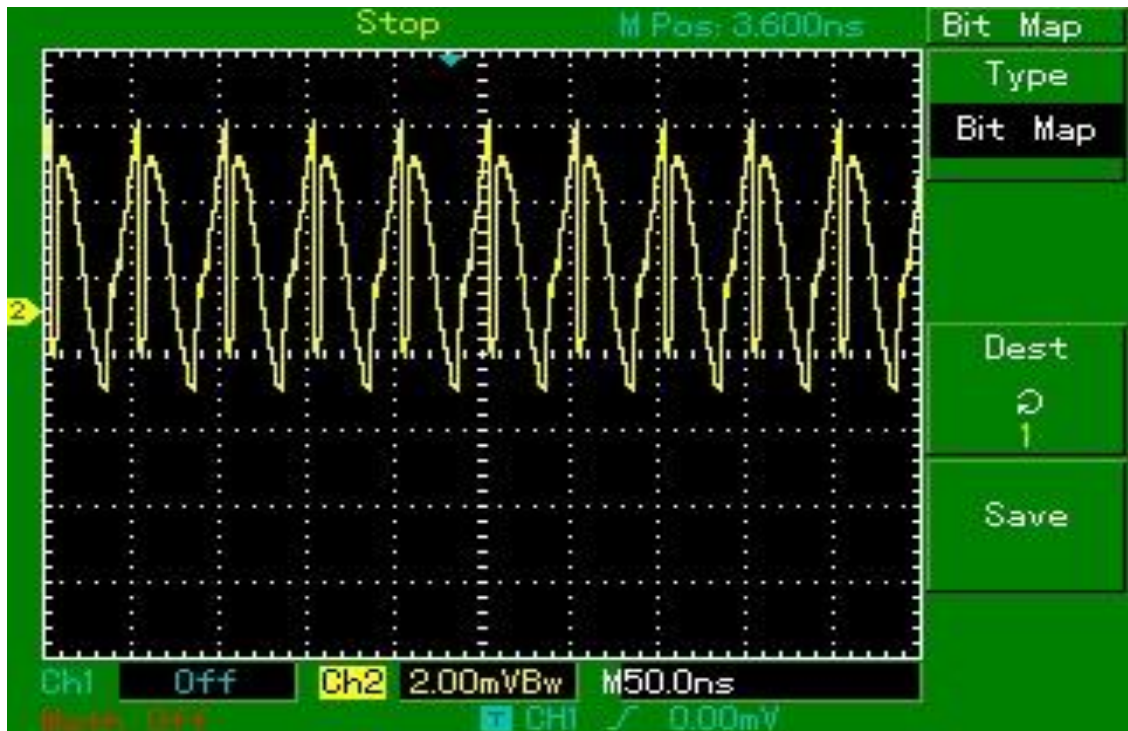


(f)

Fig. 3.3 (continued)



(g)



(h)

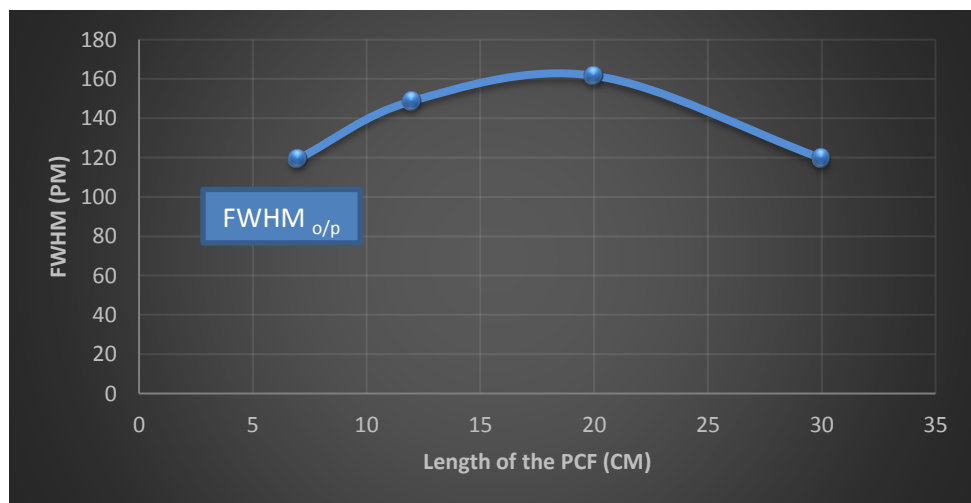
Fig. 3.3 (continued)

In order to explore the relation between the compression factor ( $F_c$ ) and the length of PCF, the results presented in Figure 3.3 are summarized in table 3.1. As can be observed the shortest length of PCF gives the highest value of the compression factor. When 7 cm PCF length is used, a compression factor of 2.43 is obtained depending on Eq. 1.37.

**Table 3.1 Relationship between 19 cells HC-PCF length, FWHM and compression factor.**

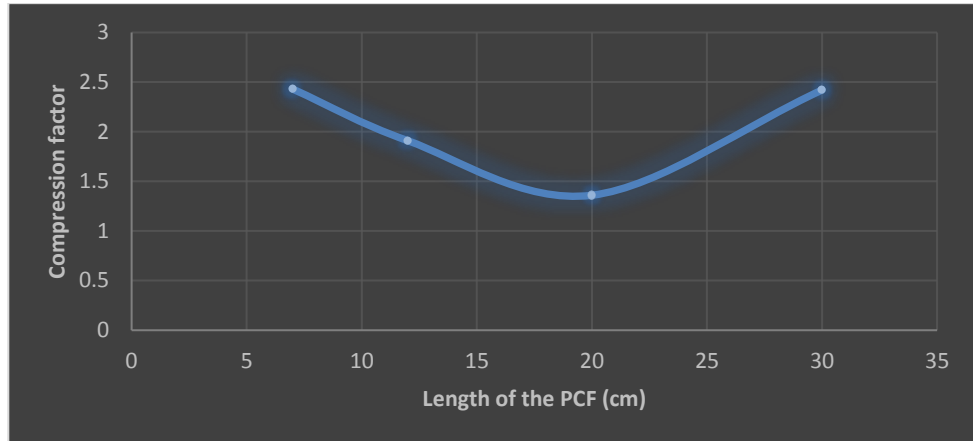
Length of 19 cells HC-PCF (cm)	FWHM (pm)	FWHM (ns)	$F_c$
7	117.26	20	2.43
12	149.511	12	1.91
20	209.27	6	1.36
30	117.78	20	2.42

In order to explore the influence of the length of PCF on the FWHM of the compressed pulse and the related compression factor, Figure 3.4 (a-b) are plotted. It can be seen that as the length of PCF ( $L_{pcf}$ ) increases the FWHM of the compressed pulsed increased until decrease dramatically with the maximum length of PCF (30 cm), as shown in Figure 3.4 (a). From Figure 3.4 (b), the compression factor decreases as the PCF length increases and rapidly increased at the maximum length of PCF (30 cm).



(a)

**Fig. 3.4 Relationship between length of 19 cells PCF and a) Full width at half maximum (FWHM), b) Compression factor ( $F_c$ ).**

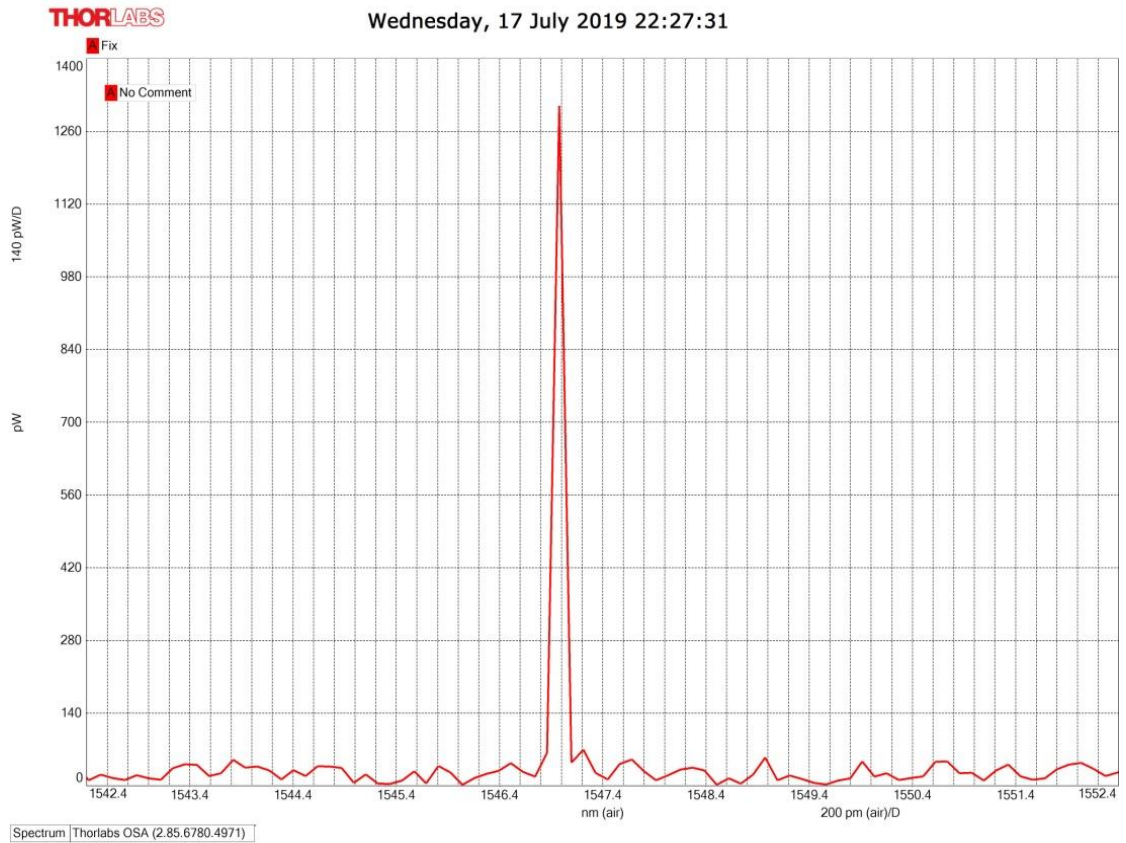


(b)

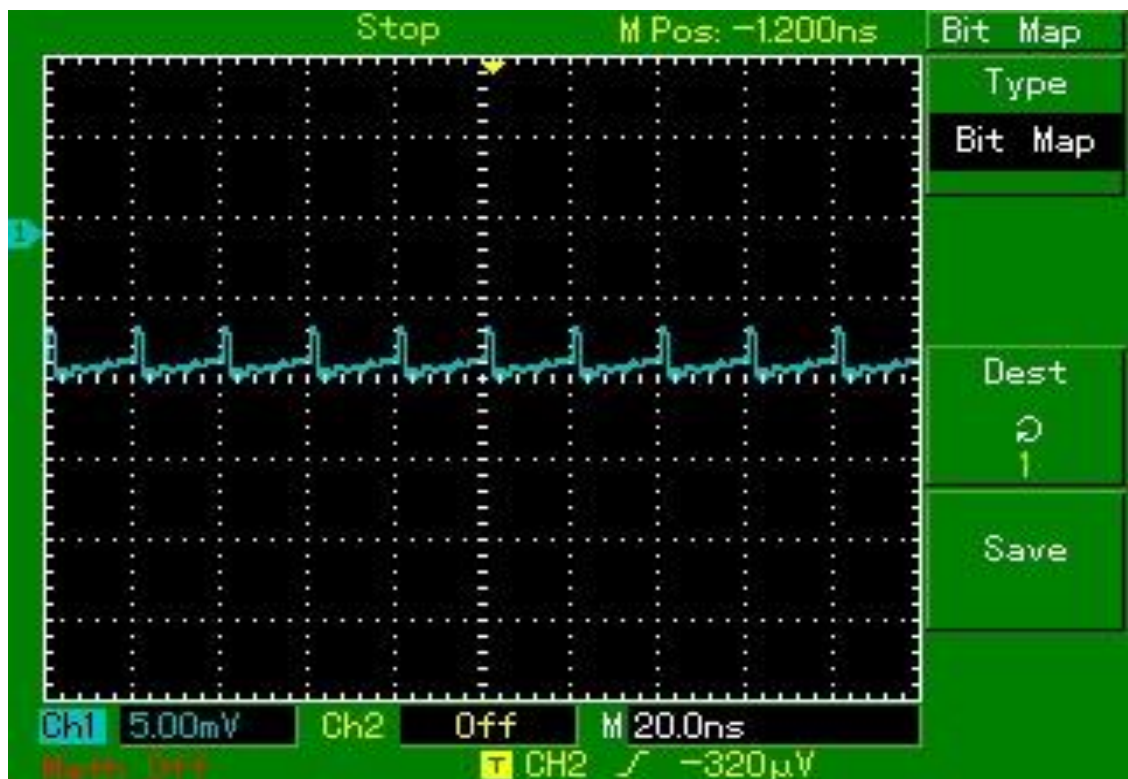
**Fig. 3.4 Continued.**

### 3.3.1.2 Pulse Compression Based on 7 cells Hollow Core Photonic Crystal Fiber

The experimental results of the pulse compression setup shown in section 2.26 are depicted in Figures 3.5 (a-h). Figure 3.5 (a-b) shows the compressed pulse in both frequency and time domain respectively using 7 cm length of 7 cells HC-PCF (HC-1550-02), the FWHM of compressed pulse of 119.384 pm was obtained. The compressed pulse with FWHM of 148.76 pm was achieved using 12 cm of PCF, as displayed in Figure 3.5 (c-d). When 20 cm and 30 cm of PCF were used, 161.622 pm and 119.583 pm FWHM of the compressed pulse were obtained as shown in Figure 3.5 (e-f) and (g-h), respectively.

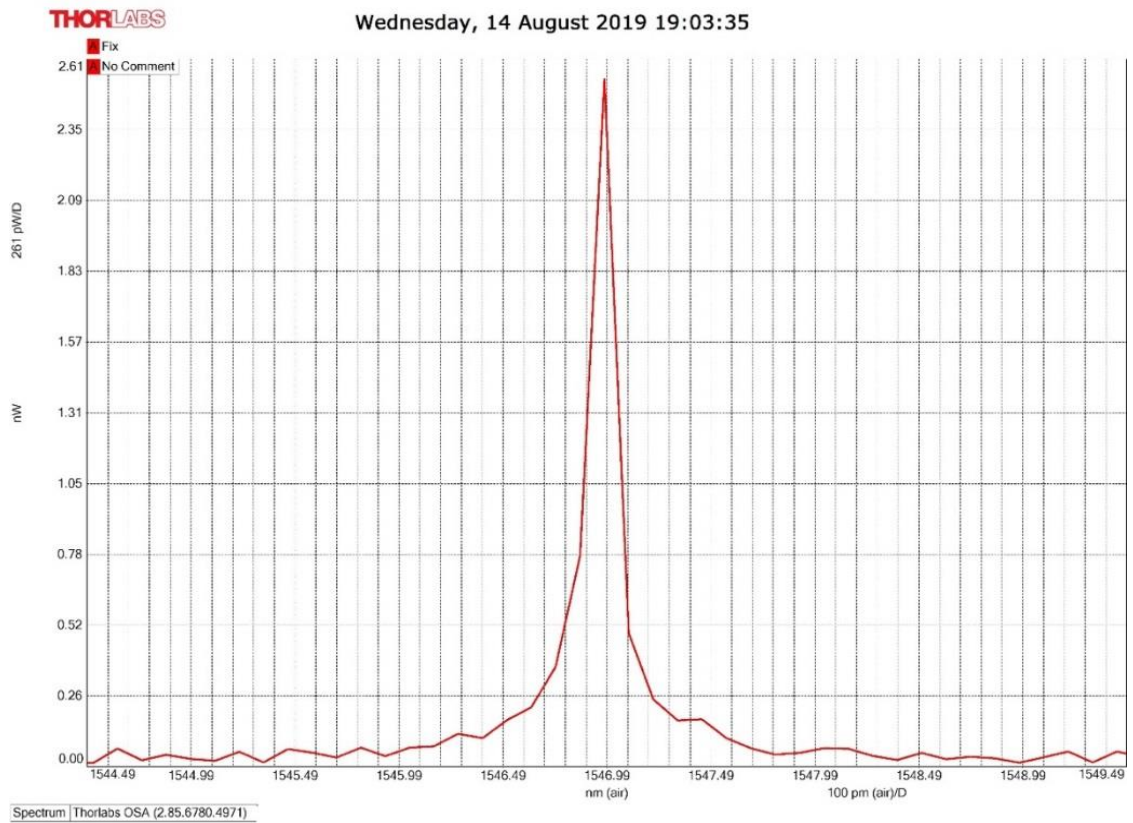


(a)

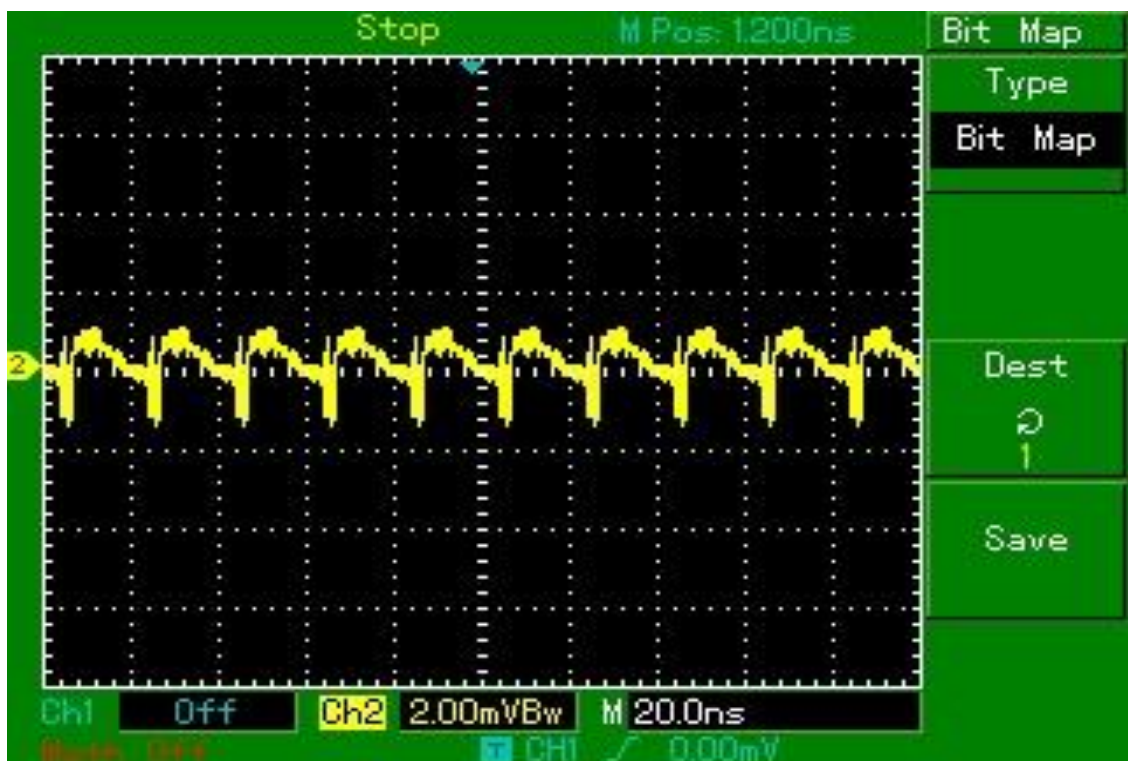


(b)

Fig. 3.5 Compressed signal in frequency and time domains for four lengths of 7 cells PCF a-b) 7 cm length, c-d) 12 cm length, e-f) 20 cm length, g-h) 30 cm length.

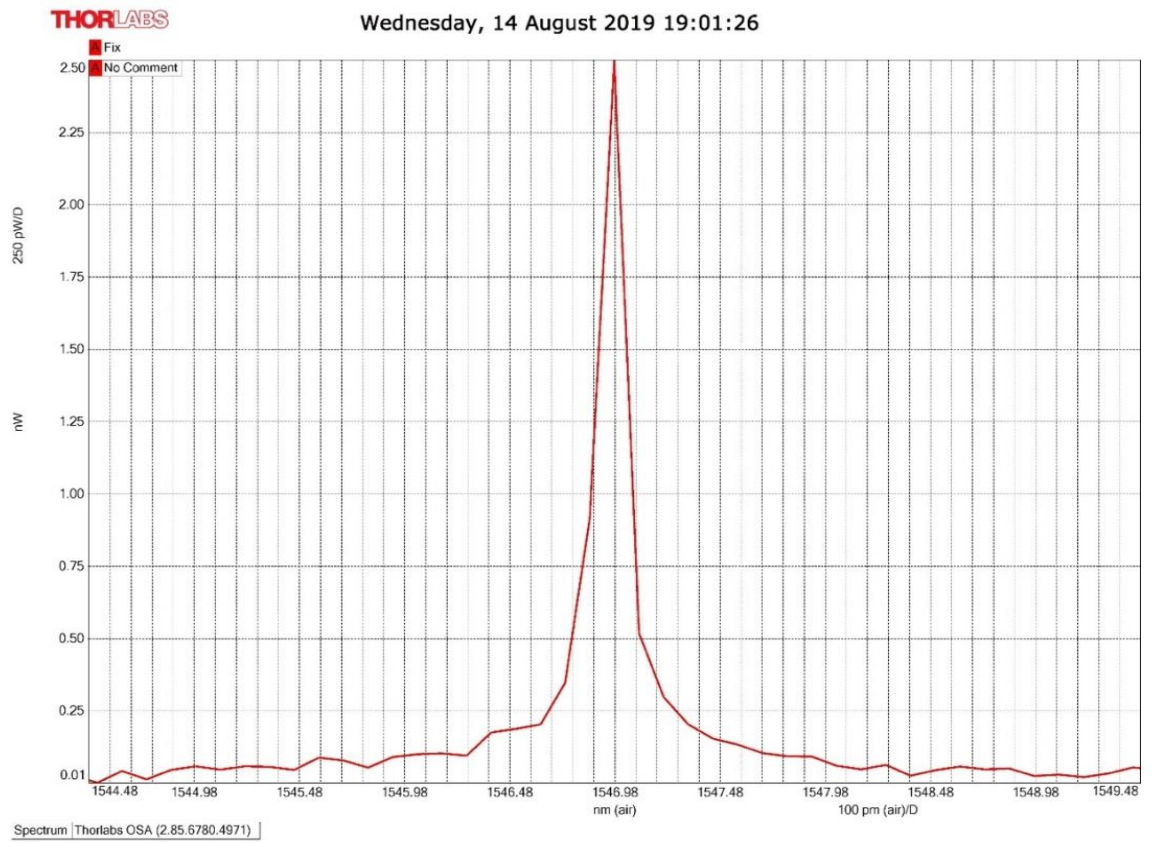


(c)

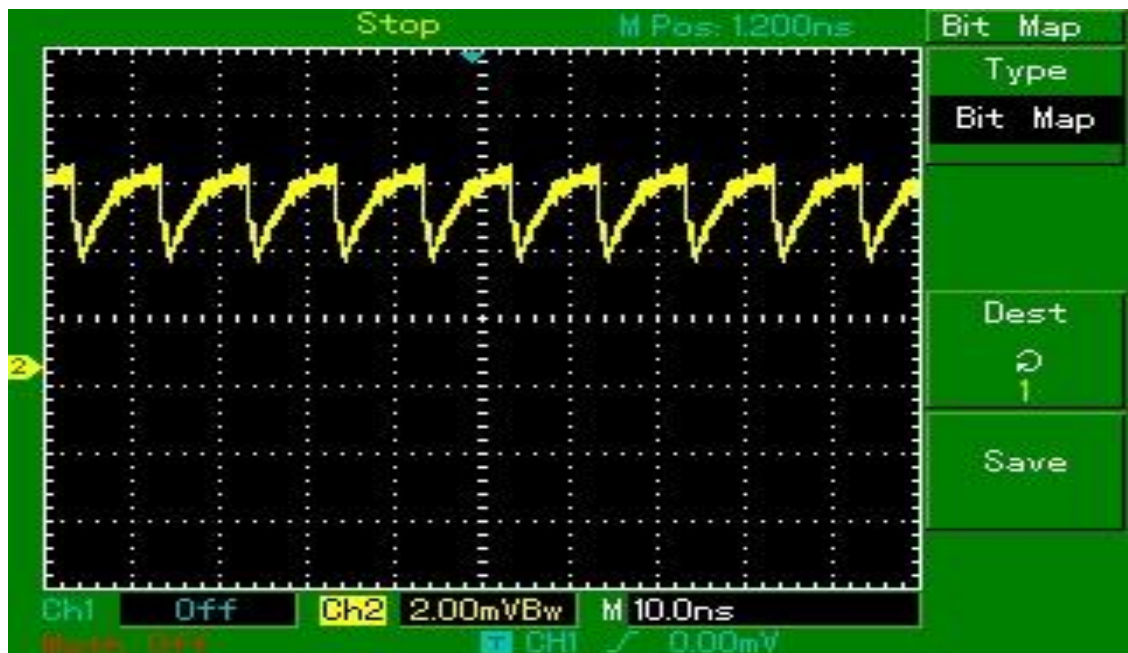


(d)

Fig. 3.5 (continued)

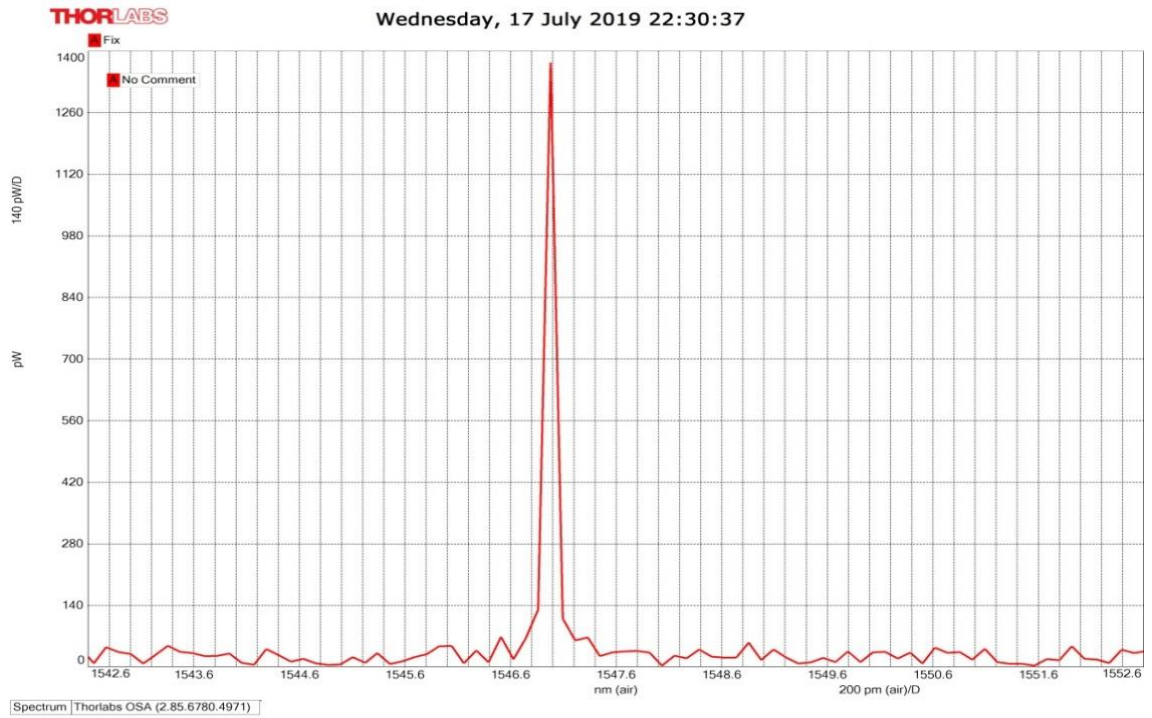


(e)

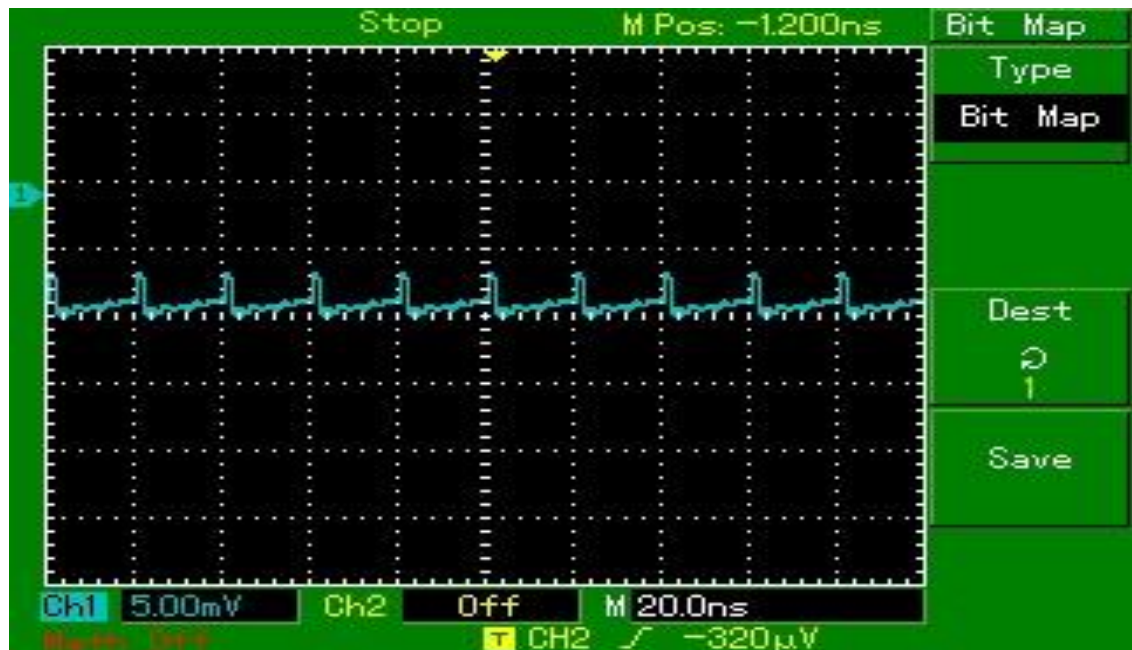


(f)

Fig. 3.5 (continued).



(g)



(h)

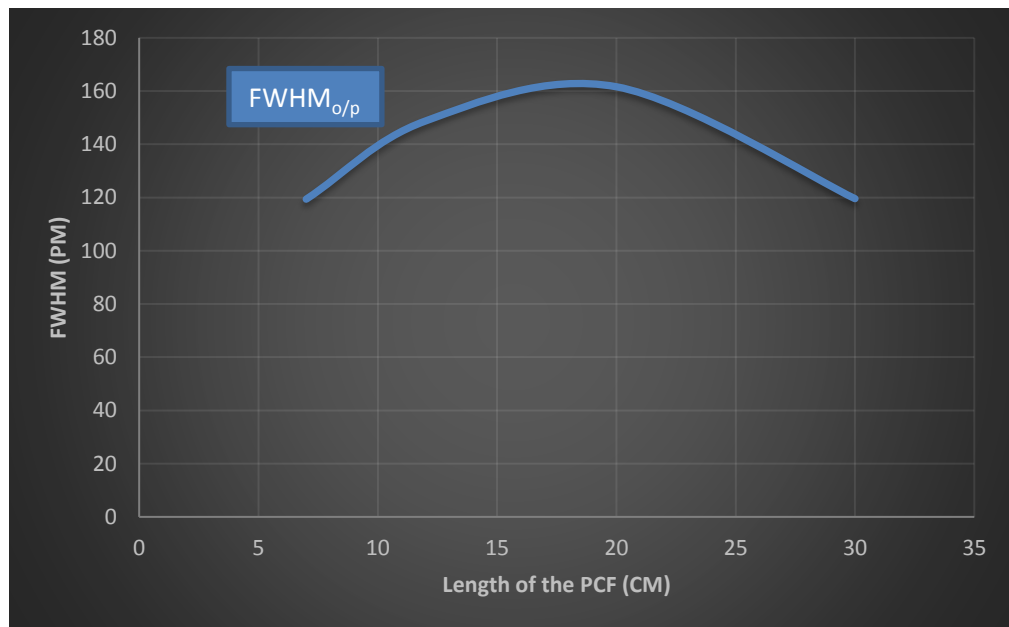
**Fig. 3.5 (continued).**

The compressed signals presented in Figure 3.5 are summarized in table 3.2, and to investigate the related compression factor. As can be observed the shortest length of PCF gives the highest value of the compression factor, when 7 cm PCF length was used, a compression factor of 2.39 is obtained depending on Eq. 1.37.

**Table 3.2 Relationship between 7 cells HC-PCF length, FWHM and compression factor.**

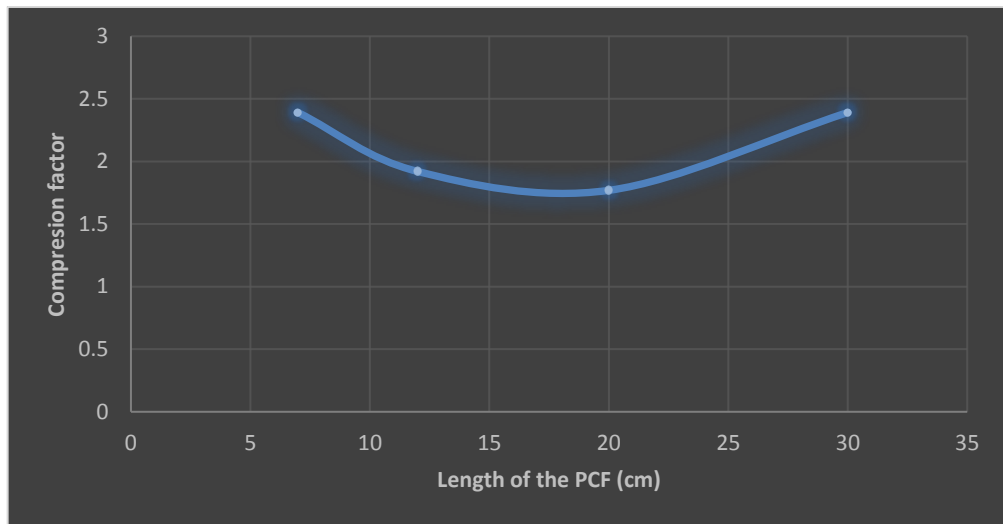
Length of 7 cells HC-PCF (cm)	FWHM (pm)	FWHM (ns)	$F_c$
7	119.384	16	2.39
12	148.76	12	1.92
20	161.622	8	1.769
30	119.583	16	2.391

To explore the influence of PCF length on the FWHM of the compressed pulse and the related compression factor, Figure 3.6 (a-b) are plotted. It can be seen that as the length of PCF increases the FWHM of the compressed pulsed increased until decrease dramatically with the maximum length of PCF (30 cm), as shown in Figure 3.6 (a). From Figure 3.6 (b), the compression factor decreases as the PCF length increases and rapidly increased at maximum length of PCF (30cm).



(a)

**Fig. 3.6 Relationship between length of 7 cells PCF and a) Full width at half maximum (FWHM), b) Compression factor ( $F_c$ ).**



(b)

**Fig. 3.6 (Continued)**

### **3.3.2 Pulse Compression Based on Infiltrated of 19 cells Hollow Core Photonic Crystal Fiber**

In order to enhance the compression of the optical pulse, infiltration technique was used. The infiltration setup was presented in 2.3.3, the 19 cell HC-PCF was infiltrated in different organic liquids as explained briefly in the following subsections:

#### **3.3.2.1 Pulse Compression using Infiltrated of 19 cells Hollow Core Photonic Crystal Fiber with Ethanol**

Figure 3.7 shows the compressed pulse obtained from 19 cell hollow core photonic crystal fiber. It can be seen that the full width at half maximum (FWHM) of the compressed pulse is 110.007 pm and the compression factor results is 2.6 depending on Eq. 1.37.

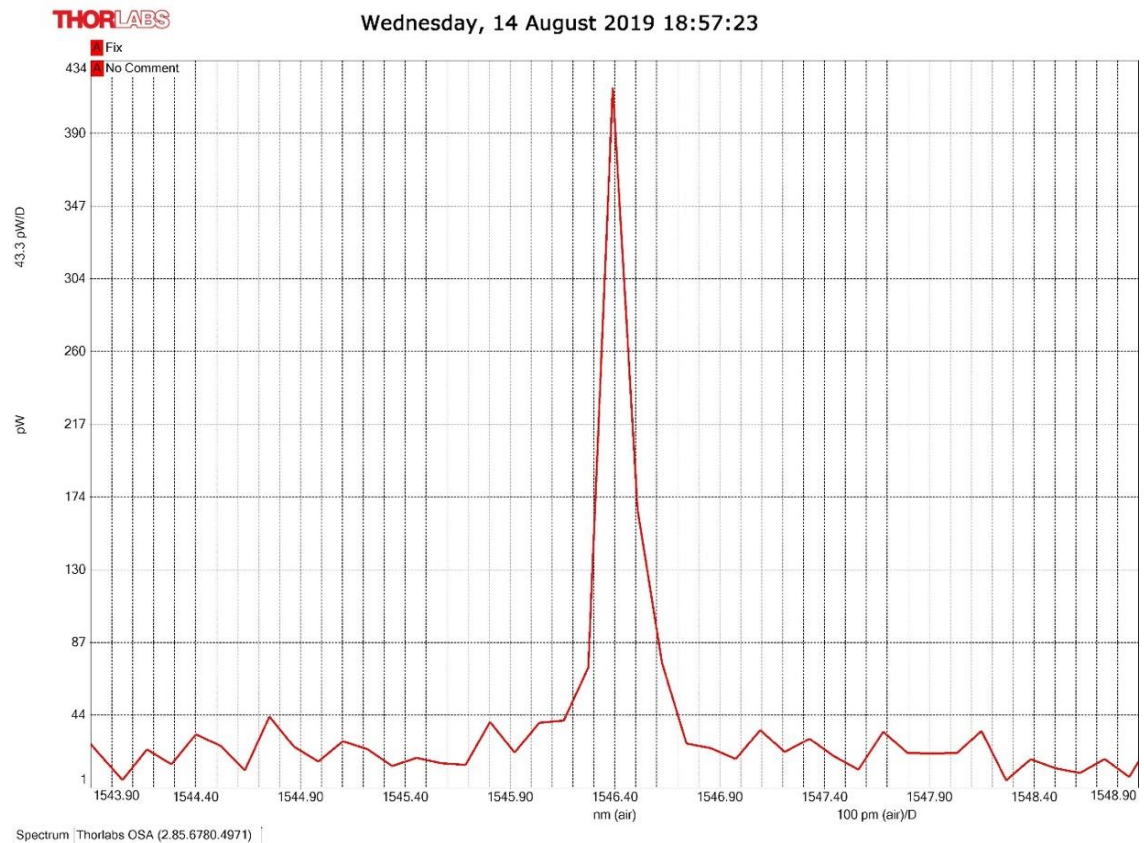


**Fig. 3.7 Optical spectrum of compressed pulse using Infiltrated sample of 19 cells HC-PCF by Ethanol.**

### **3.3.2.3 Pulse Compression Based on Infiltrated of 19 cells Hollow Core Photonic Crystal Fiber with Acrylic Acid Solution**

Infiltration process applied for two reasons:

- 1- To ensure the guiding mechanism (i.e. modified total internal reflection MTIR in SC-PCF and Photonic band gap effect PBG in HC-PCF) in 19 cells HC-PCF not change (i.e. core refractive index less than clad refractive index, which is 1.455 at 20 °C).
- 2- Acrylic acid does not use to infiltrate the fiber due to its high viscosity as explained in subsection 2.3.3.3.

Therefore, Acrylic acid was diluted in ethanol. Where 75% of Ethanol and 25% Acrylic acid are mixed well enough, the acrylic acid solution has sufficient viscosity and keep PBGE as guiding mechanism. The new refractive index had been measured experimentally, by using the

refractometer, the refractive index of the acrylic acid solution is 1.395 at 1550 nm and 20°C temperature. The resultant refractive indices can be summarized in table 3.3.

**Table 3.3 Refractive index for chemical materials.**

Chemical liquids	Refractive index	Temperature	Wavelength
Ethanol	1.353	20 ° C	1550 nm
Acrylic acid	1.5	20 ° C	1550 nm
Acrylic acid solution	1.395	20 ° C	1550 nm

In order to improve the pulse compression, Acrylic acid solution is infiltrated in 7cm of 19 cell HC-PCF. Figure 3.8 shows the compressed pulse from infiltrated fiber. From this figure, it can be observed that the FWHM of 58.367 and the compression factor of 4.9 were obtained depending on Eq. 1.37.

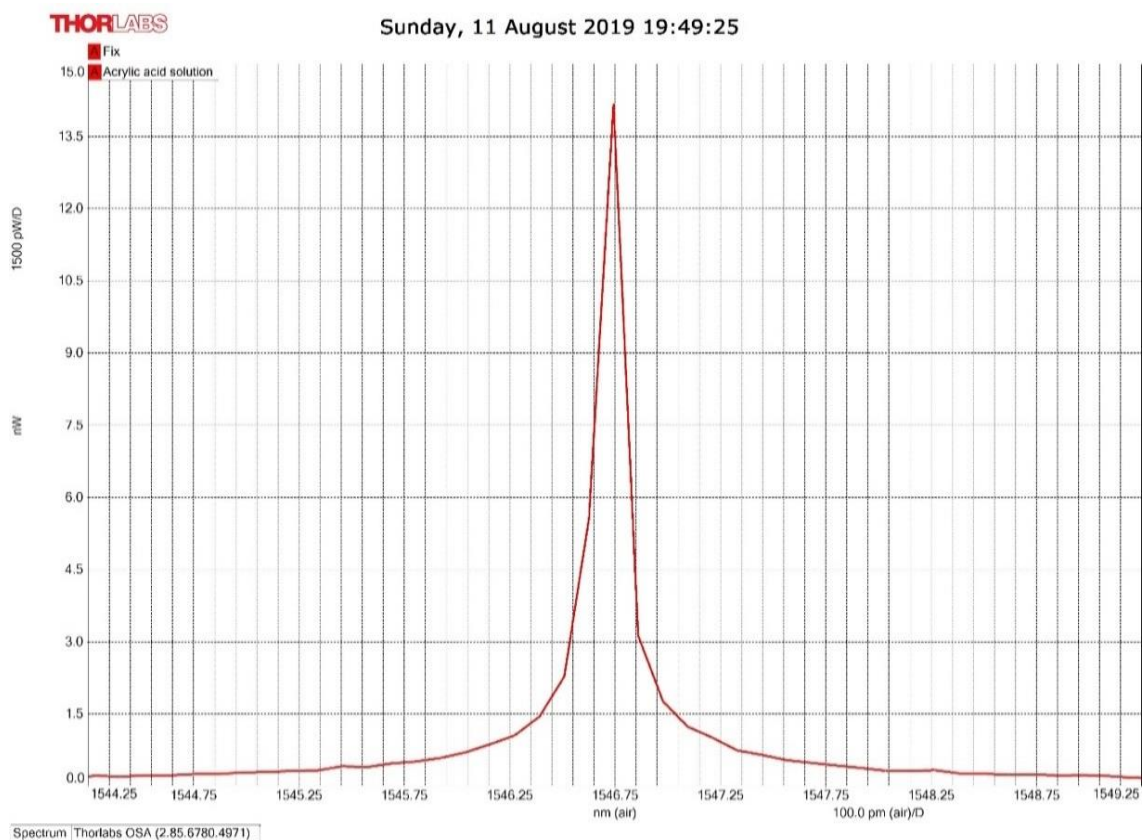


**Fig. 3. 8 Optical spectrum of the compressed pulse using Infiltrated 19 cells HC-PCF by Acrylic acid solution.**

### 3.4 Pulse Compression Based on Solid Core Photonic Crystal Fiber

The results of pulse compression based on Mach-Zehnder interferometers are given in this section. These interferometers were constructed using solid core PCF (ESM and PM) as explained in section 2.3.2. To enhance the pulse compression, dispersion compensation fiber (DCF) is connected in cascaded manner with Mach-Zehnder interferometers.

#### 3.4.1 Pulse Compression Based on Polarization Maintaining Fiber

The experimental results of the pulse compression setup that depicted in Figure 2.27 are introduced in Figure 3.9. This figure shows the compressed pulse obtained from solid core photonic crystal polarization maintaining fiber (SC-PCF: PM-1550-01) using 7 cm long of PM SC-PCF. The PM-1550-01 has a strong form-birefringence and is optimized to create a short beat length between the polarizations. Furthermore, it has reduced bend-induced coupling between polarization states, an improved polarization extinction ratio. The FWHM of compressed pulse is 117.672 pm and the compression factor obtained was 2.43 depending on Eq. 1.37 as shown in Figure 3.9.

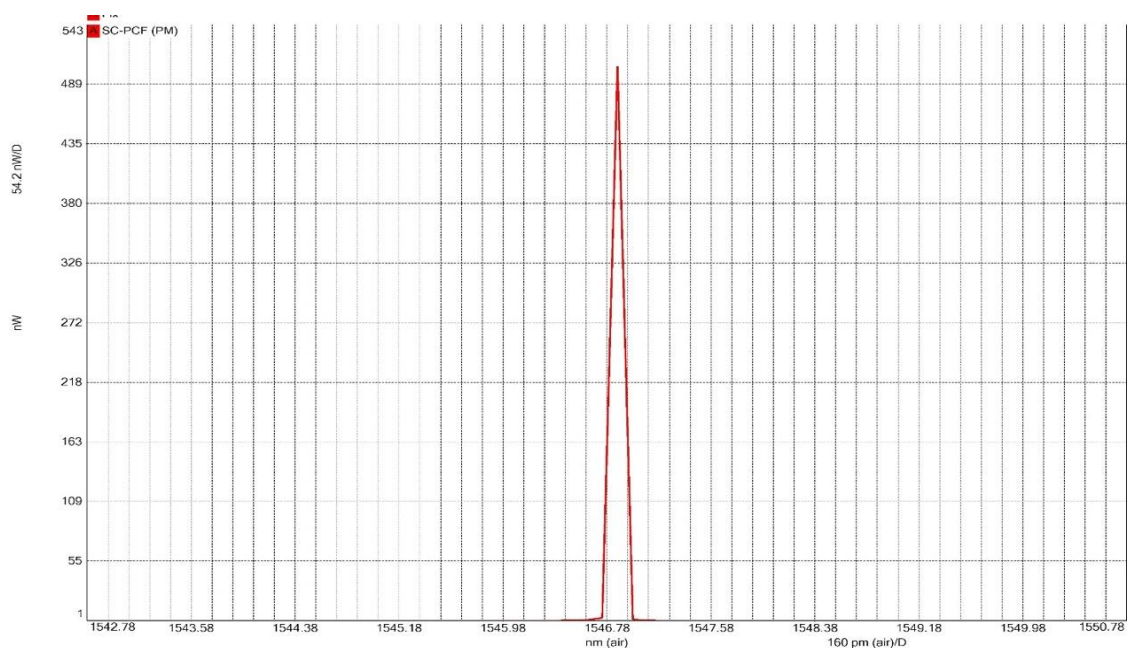


**Fig. 3.9 Optical spectrum of the compressed pulse using PM-1550-01.**

### 3.4.2 Pulse Compression Based on Endless Single Mode

The experimental results of the pulse compression setup shown in Figure 2.27 are depicted in Figure 3.10. This figure shows the compressed pulse using 7 cm long of ESM-12 SC-PCF; this single-mode photonic crystal fiber is optimized to low loss across 700 nm to above 1700 nm while keeping an almost constant mode field diameter (MFD). The fiber is endlessly single-mode with no higher order mode cut-off and delivers excellent mode quality at all wavelengths. The full width at half maximum (FWHM) of the compressed pulse is 135.52 pm while the compression factor of 2.11 was obtained.

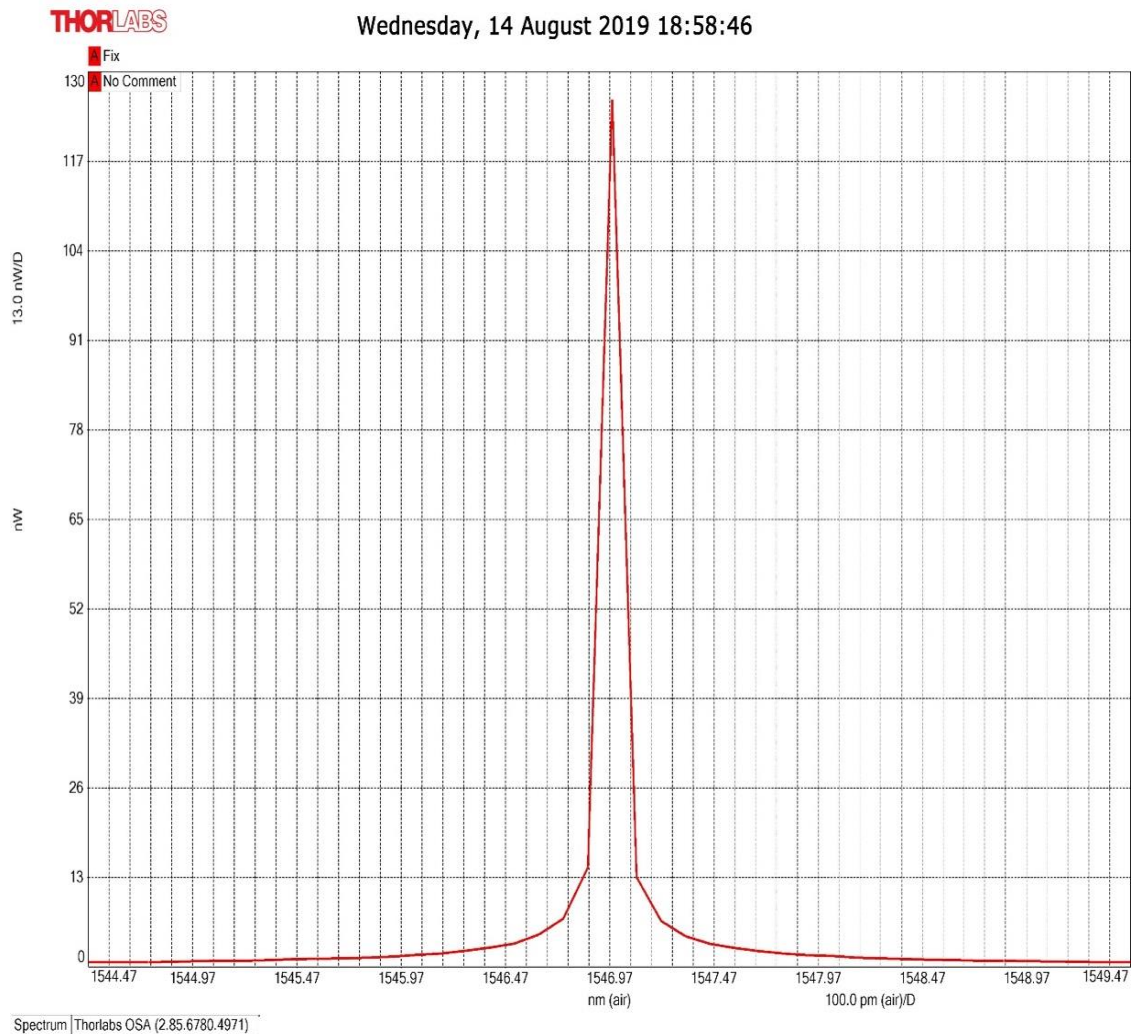
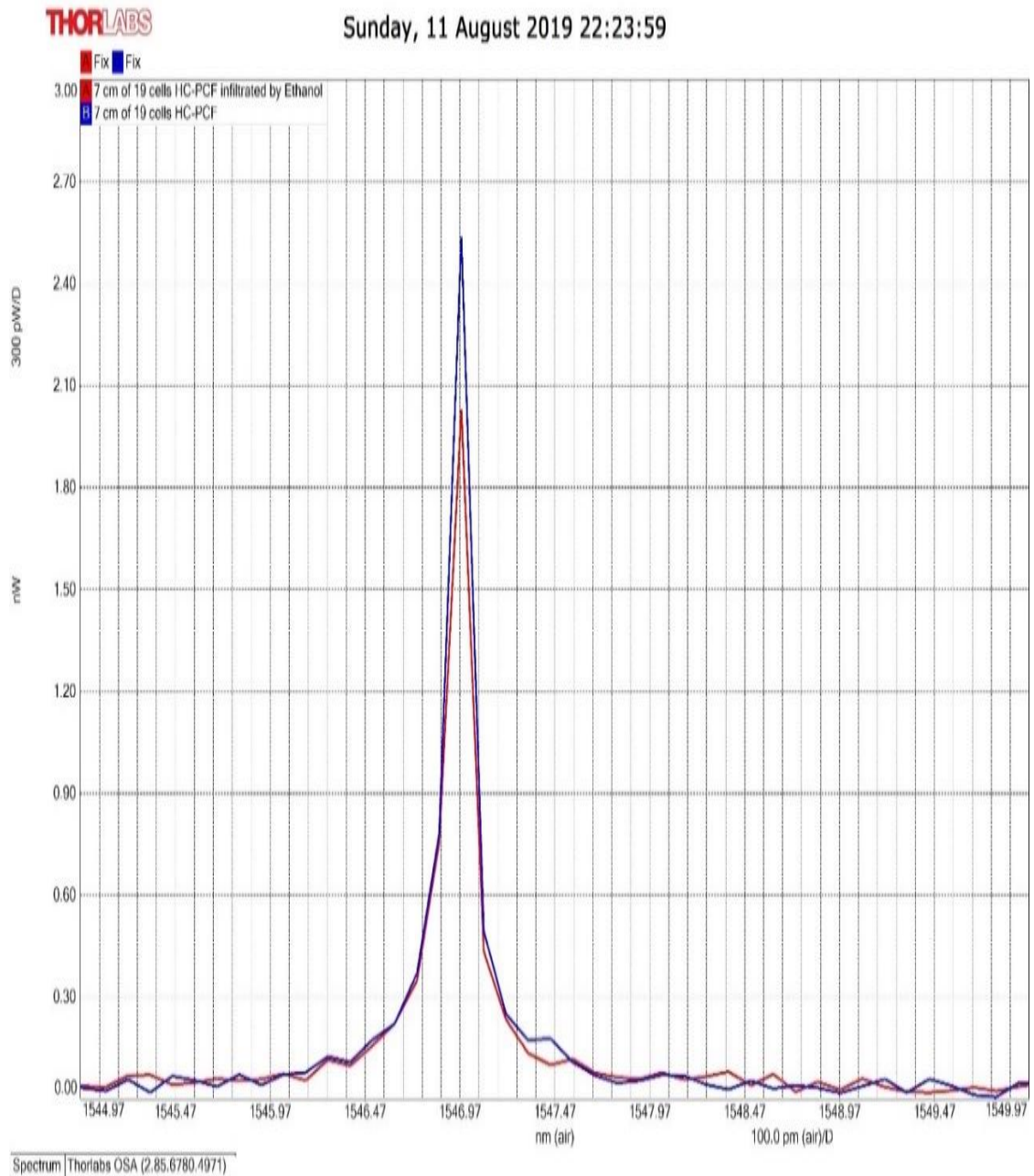


**Fig. 3.50** Optical spectrum of the compressed pulse using ESM.

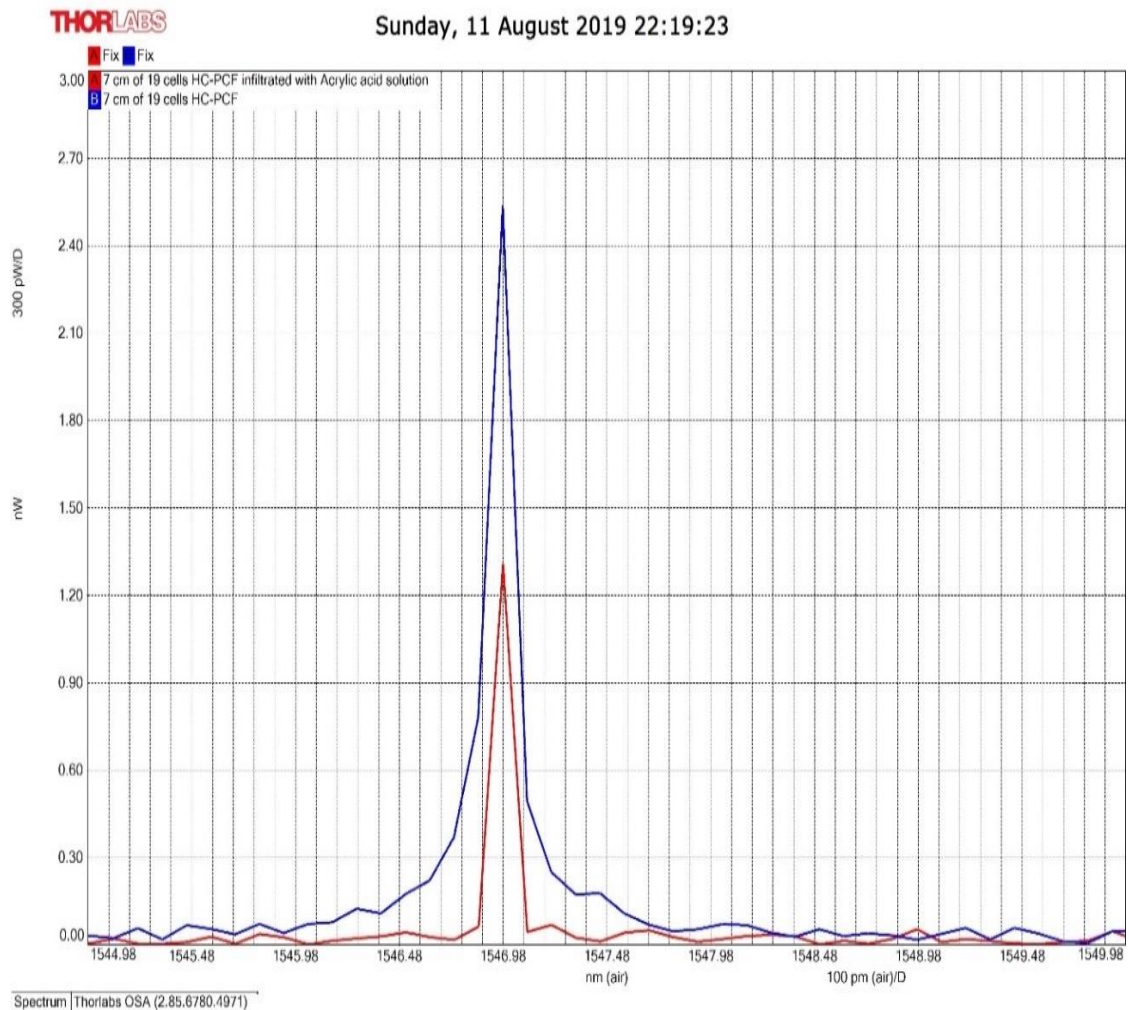
### 3.5 Performance comparison of 19 cells Hollow Core Photonic Crystal Fiber

This section introduce comparison between full width at half maximum and compression factor in 19 cells HC-PCF before and after infiltration by different chemical materials (i.e. ethanol and acrylic acid solution) as explained in Figure 3.11 (a-b).



(a)

**Fig. 3.11 Optical spectra of 19 cells HC-PCF infiltrated by a) ethanol b) acrylic acid solution.**



(b)

**Fig. 3.11 Continued.**

To explore the compression factor and full width at half maximum that obtained from 7 cm length of 19 cells HC-PCF before and after infiltration by ethanol and acrylic acid solution, table 3.4 summarizes the compression factor obtained by infiltration with ethanol has increased by 0.17 while FWHM decreased by 7.253, and when infiltrate by acrylic acid solution, the compression factor has increased by 2.47 and FWHM decreased by 58.893, as explained in Figures 3.11 (a) and (b), respectively.

**Table 3.4 Effects of infiltration on compression factor and full width at half maximum.**

<b>19 cells HC-PCF</b>	<b>FWHM (pm)</b>	<b>F<sub>c</sub></b>
Air filled holes fiber	117.26	2.43
Infiltrated fiber by Ethanol	110.007	2.6
Infiltrated fiber by Acrylic acid solution	58.367	4.9

Table 3.5 summarizes the obtained compression factor and FWHM in all experiments that occurs with respect to obtained F<sub>c</sub> from infiltration of 19 cells HC-PCF by acrylic acid solution and to FWHM of the source. It seems that infiltration process gives more compression factor than using merely HC-PCF, also 19 cells HC-PCF gives compression factor larger than 7 cells for same optimum length obtained in experiments.

**Table 3.5 percentage values of F<sub>c</sub> and FWHM**

Fiber		Length of Fiber in cm	F <sub>c</sub> %	FWHM %
HC-PCF	19 cells	7	0.49	0.41
		12	0.38	0.52
		20	0.27	0.37
		30	0.49	0.41
	7 cells	7	0.48	0.417
		12	0.39	0.52
		20	0.36	0.56
		30	0.48	0.418
Infiltrated 19 cells HC-PCF	Ethanol	7	0.53	0.384
	Acrylic acid solution	7	100 %	100 %
SC-PCF	PM	7	0.49	0.411
	ESM	7	0.43	0.473

### 3.6 Conclusion

The figure of merit to study the pulse compression is the fiber normalized frequency which is decided the number of guided modes in fiber core that is means de-excitation of the higher order modes in the fiber core-cladding region. In this thesis, the difference between core-clade refractive indices in the hollow core photonic crystal fibers were be controlled, minimized. After replacing of the air in the holes by a chemical compounds.

- 1- Compression pulse laser was obtained by designing electronic chopping circuit to achieve 10 ns pulse width, 30 MHz as a pulse repetition rate that aids to minimize the chromatic dispersion.
- 2- The maximum compressed optical pulse was obtained in the case of Fabry-Perot etalon 19 cell hollow core photonic crystal fiber and 7 cm length because of its minimum dispersion at 1550 nm which equal to 18 ps/nm/km.
- 3- After replacing the air holes of 7 cm, 19 cell hollow core photonic crystal fiber that formed Fabry-Perot etalon interferometer with acrylic acid solution (25% ethanol and 75% acrylic acid), maximum compression factor ( $F_C$ ) was obtained is equal to 4.9 because of decreasing the fiber index contrast.
- 4- Maximum guiding mode fiber core can be obtained in the case of replacing the fiber air holes with the material that has refractive index closer to index of silica which minimized the normalized frequency with fixed fiber core and pulse propagation wavelength.
- 5- The fiber's full width at half maximum has a zig-zag shape with respect to core refractive index and fiber length variations caused by fiber sensitivity to polarization according to the Faraday Effect.

### 3.7 Future Work

In this work, in line photonic crystal fiber was built as pulse compressor device and many works can be established in future that are listed below:-

- 1- Using cascade in line photonic crystal fiber interferometer for generating comp laser source.
- 2- Using non-linear Mach-Zhender interferometer for generating four wave mixing (FWM) and cross phase modulation (XPM).
- 3- Propagate the compressed data via optical communication link for studying the generating of soliton wave.
- 4- Using a microfiber instead of PCF as a fiber compressor.
- 5- Replace the photonic crystal fiber air holes by a Nano fluid material.
- 6- Build a new type of interferometer using multi core photonic crystal fiber.
- 7- Using selectively infiltrate of photonic crystal fiber for pulse compressor technique.
- 8- Study the effect of infiltration and core size on the propagation of guided mode in the case of high laser peak power ( $P_p$ ).
- 9- Analysis and studying the two air micro cavity region on the quality of the guided mode.
- 10- Calculating the nonlinear refractive index of organic liquid with different dilution ratios.

## References

- [1] Y. Wang, L. Xiao, D. N. Wang, and W. Jin, "In-fiber polarizer based on a long-period fiber grating written on photonic crystal fiber," *Opt. Letters* 32, 1035-1037, 2007.
- [2] J. C. Knight, T. A. Birks, P. S. J. Russell, and D. M. Atkin, "All-silica single-mode optical fiber with photonic crystal cladding," *Opt. Lett.*, vol. 21, no. 19, pp. 1547–1549, Oct. 1996.
- [3] Y. Wang, W. Jin, J. Ju, H. Xuan, H. L. Ho, L. Xiao, and D. Wang, "Long period gratings in air-core photonic bandgap fibers," *Opt. Express* 16, 2784-2790, 2008.
- [4] J.C. Knight, "Photonics crystal fibers", *Nature*, pp 424, 2003.
- [5] P. St. J. Russell, "Photonic-crystal fibers," *J. Lightwave Technol.* 24(12), 4729–4749, 2006.
- [6] Sinha, R. K., Varshney, S. K., "Estimation of Splice loss in Photonic Crystal Fibers", *Photonic Bandgap Materials and Devices*, Vol. 4655, 2002.
- [7] Ali Reza Bahrampour, Sara Tofighi, Marzieh Bathaee and Farnaz Farman "Optical Fiber Interferometers and Their Applications" *Intach*, Vol.41, No.22, pp.4460-4483, 2012.
- [8] Bahrampour.A.R, Bathaee.S.M, and Farman .F." Optical Fiber Interferometers and Their Applications" *Optics Communications*, Vol. 282, No. 12, pp. 2451-2456, 2012.
- [9] Sagnac, G," L'ether lumineux demontre par l'effet du vent relatif d'ether dans un interferometre en rotation uniforme" *C. R. Acad. Sci*, Vol. 157, pp. 708-710, 1913.
- [10] Burns, W.K.," Optical Fiber Rotation Sensing ", Academic Press, 1993.
- [11] W. H. Reeves, J. C. Knight, P. S. J. Russell, and P. J. Roberts, "Demonstration of ultra-flattened dispersion in photonic crystal fibers", *Opt. Express*, Vol.10, pp.609-613, 2002.

- [12] H. Y. Choi, M. J. Kim, and B. H. Lee, "All-fiber Mach-Zehnder type interferometers formed in photonic crystal fiber," *Optics express*, vol. 15, no. 9, pp. 5711–5720, 2007.
- [13] Shizhuo Yin, S.; Ruffin, P.B." *Fiber Optic sensor*", CRC Press, pp.978-982, 2008.
- [14] Y. J. Rao, T. Zhu, X. C. Yang, and D. W. Duan," *In-line fiber-optic etalon formed by hollow-core photonic crystal fiber*",*Optics Letters*, Vol.32,No.18, pp. 2662-2664, 2007.
- [15] R. Buczynski, "photonic crystal fiber Borofsky making history," vol. 106, no. 2, pp. 141–167, 2004.
- [16] F. Poli, A. Cucinotta, and S. Selleri, "Photonic crystal fibers: properties and applications", vol. 470, no. 7332. 2007.
- [17] J. J. D. Joannopoulos, S. Johnson, J. N. J. Winn, and R. R. D. Meade, "Photonic crystals: molding the flow of light", 2008.
- [18] L. Tan, S. Cao, Y. Wang, and B. Zhu, "Direct and inverse iterative design method for centrifugal pump impellers," *Proceedings of the Institution of Mechanical Engineers, Part A: Journal of Power and Energy*, vol. 226, no. 6, pp. 764–775, 2012.
- [19] F. Poletti, "Direct and inverse design of microstructure optical fiber," PhD thesis, Southampton, 2007.
- [20] R. Paschotta, "field guide to optical fiber Technology," 1st edition, 2010.
- [21] A.D. Kersey, M. A. Davis, H. J. Patrick, M. LeBlanc, K. P. Koo, C. G. Askins, M. A. Putnam, and E. J. Friebele, "Fiber grating sensors," *Journal of Lightwave Technology*, vol. 15, no. 8, pp. 1442–1463, 1997.
- [22] O. De-qin, G. Chun- yu, R. Shuang, W. Yi-ming, Y. Jin-hui, W. Hui-feng, "theoretical and experimental analysis of splicing between the Photonic crystal fiber and the conventional fiber using grin fibers," *Applied optics*, Vol 51, pp.8520-8520, 2012.

- [23] A.D. Yablon and R. T. Bise, "Low-loss high-strength microstructured fiber fusion splices using GRIN fiber lenses," *IEEE Photonics Technology Letters*, vol. 17, no. 1, pp. 118–120, 2005.
- [24] C. L. Yu, D. P. Gao, F. Wang, R. J. Huo, X. M. Hao, and X. L. Xie, "Interpretation of Frenkel's theory of sintering considering evolution of activated pores: III. Determination of equilibrium sintering time," *Sci. Sinter.*, vol. 47, no. 2, pp. 215–219, 2015.
- [25] S. Zuoming, S. Ningfang, J. Jing, S. Jingming, and M. Pan, "Low loss fusion splicing polarization-maintaining photonic crystal fiber and conventional polarization-maintaining fiber," *Optical Fiber Technology*, vol. 18, no. 6, pp. 452–456, 2012.
- [26] P. J. Bennett, T.M. Monro, and D. J. Richardson, "Toward practical holey fiber technology: Fabrication, splicing, modeling and characterization," *optics Letters*, vol.24, no.17, pp.1203-1220, 1999.
- [27] M. Murawski, L. R. Jaroszewicz, and K. Stasiewicz, "A photonic crystal fiber splice with a standard single mode fiber," *Photonics Letters of Poland*, vol. 1, no. 3, pp. 115–117, 2009.
- [28] Z. Chen, X. Xi, W. Zhang, J. Hou, and Z. Jiang, "Low-loss fusion splicing photonic crystal fibers and double cladding fibers by controlled hole collapse and tapering," *Journal of Lightwave Technology*, vol. 29, no. 24, pp. 3744–3747, 2011.
- [29] W. Jin, Z. Wang, and J. Ju, "Two-mode photonic crystal fibers.," *Optics express*, vol. 13, no. 6, pp. 2082–8, 2005.
- [30] K. Hansen, "Dispersion flattened hybrid-core nonlinear photonic crystal fiber," *Optics Express*, vol. 11, no. 13, p. 1503, 2003.
- [31] B. T. KUHLMEY, "Theoretical and Numerical Investigation of the Physics of Microstructured Optical Fibres", PhD thesis, 2004.
- [32] OFS Furukawa Company, "Understanding fiber optic attenuation" springer series, 2007.

- [33] N. Massa, "Fundamental of Photonics Fiber Optic Telecommunication" Springer series, 2000.
- [34] X. Feng, A. K. Mairaj, D. W. Hewak and T. M. Monro, "Towards high-index glass based monomode holey fiber with large mode area," *Electronics Letters* Vol.40, pp.167-169, 2004.
- [35] F. Poletti, "Direct and inverse design of microstructure optical fiber," PhD thesis, Southampton, 2007.
- [36] J. Kim, "Analysis and Application of Microstructure and Holey Optical Fibers", Ph.D Thesis, 2003.
- [37] N. Massa, "Fundamental of Photonics Fiber Optic Telecommunication", *Opt. Express* Vol.12, pp.835-840, 2000.
- [38] V. Finazzi, T. M. Monro, and D. J. Richardson, "The Role of Confinement Loss in Highly Nonlinear Silica Holey Fibers", *IEEE photonics technology letters*, Vol. 15, No.9, 2003.
- [39] J. Vijay and M. Sabir, "Low-Flattened Dispersion Hexagonal Photonic Crystal Fiber With Low Confinement Loss" *International Journal of Emerging Technology and Advanced Engineering*, Vol. 3, No. 1, 2013.
- [40] T. M. Monro; J. C. Baggett and D. J. Richardson, "Comparative Study of Bend loss in large Mode Holey and conventional Fibers", PH.D, 2001.
- [41] M. D. Nielson; N. A. Mortensen; M. Albertsen; j. r. Folken Berg; A. Bjarklev; and D. Bonacinni, "Predicting Macrobending loss for large Mode Area Photonic Crystal Fibers", *Optics Express*, Vol.12, pp. 1775-1779, 2004.
- [42] M. Ming –K.Liu, "Principles and Applications of – Optical Communication", McGraw –Hill, 1996.
- [43] K. L. G. Wong, "Non Linear Optics in Photonic crystal fiber" MS.c thesis, 2003.
- [44] T. A. Birks; D. M. Bird; T. D. Hedley; J. M. Pottage; and P. St. J. Russell, "Scaling laws and Vector effects in Bandgap Guiding Fibers" *Optics Express*, Vol.12, pp. 69 -74, 2004.

- [45] Elden, Metrologia, "Refractive index of air" Optics Express, Vol. 2 No.71, 1966.
- [46] F. A. Jenkis and H. E. White, "Fundamentals of optics" McGraw –Hill, 3rd edition, 1957.
- [47] K. Okamoto, "Fundamentals of optical waveguides" academic press, 2000.
- [48] P. G Agrawal, "Nonlinear Fiber Optics," Third Edition, 2001.
- [49] G. Antonopoulos; F. Benabid; T.A. Birks; D. M.Bird; J. C. Knight and P. St. J.Russel, "Experiment Demonstration of the Frequency Shift of Bandgaps in Photonic Crystal fibers Due to Refractive index Scaling", Optics Express Vol.14, No. 7, April 2006.
- [50] E. Wintner,"Ultra-Short-Pulse Laser Technology" M.Sc. thesis, 2001.
- [51] G. Keiser, "Optical Fiber Communications," 3rd edition, 2000.
- [52] John E. Greivenkamp "Field guide to Optical Fiber Technology", spie series, 2010.
- [53] B. Zsigri, "Photonic Crystal Fiber as Transmission Medium for Future Optical Communication Systems", Technical university of Denmark, Vol. 10, 2006.
- [54] J. Kim, "Analysis and Application of Microstructure and Hollow Optical Fibers", Ph.D Thesis, 2003.
- [55] D. A. Zheltikova; M. Scalova; A. M. Zhdtikov; M. J. Bloemer; M. N. Shneider; G. D. Aguanno; and R. B. Milles, "Switching intense Laser pulses Guided by Kerr-Effect-Modified Modes Of a Hollow –core Photonic crystal Fiber", Physical Review E71, 2005.
- [56] G. Agrawal, "Applications of Nonlinear Fiber Optics", Academic Press, ch.2, pp.160, 2001.
- [57] A. K. Abeeluck and C. Headley, "Continuous-wave pumping in the anomalous- and normal-dispersion regimes of nonlinear fibers for supercontinuum generation", Opt. Lett.Vol.30, pp. 61-63, 2005.

- [58] D. Yevick and B. Hermansson, "Efficient beam propagation techniques", IEEE J. Quantum Electron. Vol.26, pp.109-112, 1990.
- [59] N. A. Mortensen, "Effective area of photonic crystal fibers", Opt. Express, Vol.10, pp.341-348, 2002.
- [60] D.G. Ouzounov, C.J. Hensley, A.L. Gaeta, N. Venkateraman, M.T. Gallagher, K.W. Koch, "Soliton pulse compression in photonic band-gap fibers" Optics Express 13 , 2005.
- [61] Dimitre G. Ouzounov, Christopher J. Hensley and Alexander L. Gaeta "Soliton pulse compression in photonic band-gap fibers", Optics Express, Vol.13, No.16, pp.6153, 2005.
- [62] Yingying Wang, Meshaal Alharbi , Thomas D. Bradley, Coralie Fourcade-Dutin, Benoît Debord, Benoît Beaudou, Frédéric Gerôme, and Fetah Benabid "Hollow-core photonic crystal fibre for high power laser beam delivery" High Power Laser Science and Engineering , Vol.1, No. 1, pp.17–28, 2013.
- [63] Tuomo Ritari "Novel Sensor and Telecommunication Application of Photonic Crystal Fibers" TKK Dissertations, Vol.39, 2006.
- [64] Yashar E. Monfared, A. Mojtahedinia, A. R. Maleki Javan, A. R. Monajati Kashani "Highly nonlinear enhanced-core photonic crystal fiber with low dispersion for wavelength conversion based on four-wave mixing" Front. Optoelectron, Vol.6, No.3, pp.297–302, 2013.
- [65] John E. Greivenkamp "Field guide to Optical Fiber Technology", spie series, 2010.
- [66] J. Rheims, J Köser and T Wriedt. Refractive-index measurements in the near-IR using an Abbe refractometer, Meas. Sci. Technol. 8, 601-605, 1997.

# Appendices

## Appendix A

### Corning® SMF-28™ Optical Fiber Product Information



PI1056  
 Issued: April 2002  
 Supersedes: December 2001  
 ISO 9001 Registered

### Corning® Single-Mode Optical Fiber

#### The Standard For Performance

Corning® SMF-28™ single-mode optical fiber has set the standard for value and performance for telephony, cable television, submarine, and utility network applications. Widely used in the transmission of voice, data, and/or video services, SMF-28 fiber is manufactured to the most demanding specifications in the industry. SMF-28 fiber meets or exceeds ITU-T Recommendation G.652, TIA/EIA-492CAAA, IEC Publication 60793-2 and GR-20-CORE requirements.

Taking advantage of today's high-capacity, low-cost transmission components developed for the 1310 nm window, SMF-28 fiber features low dispersion and is optimized for use in the 1310 nm wavelength region. SMF-28 fiber also can be used effectively with TDM and WDM systems operating in the 1550 nm wavelength region.

#### Features And Benefits

- Versatility in 1310 nm and 1550 nm applications
- Enhanced optical properties that optimize transmission performance
- Outstanding geometrical properties for low splice loss and high splice yield
- OVD manufacturing reliability and product consistency
- Optimized for use in loose tube, ribbon, and other common cable design

#### The Sales Leader

Corning SMF-28 fiber is the world's best selling fiber. In 2001, SMF-28 fiber was deployed in over 45 countries around the world. All types of network providers count on this fiber to support network expansion into the 21st Century.

## Protection And Versatility

SMF-28 fiber is protected for long-term performance and reliability by the CPC<sup>®</sup> coating system. Corning's enhanced, dual acrylate CPC coatings provide excellent fiber protection and are easy to work with. CPC coatings are designed to be mechanically stripped and have an outside diameter of 245  $\mu\text{m}$ . They are optimized for use in many single- and multi-fiber cable designs including loose tube, ribbon, slotted core, and tight buffer cables.

## Patented Quality Process

SMF-28 fiber is manufactured using the Outside Vapor Deposition (OVD) process, which produces a totally synthetic ultra-pure fiber. As a result, Corning SMF-28 fiber has consistent geometric properties, high strength, and low attenuation. Corning SMF-28 fiber can be counted on to deliver excellent performance and high reliability, reel after reel. Measurement methods comply with ITU recommendations G.650, IEC 60793-1, and Bellcore GR-20-CORE.

## Optical Specifications

### Attenuation

Wavelength (nm)	Attenuation* (dB/km)	
	Premium	Standard
1310	$\leq 0.34$	$\leq 0.35$
1550	$\leq 0.20$	$\leq 0.22$

\*Alternate attenuation values available upon request.

### Point Discontinuity

No point discontinuity greater than 0.10 dB at either 1310 nm or 1550 nm.

### Attenuation at the Water Peak

The attenuation at  $1383 \pm 3$  nm shall not exceed 2.1 dB/km.

### Attenuation vs. Wavelength

Range (nm)	Ref. $\lambda$ (nm)	Max. $\alpha$ Difference (dB/km)
1285 - 1330	1310	0.05
1525 - 1575	1550	0.05

The attenuation in a given wavelength range does not exceed the attenuation of the reference wavelength ( $\lambda$ ) by more than the value  $\alpha$ .

## Attenuation with Bending

Mandrel Diameter (mm)	Number of Turns	Wavelength (nm)	Induced Attenuation* (dB)
32	1	1550	$\leq 0.50$
50	100	1310	$\leq 0.05$
50	100	1550	$\leq 0.10$
60	100	1550	$\leq 0.05$

\*The induced attenuation due to fiber wrapped around a mandrel of a specified diameter.

### Cable Cutoff Wavelength ( $\lambda_{\text{cutoff}}$ )

$$\lambda_{\text{cutoff}} \leq 1260 \text{ nm}$$

### Mode-Field Diameter

$$9.2 \pm 0.4 \mu\text{m} \text{ at } 1310 \text{ nm}$$

$$10.4 \pm 0.8 \mu\text{m} \text{ at } 1550 \text{ nm}$$

### Dispersion

Zero Dispersion Wavelength ( $\lambda_0$ ):

$$1302 \text{ nm} \leq \lambda_0 \leq 1322 \text{ nm}$$

Zero Dispersion Slope ( $S_0$ ):

$$\leq 0.092 \text{ ps}/(\text{nm}^2 \cdot \text{km})$$

$$\text{Dispersion} = D(\lambda) = -\frac{S_0}{4} \left[ \lambda - \frac{\lambda_0^4}{\lambda} \right] \text{ ps}/(\text{nm} \cdot \text{km}),$$

for  $1200 \text{ nm} \leq \lambda \leq 1600 \text{ nm}$

$\lambda$  = Operating Wavelength

## Polarization Mode Dispersion

### Fiber Polarization Mode Dispersion (PMD)

	Value (ps/ $\sqrt{\text{km}}$ )
PMD Link Value	$\leq 0.1^*$
Maximum Individual Fiber	$\leq 0.2$

\* Complies with IEC 60794-1:2001, version 5.5, Method 1, September 2001.

The PMD link value is a term used to describe the PMD of concatenated lengths of fiber (also known as the link quadrature average). This value is used to determine a statistical upper limit for system PMD performance.

Individual PMD values may change when cabled. Corning's fiber specification supports network design requirements for a  $0.5 \text{ ps}/\sqrt{\text{km}}$  maximum PMD.

## Environmental Specifications

Environmental Test Condition	Induced Attenuation 1310 nm/1550 nm (dB/km)
Temperature Dependence -60°C to +85°C <sup>a</sup>	≤0.05
Temperature-Humidity Cycling -10°C to +85°C <sup>a</sup> , up to 98% RH	≤0.05
Water Immersion, 23±2°C <sup>a</sup>	≤0.05
Heat Aging, 85±2°C <sup>a</sup>	≤0.05

<sup>a</sup>Reference temperature = +23°C

## Operating Temperature Range

-60°C to +85°C

## Dimensional Specifications

**Length (km/reef):** fiber lengths available up to 50.4\*

\* Longer spliced lengths available as a premium.

## Glass Geometry

Fiber Curl: ≥ 4.0 m radius of curvature

Cladding Diameter: 125.0 ± 0.7 μm

Core-Clad Concentricity: ≤ 0.5 μm

Cladding Non-Circularity: ≤ 1.0%

Defined as:  $\left[1 - \frac{\text{Min. Cladding Diameter}}{\text{Max. Cladding Diameter}}\right] \times 100$

## Coating Geometry

Coating Diameter: 245 ± 5 μm

Coating-Cladding Concentricity: <12 μm

## Mechanical Specifications

### Proof Test

The entire fiber length is subjected to a tensile proof stress ≥ 100 kpsi (0.7 GN/m<sup>2</sup>)\*.

\* Higher proof test levels available as a premium.

## Performance Characterizations

*Characterized parameters are typical values.*

**Core Diameter:** 8.2 μm

**Numerical Aperture:** 0.14

NA is measured at the one percent power level of a one-dimensional far-field scan at 1310 nm.

**Zero Dispersion Wavelength (λ<sub>0</sub>):** 1313 nm

**Zero Dispersion Slope (S<sub>0</sub>):** 0.086 ps<sup>2</sup>/(nm<sup>2</sup>·km)

**Refractive Index Difference:** 0.36%

**Effective Group Index of Refraction**  
(N<sub>eff</sub> @ nominal MFD):

1.4677 at 1310 nm

1.4682 at 1550 nm

**Fatigue Resistance Parameter (n<sub>d</sub>):** 20

**Coating Strip Force:**

Dry: 0.6 lbs. (3N)

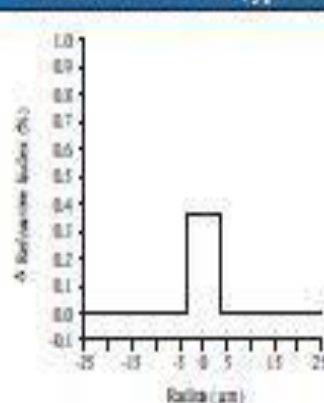
Wet, 14-day room temperature: 0.6 lbs. (3N)

**Rayleigh Backscatter Coefficient**  
(for 1 ns pulse width):

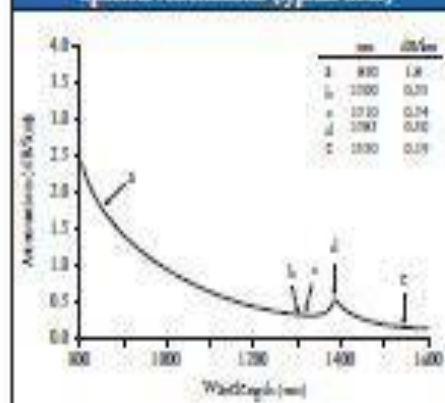
1310 nm: -77 dB

1550 nm: -82 dB

Refractive Index Profile (typical fiber)



Spectral Attenuation (typical fiber)



## Ordering Information

To order Corning® SMF-28® fiber, contact your sales representative, or call the Optical Fiber Customer Service Department at 607-248-2000 or +44-1244-287-437 in Europe. Please specify the following parameters when ordering.

**Fiber Type:** Corning® SMF-28® Fiber

**Fiber Attenuation:** dB/km

**Fiber Quantity:** km

**Other:** (Requested ship date, etc.)

**Corning Incorporated**  
[www.corning.com/opticalfiber](http://www.corning.com/opticalfiber)

One Riverfront Plaza  
 Corning, NY 14831  
 U.S.A.

Phone: 800-525-2524 (U.S. and Canada)  
 607-786-8125 (International)

Fax: 800-529-3632 (U.S. and Canada)  
 607-786-8344 (International)

E-mail: [cofc@corning.com](mailto:cofc@corning.com)

### Europe

Phone: 00 800 6620 6621 (U.K., Ireland, Italy, France, Germany, The Netherlands, Spain and Sweden)

+1 607 786 8125 (All other countries)

Fax: +1 607 786 8344

### Asia Pacific

**Australia**  
 Phone: 1-800-148-600  
 Fax: 1-800-148-568

**Indonesia**  
 Phone: 001-800-015-721-1261  
 Fax: 001-800-015-721-1262

**Malaysia**  
 Phone: 1-800-80-3156  
 Fax: 1-800-80-3155

**Philippines**  
 Phone: 1-800-1-116-0128  
 Fax: 1-800-1-116-0129

**Singapore**  
 Phone: 800-1300-955  
 Fax: 800-1300-956

**Thailand**  
 Phone: 001-800-1-3-721-1261  
 Fax: 001-800-1-3-721-1264

### Latin America

**Brazil**  
 Phone: 00817-762-4772  
 Fax: 00817-762-4996

**Mexico**  
 Phone: 001-800-225-1713  
 Fax: 001-800-129-1472

**Venezuela**  
 Phone: 800-1-4418  
 Fax: 800-1-4419

### Greater China

**Beijing**  
 Phone: (86) 10-6505-5066  
 Fax: (86) 10-6505-5077

**Hong Kong**  
 Phone: (852) 2807-2723  
 Fax: (852) 2807-2152

**Shanghai**  
 Phone: (86) 21-3222-4668  
 Fax: (86) 21-6288-3575

**Taiwan**  
 Phone: (886) 2-2716-0338  
 Fax: (886) 2-2716-0129

E-mail: [GCCoC@corning.com](mailto:GCCoC@corning.com)

Corning is a registered trademark. SMF-28 and CPC are trademarks of Corning Incorporated, Corning, NY.

Any warranty of any nature relating to any Corning optical fiber is only contained in the written agreement between Corning Incorporated and the direct purchaser of such fiber.

©2002 Corning Incorporated

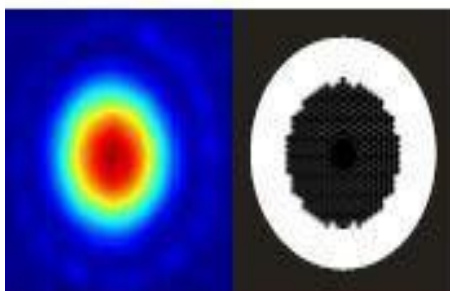




# HCI9-1550

## Hollow Core Photonic Bandgap Fiber

- < 3% of optical power located in silica
- Negligible bend loss
- Gaussian like fundamental mode



### Applications

- Fiber optic gyroscopes
- Pulsed lasers (delivery and/or compression)
- Gas spectroscopy
- Low latency communication



NKT Photonics A/S (Headquarters)  
 Blokken 84, 3460 Birkerød, Denmark  
 Phone: +45 4348 3900  
 Fax: +45 4348 3901

NKT Photonics GmbH  
 Schwanenstrasse 39, Bldg D9-013  
 51063 Cologne, Germany  
 Phone: +49 221 99511-0  
 Fax: +49 221 99511-450

NKT Photonics Inc.  
 1400 Campus Drive West  
 Morganville NJ 07751, USA  
 Phone: +1 732 972 9937  
 Fax: +1 732 814 4034

Hollow core Photonic Bandgap Fibers guide light in a hollow core, surrounded by a microstructured cladding of air holes and silica. Since only a small fraction of the light propagates in silica, the effect of material nonlinearities is insignificant and the fibers do not suffer from the same limitations on loss as conventional fibers made from solid material alone.

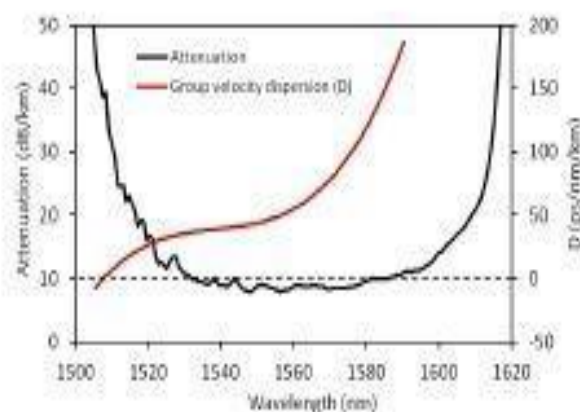
### Specifications

Optical	
Design wavelength	1550 nm
Attenuation @ 1550 nm	< 20 dB/km
Mode field diameter @ 1550 nm <sup>1</sup>	13 ± 2 μm
Operating wavelength <sup>2</sup>	1520-1600 nm

Physical	
Core diameter	20 ± 2 μm
Air filling fraction of the holey region	≥ 90 %
Diameter of the holey region	70 ± 5 μm
Outer cladding diameter	115 ± 3 μm
Coating diameter	220 ± 30 μm
Coating material	Single layer acrylate

1. Full 1/e<sup>2</sup>-width of the near field intensity distribution
2. Over which the attenuation is < 30 dB/km

### Typical attenuation and dispersion



All NKT Photonics products are produced under our quality management system certified in accordance with ISO 9001:2008 standard.



## HC-1550-02

### Hollow Core Photonic Bandgap Fiber



- < 5% of optical power located in silica
- Gaussian-like fundamental mode
- Can be filled with gas
- Negligible bend loss
- Fresnel reflection of core mode to air (10%)
- Mode effective index close to unity
- Numerical Aperture ~ 0.2
- Pure silica for good temperature stability

Hollow core Photonic Bandgap Fibers guide light in a hollow core, surrounded by a microstructured cladding of air holes and silica.

Since only a small fraction of the light propagates in silica, the effect of material nonlinearities is insignificant and the fibers do not suffer from the same limitations on loss as conventional fibers made from solid material alone.

#### Applications

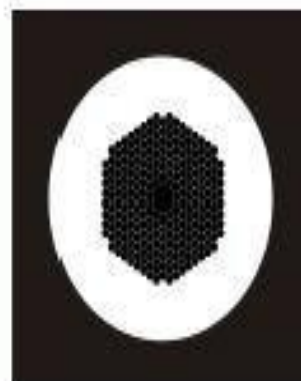
- Fiber optic gyroscopes
- Pulsed lasers (pulse delivery and/or compression)
- Gas spectroscopy
- Low latency communication

Physical properties	
Core diameter	10 ± 1 µm
Cladding pitch	3.8 ± 0.1 µm
Diameter of PCF region	70 ± 5 µm
Cladding diameter	120 ± 2 µm
Coating diameter	220 ± 30 µm
Coating material	Single layer acrylate

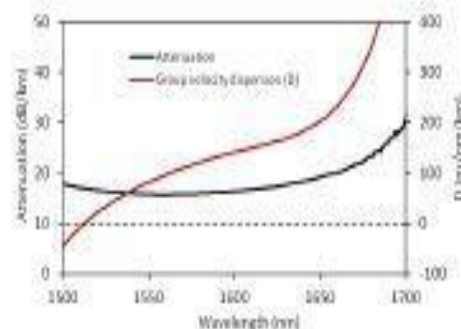
Optical properties	
Design wavelength	1550 nm
Attenuation @ 1550 nm	< 30 dB/km
Typical GVD @ 1550 nm	90 ps <sup>2</sup> /nm/km
Operating wavelength <sup>1)</sup>	1490-1680 nm
Mode field diameter @ 1550 nm <sup>2)</sup>	9 ± 1 µm

1. Over which the attenuation is < 30 dB/km
2. Full 1/e-width of the near field intensity distribution

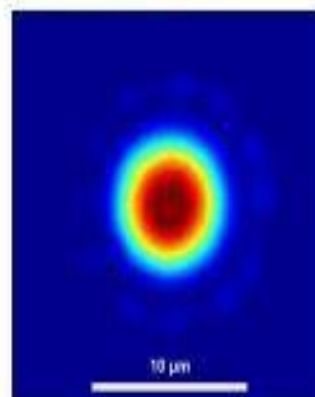
#### Schematic fiber cross section



#### Typical attenuation and dispersion



#### Typical near field intensity profile



HC-1550-02-111221

## PM-1550

Single mode polarization-maintaining fiber with short beat length

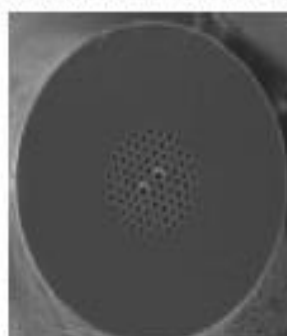
- Low loss fiber from 600 to 1700 nm
- Single mode at all wavelengths
- Polarization Maintaining
- Radiation hard pure silica fiber
- Wavelength independent MFD

The PM-1550 has a strong form-birefringence and is optimized to create a short beat length between the polarizations.

Furthermore it has reduced bend-induced coupling between polarization states, an improved polarization extinction ratio, and is 30 times less temperature sensitive than conventional Hi-Bi fiber.

Optical properties at 1550 nm	
Single mode	Yes
Attenuation	<3 dB/km
Mode field diameter ( $1/e^2$ )	5.5/3.8 ± 0.8 $\mu$ m
Mode field ellipticity	~ 1.5
Birefringence	≥ 4e-4
PER	Typical > 10dB
Chromatic dispersion	55 ± 10 ps/nm/km

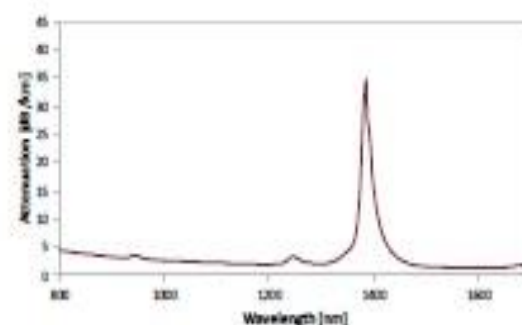
Physical properties	
Core diameter	6.3/4.4 ± 0.5 $\mu$ m
Outer cladding diameter, OD	125 ± 5 $\mu$ m
Coating diameter	240 ± 10 $\mu$ m
Core and cladding material	Pure silica
Coating material, single layer	Single layer Acrylate
Coating concentricity	< 10 $\mu$ m
Proof test level	0.5 %



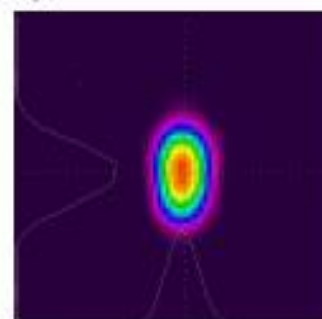
### Applications

- Sensors
- Gyroscopes
- Interferometers

### Typical spectral attenuation



### Near field image



PM-1550-180631

NKT Photonics A/S (Headquarters)  
Blåsten 84 • 3490 Birkerød • Denmark  
Phone: +45 4348 3900  
Fax: +45 4348 3901  
www.nktphotonics.com

NKT Photonics GmbH  
Schanzenstrasse 39 • Bldg D9-D13  
51083 Cologne • Germany  
Phone: +49 221 99511-0  
Fax: +49 221 99511-650

NKT Photonics Inc.  
3514 N Vancouver Avenue, Suite 310 •  
Portland, OR 97227 • USA  
Phone: +1 (503) 444-8404  
Fax: +1 (503) 914-1884



**THORLABS****Dispersion Compensating Fiber****DCF38****Description**

Thorlabs' dispersion compensating bare fiber delivers high performance across a broad spectral range in the telecom region. These fibers have both high mechanical reliability and high optical stability. The DCF38 fiber has dispersion designed specifically to match and compensate Corning L1000 or S1/F-28e-fiber.

**Specifications****Dispersion Specifications**

Dispersion @ 1550 nm	-49.00 to -30.00 ps/nm <sup>2</sup> km
Dispersion Slope @ 1550 nm	-0.155 to -0.075 ps/nm <sup>3</sup> km
Typical Effective Area	≥26.8 μm <sup>2</sup>
Polarization Mode Dispersion	≤0.05 ps/km

**General Specifications**

Mode Field Diameter @ 1550 nm	5.72 to 6.30 μm
Cladding Diameter	125.0 ± 1.0 μm
Coating Diameter	250 ± 5 μm
Coating-Cladding Concentricity	<12 μm
Core-Clad Concentricity	≤0.5 μm
Cutoff Wavelength	≤1520 nm
Attenuation @ 1550 nm	≤0.265 dB/km
Attenuation Slope from 1530 to 1565 nm	-0.00040 ≤ to ≤ -0.00011 dB/nm <sup>2</sup> km
Point Discontinuity	≤0.10 dB @ 1550 nm
Optical Return Loss	≥60 dB
Typical Splice Loss @ 1550 nm (Splice DCF38/DCF38)	≤0.15 dB

US, Canada, & South America: +1-973-300-3000 | France: +33 (0) 970 444 844 | Europe: +49 (0) 8131-5956-0 | UK & Ireland: +44 (0)1353-654440  
 Brazil: +55-16-3413 7062 | Scandinavia: +46-31-733-30-00 | Japan & Asia: +81-3-5979-8889 | China: +86 (0)21-60581122

www.thorlabs.com

April 1, 2013  
 23057-501, Rev B

## Appendix B

Technical passport / EDFA-1550

---



1550nm Optical Amplifier

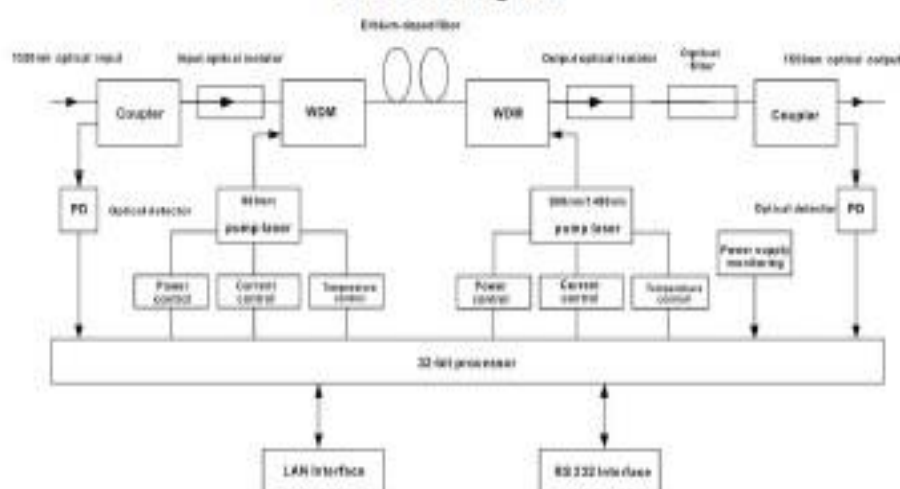
EDFA-1550/24 (4×17)



## 2. Performance Characteristics

- Automatic control the output optical power.
- The output optical power is adjustable, attenuation range is 0-3dB.
- Adopt high-performance erbium doped fiber, high efficiency energy conversion.
- Adopt advanced 32 bit processor, coordinate with perfect automatic monitoring systemic circuit. It can timely and accurately monitor optical output power and various work status of the pump laser, ensures the stable optical output power and can effectively extend the working life of the pump laser.
- Built-in blue screen 160×32 dot matrix LCD monitor on the front panel, accurately showing all working status parameters.
- 19"1U height standard rack mount, equipped standard IEEE802.3 10Base-T Ethernet interface and RS232 interface, can expediently realizes network management monitoring.

## 3. Block diagram



## 4. Technique Parameter

### 4.1 Link test conditions

**Special instructions:** The performance parameters of this manual according to the measuring method of GY/T 184-2002 < CATV system analog optical fiber amplifier technical requirements and measuring method>, and tested in the following conditions.

**Test condition:** With standard optical fiber and standard optical receiver composed the test link. Set 59 PAL-D analog TV channel signal at 550MHz frequency range under the specified link loss. Transmit digital modulation signal at range of 550 MHz ~ 862MHz, the digital modulation signal level (in 8 MHz bandwidth) is 10dB lower than analog signal carrier level. When the input optical power of optical receiver is -1dBm, measure the C/CTB, C/CSO and C/N.

#### 4.2 Technique Parameters

Item	Unit	Technique parameter	Remark
Operating bandwidth	nm	1535 - 1565	
Input optical power range	dBm	-3 - +10	
Total optical output power	dBm	24	Optional
One way optical output power	dBm	17	
Output power stability	dBm	±0.5	
Noise figure	dB	≤ 5.0	Input optical power 0dBm
Return loss	Input	dB	≥ 45
	Output	dB	≥ 45
Pump leakage power	Input	dBm	≤ -30
	Output	dBm	≤ -30
Optical connector type		SC/APC	
Power supply voltage	V	AC160V - 250V (50 Hz)	
Consumption	W	< 30	
Operating Temperature Range	°C	-5 - +55	
Maximum operating relative humidity	%	Max 95% No Condensation	
Storage Temperature Range	°C	-30 - +70	
Maximum storage relative humidity	%	Max 95% No Condensation	
Dimension	mm	483(W)×340(D)× 44(H)	

---

**THORLABS**

## Manual Fiber Polarization Controllers

### User Guide



## Chapter 4 Specifications

### 4.1. 3-Paddle Polarization Controllers

Item #	FPC030	FPC031	FPC032
Paddle Material	Black Delrin		
Number of Paddles	3		
Loop Diameter	1.08" (27 mm)		
Paddle Rotation	$\pm 117.5^\circ$		
Foot Print (L x W)	8.5" x 1.0" (215.9 mm x 25.4 mm)		
Fiber	None	CCC1310-J9	
Operating Wavelength Range <sup>a</sup>	N/A	1280 - 1625 nm	
Design Wavelength <sup>b</sup>	N/A	1310 nm	
Mode Field Diameter	N/A	8.6 $\pm$ 0.4 $\mu$ m @ 1310 nm 9.7 $\pm$ 0.5 $\mu$ m @ 1550 nm	
Cladding Diameter	N/A	125 $\pm$ 0.7 $\mu$ m	
Coating Diameter	N/A	242 $\pm$ 5 $\mu$ m	
Tubing Diameter	N/A	$\varnothing$ 900 $\mu$ m Tight Buffer	
Numerical Aperture	N/A	0.14	
Loop Configuration <sup>c</sup>	N/A	2-3-2	
Connectors	N/A	FC/PC	FC/APC
Bend Loss	N/A	$\leq 0.1$ dB	

- Retardance varies as a function of wavelength. Refer to Chapter 2 for more information.
- Devices with preloaded fiber are optimized for this wavelength.
- For polarization controllers with fiber preinstalled.

---

**THORLABS**

# Optical Spectrum Analyzers

## User Guide



6501  $\text{cm}^{-1}$ . To distinguish between these signals in the interferogram, we would need to move away 1 cm from the point of zero path difference (ZPD). The OSA can move  $\pm 4$  cm in OPD, and so it can resolve spectral features 0.25  $\text{cm}^{-1}$  apart. The resolution of the instrument can be calculated as follows:

$$\Delta\lambda = \Delta k \times 100 \times \lambda^2$$

Here,  $\Delta\lambda$  is the resolution in  $\mu\text{m}$ ,  $\Delta k$  is the OPD in  $\text{cm}^{-1}$  (maximum of 0.25  $\text{cm}^{-1}$  for this instrument) and  $\lambda$  is the wavelength in  $\mu\text{m}$ .

The resolution of the OSA can be set to High or Low in the main window of the software. In high resolution mode, the retroreflectors translate by the maximum of  $\pm 1$  cm ( $\pm 4$  cm in OPD), while in low resolution mode, the retroreflectors translate by  $\pm 0.25$  cm ( $\pm 1$  cm in OPD). In the Setup section of the OSA software (Chapter 7), the length of the interferogram that is used in the calculation of the spectrum can be cut to remove spectral contributions from high-frequency components.

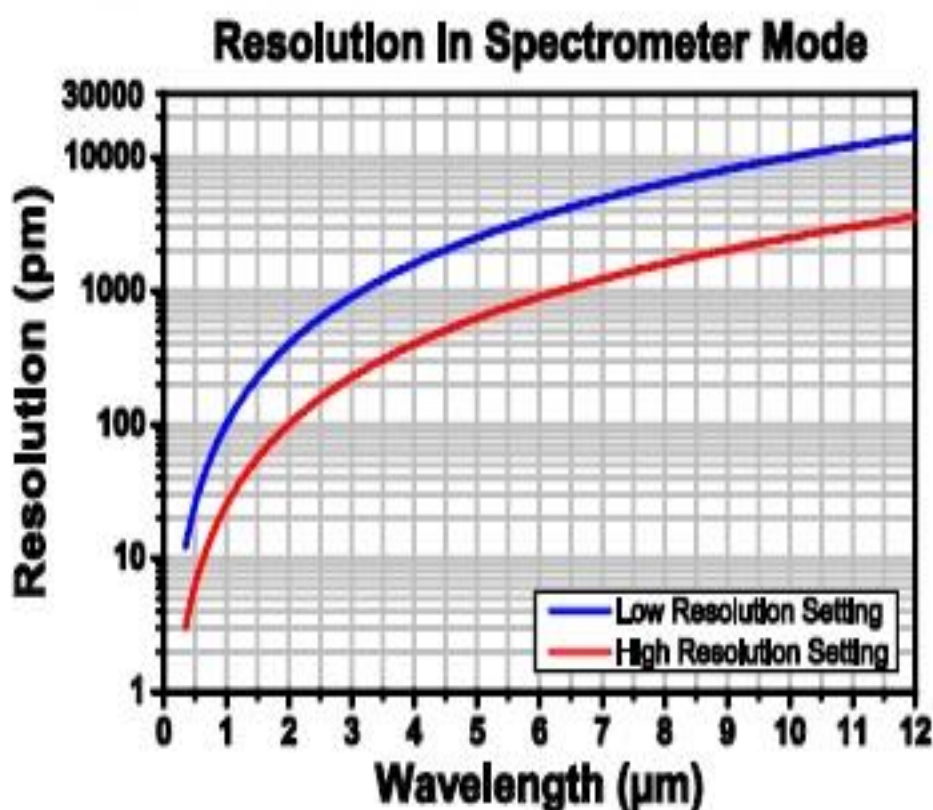


Figure 3 Resolution as a Function of Wavelength

The sensitivity of the instrument depends on the electronic gain used in the sensor electronics. Since an increased gain setting reduces the bandwidth of the detectors, the instrument will run slower when higher gain settings are used. Figure 4 and Figure 5 on the following page show the dependence of the noise floor on the wavelength and OSA model.

## Chapter 13 Technical Data

### 13.1. Common Specifications

Specification	Notes	Value
Spectral Resolution	-	7.5 GHz (0.25 cm <sup>-1</sup> )
Spectral Accuracy <sup>a</sup>		±2 ppm <sup>b</sup>
Spectral Precision <sup>c</sup>		1 ppm
Wavelength Meter Resolution	Wavelength Meter Mode (Linewidth <10 GHz) See Section 4.6	0.1 ppm
Wavelength Meter Display Resolution <sup>d</sup>		9 Decimals
Wavelength Meter Accuracy <sup>e</sup>		±1 ppm
Wavelength Meter Precision <sup>f</sup>		0.2 ppm
Input Power (Max)	CW Source	10 mW (10 dBm)
Input Damage Threshold <sup>g</sup>	-	20 mW (13 dBm)
Power Level Accuracy <sup>h</sup>	-	±1 dB
Optical Rejection Ratio	See Section 4.13	30 dB
Input Fiber Compatibility	-	FC/PC Connectors <sup>h</sup> All Single Mode Patch Cables, Including Fluoride SM Patch Cables Silica Multimode Patch Cables with ≤Ø50 µm Core and NA ≤ 0.22 Fluoride Multimode Patch Cables with ≤Ø100 µm Core and NA ≤ 0.26
Free-Space Input	-	Accepts Collimated Beams up to Ø6 mm Red Alignment Laser Beam Four 4-40 Taps for 30 mm Cage Systems
Dimensions	-	320 mm x 149 mm x 475 mm (12.6" x 5.9" x 18.7")

- a. After a 45-minute warm-up, for a single mode FC/PC-terminated patch cable at an operating temperature of 20 - 30 °C.
- b. Specified in parts per million. For instance, if the wavelength being measured is 1 µm, the spectral accuracy will be ±2 pm. (±2 pm of accuracy for every 1,000,000 pm, or 1 µm, of wavelength.)
- c. Spectral Precision is the repeatability with which a spectral feature can be measured using the peak search tool.
- d. Can be set from 0-9 decimals and have an auto option that estimates the relevant number of decimals.
- e. Using the same input single mode fiber for all measurements.
- f. Limited by the damage threshold of the internal components.
- g. Specified using Absolute Power Mode, Zero Fill = 2, and Hann apodization, after a 45-minute warm-up, for an operating temperature of 20 - 30 °C. (The different apodization modes available in the OSA software are described in Section 15.2.) The specified wavelength range is 400 - 1000 nm for OSA201C, 600 - 1600 nm for OSA202C, 1.0 - 2.4 µm for OSA203C, 1.3 - 5.0 µm for OSA205C, and 2.0 - 11.0 µm for OSA207C. Each specification is valid for a single mode FC/PC-terminated patch cable, as well as for a collimated free-space beam with diameter < 3 mm and divergence < 3 mrad, assuming the included protective window is installed in the free-space aperture.
- h. Connectors for other fiber input receptacles are available upon request. Contact [techsupport@thorlabs.com](mailto:techsupport@thorlabs.com) for details.



## 1270~1610nm CWDM Pigtailed Components

### Features

- Built - in optical isolator
- Low capacitance and low dark current
- High stability of CWDM lasers diode
- Low threshold current, low operating current
- Integrated high isolation , low insertion loss



### Applications

CATV Reverse Transmission

Other Analog or Digital Optical Transmission

### Absolute Maximum Ratings

Parameter	Symbol	Min.	Max.	Unit	Test Condition
Storage Temperature	Tstg	-40	100	°C	-
Operating Temperature	Top	-40	85	°C	I=Iop
Laser Forward Current	If	-	150	mA	-
LD Reverse Voltage	Lvr	-	2	V	-
PD Reverse Voltage	Pvr	-	15	V	-
Soldering Temp	-	-	260	°C	-
Soldering Time	-	-	10	S	-

### Optical & Electrical Characteristics

Parameter	Symbol	Min.	Typ.	Max.	Unit	Test condition
Rated Power	Po	1	-	3	mW	Ith+20mA
Threshold Current	Ith	5	-	15	mA	CW
Forward Voltage Drop	Vop	-	1.0	1.2	V	-
Cent Wavelength	$\lambda_c$	Note 2			nm	Note 1
Spectrum Width(-3dB)	$\Delta\lambda$	-	0.5	1	nm	CW,-3dB
Side-mode Suppression Ratio	SMSR	35	-	-	dB	-
Monitor Current	Im	100	-	900	uA	CW, Ith+20mA
Dark Current of Monitor	Id	-	-	100	nA	-
Optical Isolation	ISO	30	40	-	dB	25°C
Frequency Range	F	2.5			GHz	RI=50Ω
Cut-off Frequency	Fc	6			GHz	If=Iop
Relative intensity noise	RIN	-	-155	-150	dB/Hz	CW, If=Iop, f=4500MHz
RF Bandpass Flatness	BF		±1.5		dB	If=Iop,45MHz-4500MHz,T=25 °C

**Technology to lead the Shengshi**

Version Mar.2016



Shengshi Optical  
Shengshi Optical

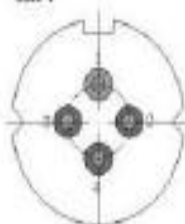
Note 1. 2.5Gb/s NRZ, pseudo-random,  $P_b=0.2mW$ ,  $P_{peak}=1.0mW$

Note 2. The selected wavelength is available as follow:

Wavelength (nm) (Tl=Tser) (in vacuum)	Tolerance(nm)
1271	$\pm 2$ or $\pm 3$
1291	$\pm 2$ or $\pm 3$
1311	$\pm 2$ or $\pm 3$
1331	$\pm 2$ or $\pm 3$
1351	$\pm 2$ or $\pm 3$
1371	$\pm 2$ or $\pm 3$
1391	$\pm 2$ or $\pm 3$
1411	$\pm 2$ or $\pm 3$
1431	$\pm 2$ or $\pm 3$
1451	$\pm 2$ or $\pm 3$
1471	$\pm 2$ or $\pm 3$
1491	$\pm 2$ or $\pm 3$
1511	$\pm 2$ or $\pm 3$
1531	$\pm 2$ or $\pm 3$
1551	$\pm 2$ or $\pm 3$
1571	$\pm 2$ or $\pm 3$
1591	$\pm 2$ or $\pm 3$
1611	$\pm 2$ or $\pm 3$

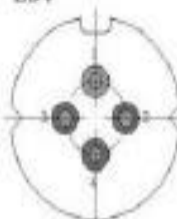
## PIN Definition

LD:



Type A:  
**【1】** LD + /CASE  
**【2】** LD -  
**【3】** PD +  
**【4】** PD -

LD:



Type B:  
**【1】** CASE  
**【2】** LD -  
**【3】** LD+/PD-  
**【4】** PD +

Bottom View

Address: 5-floor,Block B Creative Building, Wenzhi St.,Hongshan District,Wuhan,City,Hubei,P.R.China 430074

Tel: 0086-27-87179709\*601    Cell: 0086-158 7177 5837    Fax: 0086-27-87172995

<http://en.op.en.alibaba.com>    [Skype:vicky\\_wgy](http://skype:vicky_wgy)    [www.laserdiodedevice.com](http://www.laserdiodedevice.com)

## DVP-740 Single Fiber Fusion Splicer

### Features

- *Compact & Light weight*
- *Fully Automatic Operation*
- *5000m altitude ensures Splice Quality*
- *SYSTEM TEST ensures the best working condition*
- *Color LCD monitor*
- *Pause function, convenient for scientific research*
- *Store 8000 groups of splice results*
- *USB&DC interface*
- *High battery capacity, up to 120 times of continuous splice and heat*



### SPECIFICATIONS

Applicable fibers	SM, MM, DS, NZ-DS(G655), EDF, Bending Loss Insensitive fiber(G657), Pigtail, Drop cable and connector.
Fiber cleaved length	8-22mm
Average splice loss	0.02dB(SM)、0.01dB(MM)、0.05dB(DS)、0.04dB(NZDS)
Return loss	≥60dB
Tension test	2.0N(200gf)(Standard)
Protection sleeve length	20mm, 40mm, 60mm and more .
Splice Program	15 groups of preset programs, 1 group of manual setting
Language	English, Chinese, Korean, Russian, Spanish, Portuguese, German, French
Environment conditions	-25 ~ + 50℃ (operation temperature), 0 ~ 95%RH (humidity), 0 ~ 5000m (altitude)
Storage environment	-40~ +80℃ (temperature) , 0~95%RH (humidity)
Power supply	AC adaptor: 85~260V input voltage Internal battery: 12V, 6Ah, up to 120 times of continuous splice and heat
Dimensions/Weight	142 (D) × 122 (W) × 138 (H) mm/1.95kg (with battery)

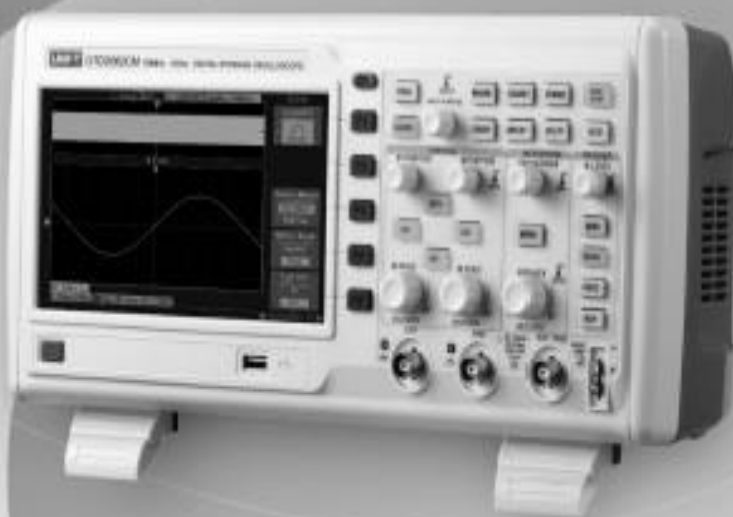
### STANDARD PACKAGE

Fusion Splicer, Internal Battery, Charger, Spare Electrodes, Cooling Tray, Manual Instruction, Carry Case, Fiber Cleaver, Fiber Stripper, AC Adaptor, AC Power Cord

# UNI-T®

## UTD2000M

### Operating Manual



**Digital Storage  
Oscilloscope**

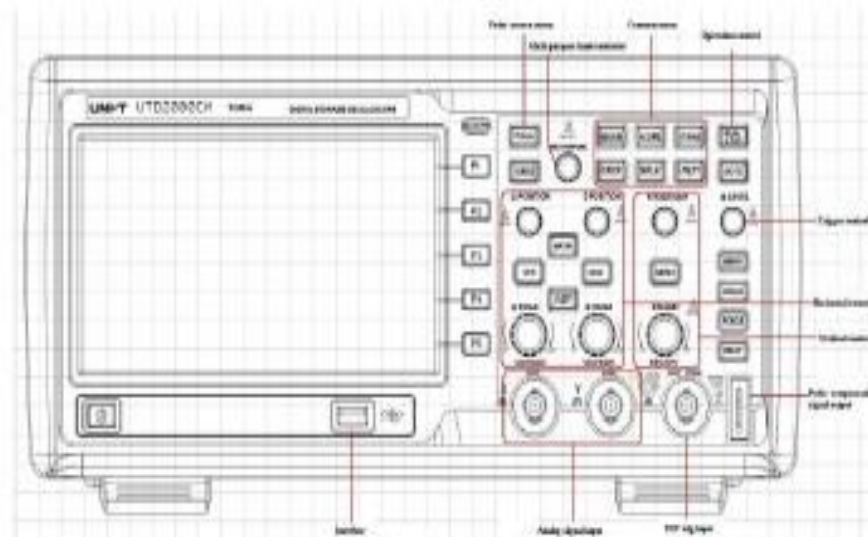


Fig 1-1 Front Panel - UTD 2000CM

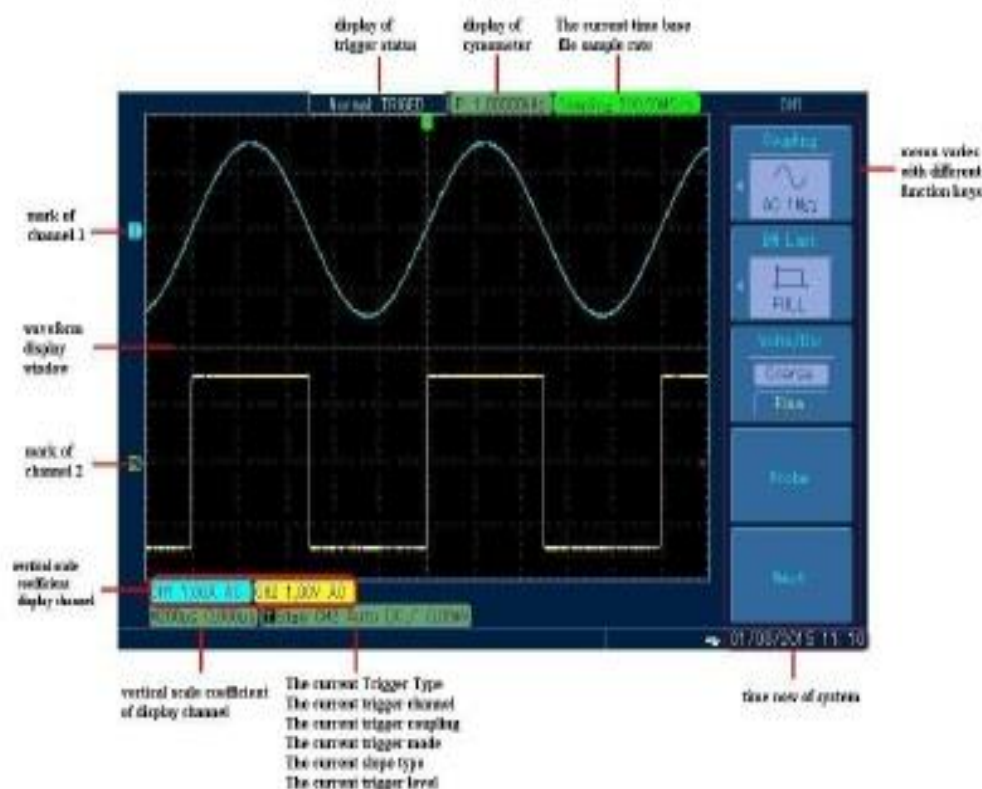


Figure 1-2 Screen Display - UTD2000CM

**Notes:** Real-time sampling rate at current time base are not available for UTD2202HM&CM.

To use the menu system, please follow the following steps:

1. Press a menu key to display the menu to be used.
2. Press F1 to F5 located to the right of the screen to select a menu item. If the menu item contains multiple submenus, then again press F1 to F5 to make a selection.
3. Some menu items require numeric entry or making multiple choices to complete the setting, in this case, a



# FiberMeter Optical Power Meter

Model #: FO600 / FO602 / FO610

## Operations Guide

Firmware Revision 4.62  
March 1, 2007

## Specifications to Power Meter

<b>Model</b>	<b>FPM-300/FLS-300/FOT-300</b>
Power meter port	Ge
Power range (dBm)	10 to -60
Range displayed	Down to -65
Number of calibrated wavelength	10
Power uncertainty	$\pm 5\% \pm 1 \text{ nW}$
Resolution (dB)	0.01
Automatic offset nulling	Yes
Display units	dB/Dbm/W
Automatic wavelength recognition	Yes
Screen refresh rate (Hz)	3
Tone detection (Hz)	270, 1 K, 2K
Battery life (hours) (typical)	>300



## Automatic Digital Refractometer RX-5000 $\alpha$

The RX-5000 $\alpha$  ( alpha ) is an automatic digital refractometer which can set measurement temperature internally and has the following features for measuring the refractive index, Brix or concentration of various liquids accurately and speedily

- Since the RX-5000 $\alpha$  ( alpha ) has a thermo-module to control temperature, a constant temperature water bath is not necessary.
- The measurement starts automatically after the sample reaches your targeted temperature.
- The refractive index and Brix at your targeted temperature are speedily displayed.
- High Brix  $\pm$  0.03% and refractive index  $\pm$  0.00004 accuracy can be obtained.
- The RX-5000 $\alpha$  ( alpha ) displays the top-and-bottom-limit-bar for your set control range.
- If the measurement value differs from that of your Standard Liquid or the other refractometer, it can be adjusted in a certain range.
- 60 kinds of user scales can be input according to your sample.
- The RX-5000 $\alpha$  ( alpha ) is capable of calling up 30 latest measurements.

\* Special model of RX-5000 $\alpha$  allows pre-programming of an additional scale (such as honey moisture, inverted sugar% or salt concentration) in addition to Refractive Index and Brix (%) at customer's request.

This product comes standard with a two (2) year limited warranty against manufacturer's defects from the date of the original purchase.

FDA 21 CFR Part 11 Software Included in Standard Delivery.

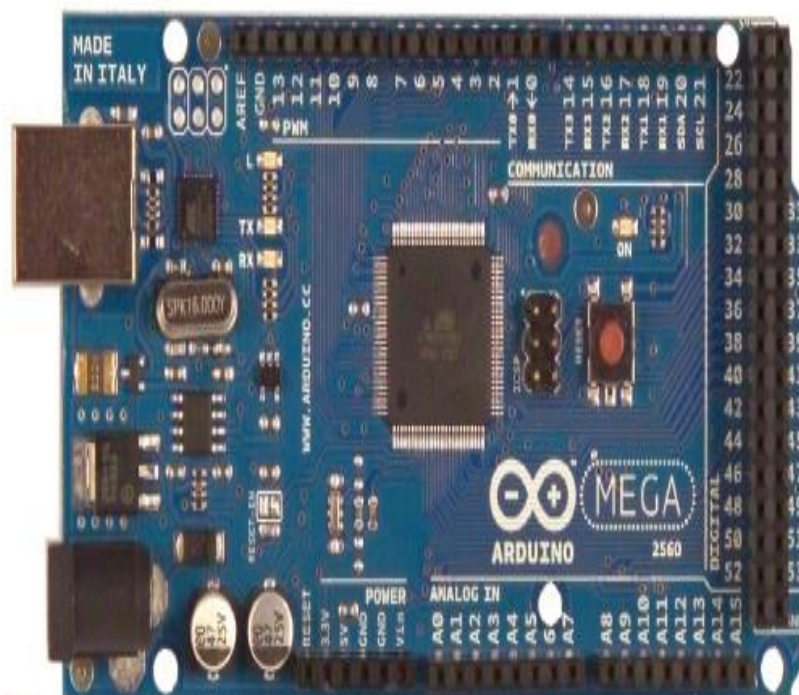


Model	RX-5000α	Cat.No	3261
Measurement Range	Refractive index (nD) : 1.32700 to 1.58000 Brix : 0.00 to 100.00% ( 5 to 60°C ATC)	Minimum indication	Refractive index (nD) : 0.00001 Brix : 0.01% Temperature: 0.01°C
Measurement Accuracy *Repeatability	Refractive index (nD) : ±0.00004 *±0.00002 Brix : ±0.03% *±0.01% [*1]	Measurement Temperature	5 to 60°C
		Power Supply	AC100V to 240V, 50/60Hz
Power consumption	65VA	Dimensions & weight	37×26×14cm, 6.4kg (Main Unit only)
Mode	<p>MODE-1: Displays the measurement value once the sample reaches the target temperature.</p> <p>MODE-2: Measures refractive index and temperature at fixed intervals and displays the estimated measurement value at the target temperature.</p> <p>MODE-3: The thermo-module can be turn off. Without temperature control, the measurement value is displayed in 4 seconds after the START key is pressed.</p> <p>MODE-S: Displays the measurement value once a certain level of sample stability is achieved.</p>		
Output terminals	<ul style="list-style-type: none"> <li>• Printer (for ATAGO digital printers)</li> <li>• Computer - RS-232C</li> </ul> <p>Connection to a USB port requires a USB to RS-232 adapter (optional)</p>		

## Appendix C



## Arduino Mega 2560 Datasheet



## DATA SHEET

**NEC****SILICON TRANSISTOR  
2SC3355****HIGH FREQUENCY LOW NOISE AMPLIFIER  
NPN SILICON EPITAXIAL TRANSISTOR****DESCRIPTION**

The 2SC3355 is an NPN silicon epitaxial transistor designed for low noise amplifier at VHF, UHF and CATV band.

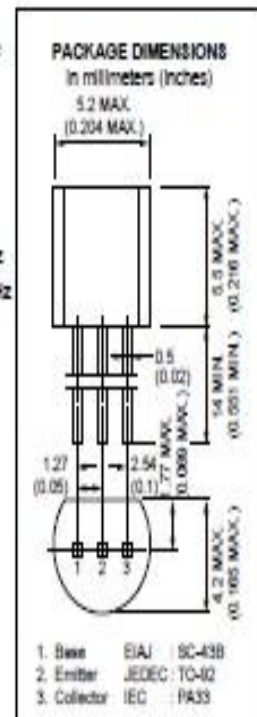
It has large dynamic range and good current characteristic.

**FEATURES**

- Low Noise and High Gain  
 $NF = 1.1$  dB TYP.,  $G_n = 8.0$  dB TYP. @  $V_{CE} = 10$  V,  $I_c = 7$  mA,  $f = 1.0$  GHz  
 $NF = 1.1$  dB TYP.,  $G_n = 9.0$  dB TYP. @  $V_{CE} = 10$  V,  $I_c = 40$  mA,  $f = 1.0$  GHz
- High Power Gain  
 $MAG = 11$  dB TYP. @  $V_{CE} = 10$  V,  $I_c = 20$  mA,  $f = 1.0$  GHz

**ABSOLUTE MAXIMUM RATINGS ( $T_A = 25^\circ\text{C}$ )**

Collector to Base Voltage	$V_{CB}$	20	V
Collector to Emitter Voltage	$V_{CE}$	12	V
Emitter to Base Voltage	$V_{EB}$	3.0	V
Collector Current	$I_c$	100	mA
Total Power Dissipation	$P_T$	600	mW
Junction Temperature	$T_j$	150	$^\circ\text{C}$
Storage Temperature	$T_{stg}$	-65 to +150	$^\circ\text{C}$

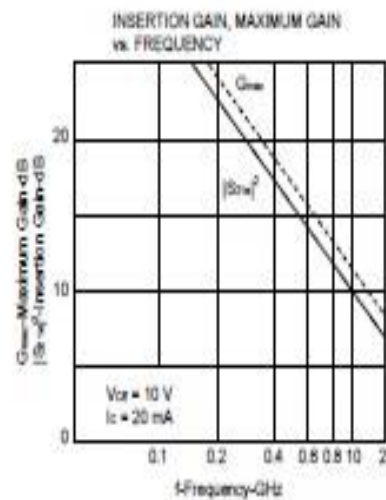
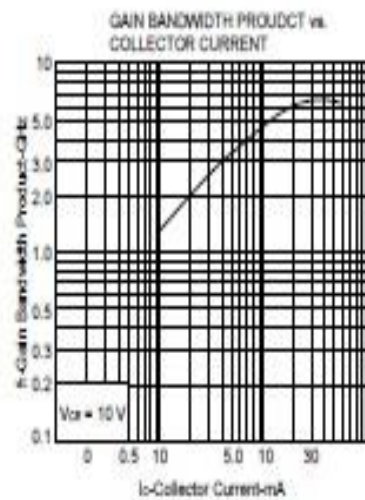
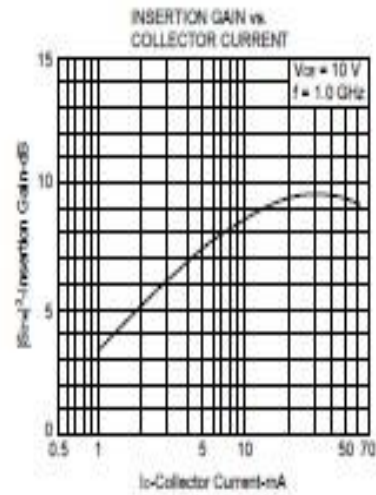
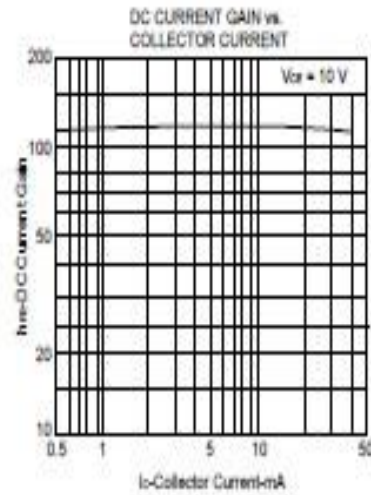
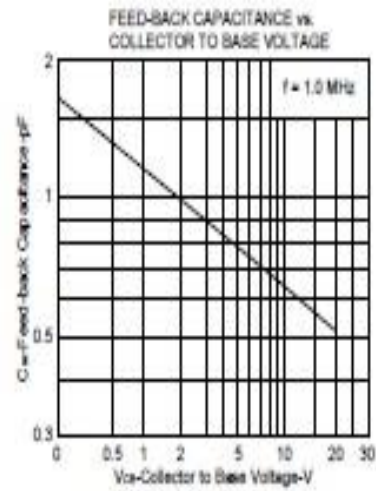
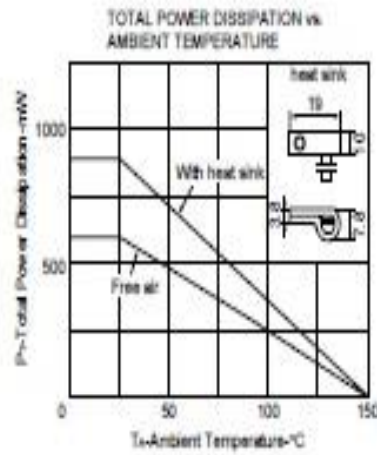
**ELECTRICAL CHARACTERISTICS ( $T_A = 25^\circ\text{C}$ )**

CHARACTERISTIC	SYMBOL	MIN.	TYP.	MAX.	UNIT	TEST CONDITIONS
Collector Cutoff Current	$I_{CO}$			1.0	$\mu\text{A}$	$V_{CE} = 10$ V, $I_B = 0$
Emitter Cutoff Current	$I_{EO}$			1.0	$\mu\text{A}$	$V_{BE} = 1.0$ V, $I_C = 0$
DC Current Gain	$h_{FE}$	50	120	300		$V_{CE} = 10$ V, $I_C = 20$ mA
Gain Bandwidth Product	$f_T$		6.5		GHz	$V_{CE} = 10$ V, $I_C = 20$ mA
Output Capacitance	$C_{ce}$		0.65	1.0	pF	$V_{CE} = 10$ V, $I_C = 0$ , $f = 1.0$ MHz
Insertion Power Gain	$S_{21}$		9.5		dB	$V_{CE} = 10$ V, $I_C = 20$ mA, $f = 1.0$ GHz
Noise Figure	NF		1.1		dB	$V_{CE} = 10$ V, $I_C = 7$ mA, $f = 1.0$ GHz
Noise Figure	NF		1.8	3.0	dB	$V_{CE} = 10$ V, $I_C = 40$ mA, $f = 1.0$ GHz

 **$h_{FE}$  Classification**

Class	K
Marking	K
$h_{FE}$	50 to 300

TYPICAL CHARACTERISTICS (T<sub>A</sub> = 25 °C)



## الخلاصة

يُعد ضغط الإشارة البصرية من أهم العمليات التي تستخدم في منظومات الاتصالات البصرية المتقدمة ذات معدل نقل البيانات العالي ان كانَ (OFDM) أو (DWDM).

في هذه الرسالة، صُمم ونفذ ضغط الإشارة ليفي التراصف من خلال انتشار مصدر الليزر الليفي الضيق في منظومتي التداخل الليفي علما ان الشعاع الليزري الصادر من هذا المصدر قد تم تقطيعه الكترونياً ليكون نبضي لتتولد لدينا نبضات بعرض ( $\tau = 10 \text{ ns}$ ) و ( $\text{FWHM} = 286 \text{ pm}$ ) وطاقة مقدارها ( $P_p = 2.3 \text{ mW}$ ) متمركزة عند الطول الموجي ( $\lambda = 1546.7 \text{ nm}$ ).

أول منظومة كانت ذات متداخل من نوع (etalon Fabry–Perot interferometer) والمتكون من لحام نوعين من الاليف البلورية الفوتونية ذات القلب المجوف أحدهما كان من نوع 7 خلايا والاخر كان من نوع 19 خلية بين قطعتين ليف بصري احادي النمط نوع (smf-28).

أما النوع الثاني من المنظومات التي تم تنفيذها هي من المتداخل من نوع (Mach-Zehnder interferometer) المنفذ من خلال لحام الليف البصري الفوتوني ذو القلب الصلب أحدهما من نوع (PM-1550-01) والاخر من نوع (ESM-12B) بين قطعتين من الليف البصري احادي النمط من نوع (smf-28) ايضاً.

تم الحصول على أقل نتيجة لقيمة (FWHM) والتي هي ( $117.26 \text{ pm}$ ) عندما كان الليف البصري الفوتوني المستخدم من نوع القلب المجوف ذو 19 خلية محذوفة بطول ( $7 \text{ cm}$ ) باستعمال جهاز محلل الليف البصري أو (Optical spectrum analyser). ثم بعد ذلك حسبت قيمة معامل التضيق او ( $F_c$ ) والتي كانت بمقدار (2.49).

ولتحسين قيمة معامل التضيق فقد استبدلت جميع الثقوب في ذلك الليف الهوائية بمادتين عضويتين هما حامض الايثانول ومحلول حامض الاكريليك ذو تركيز (75% حامض الايثانول و 25% حامض الاكريليك) وكانت قيمة معامل الانكسار لحامض الايثانول 1.369 وحامض الاكريليك 1.5 بدرجة حرارة 20 درجة سيليزية وطول موجي مقداره  $1550 \text{ nm}$ , وتمت مشاهدة افضل ( $\text{FWHM} = 58 \text{ pm}$ ) بمعامل تضيق قدره ( $\text{FC} = 4.9$ ).



وزارة التعليم العالي والبحث العلمي  
جامعة بغداد  
معهد الليزر للدراسات العليا

# تصميم وتنفيذ ضغط الاشارة المتراصف الليفي باستخدام الليف البلوري الفوتوني

رسالة مقدمة الى

معهد الليزر للدراسات العليا / جامعة بغداد / لاستكمال متطلبات نيل شهادة  
ماجستير علوم في الليزر/ الهندسة الالكترونية والاتصالات

من قبل

علي احمد داود

بكلوريوس هندسة الاتصالات – 2008

بإشراف

الأستاذ المساعد الدكتورة تحرير صفاء منصور